Investigations of LC Filter Unbalance in an Inverter-Fed Permanent Magnet Synchronous Motor Drives

Seyedeh Nazanin Afrasiabi

A Thesis

in

The Department

of

Electrical and Computer Engineering

Presented in Partial Fulfillment of the Requirements

For the Degree of

Master of Applied Science (Electrical and Computer Engineering) at

Concordia University

Montrèal, Quèbec, Canada

May 2020

CONCORDIA UNIVERSITY
SCHOOL OF GRADUATE STUDIES

This is to certify that the thesis prepared

By: Seyedeh Nazanin Afrasiabi

Entitled: Investigations of LC Filter Unbalance in an Inverter-Fed Permanent Magnet Synchronous Motor Drives

and submitted in partial fulfillment of the requirements for the degree of

Master of Applied Science (Electrical and Computer Engineering)

complies with the regulations of this University and meets the accepted standards with respect to originality and quality.

Signed by the final examining committee:

_____ Chair
Dr. P. Pillay

_____ External Examiner
Dr. A. Awasthi (CIISE)

_____ Internal Examiner
Dr. P. Pillay

_____ Supervisor
Dr. C. Lai

Approved by: _____
Dr. Y.R. Shayan, Chair
Department of Electrical and Computer Engineering

May 6, 2020

_____
Dr. M. Debbabi, Interim Dean,
Faculty of Engineering and Computer Science

Abstract

Investigations of LC Filter Unbalance in an Inverter-Fed Permanent Magnet Synchronous Motor Drives

Seyedeh Nazanin Afrasiabi MASc.

Concordia University, 2020

Permanent magnet synchronous machines (PMSMs) are usually controlled using two-level inverters. The output voltage of the inverter is in the form of the switching pulses between the positive DC-bus voltage and the negative DC-bus voltage. Such voltage waveforms have several adverse effects on the motor. These include, higher stress on winding insulation, higher eddy current losses and acoustic noise. Thus, to overcome these problems, different types of filters, typically LC-filters are used between the inverter and motor terminals to smooth the pulse width modulation (PWM) output voltages of the motor drives. Theoretically, the inductance and capacitance used for the filters are considered identical in each phase. However, in a practical scenario, it is difficult to have identical filter elements for all three phases. This non-ideal condition of filter elements amongst the three phases is considered as filter unbalance. This thesis investigates the impacts of filter unbalance on the PMSM drive system. Specifically, a comprehensive model of the motor drive system considering filter unbalance is proposed and developed at first. With the developed model, conventional field oriented control (FOC) is implemented to investigate the impact of this filter unbalance. A range of filter parameter variation and the corresponding impact on the motor drive including the motor current, torque and speed ripples is then studied in detail. Thereafter, the results obtained from the proposed model are validated through both circuit simulations and experimental tests.

Based on the investigation results, this thesis will discuss the allowable parameter variation in the LC filters to limit the motor performance deterioration within the required bounds, which will be beneficial to engineering practice in motor drive area. In addition, this investigation shows that a conventional FOC with proportional integral (PI) controller might not be capable of mitigating the negative impact on the motor due to filter unbalance, for example,

the negative sequence current. Therefore, this thesis implemented an adaptive proportional resonant (PR) controller to address negative sequence current and the corresponding impacts. A detailed mathematical framework to develop this proposed controller will also be presented in the thesis. Finally, the proposed adaptive PR controller is extensively evaluated on a laboratory PMSM drive system under different operating conditions.

Acknowledgement

First and foremost, I would like to express my deep and sincere gratitude to my supervisor, Prof. Chunyan Lai. It would not have been possible to write this thesis without her motivation, guidance, patience, and continuous support. I am also grateful for the financial support she has instilled during the course of my study.

I appreciate the valuable comments and helpful suggestions from the committee members, especially Prof. Pillay and Prof. Awasthi, who have significantly helped me to improve and shape my thesis.

Sincere vote of appreciation to my colleagues Dr. Amitkumar, Dr. Chirag, Rajendra and Dr. Mathews for addressing my different questions. Special thanks to Dr. Amitkumar for the stimulating discussions, troubleshooting skills, valuable insights without his consultations, this research work would not have been possible. And I would like to appreciate Dr. Chirag for helping me with appropriate tools to prepare my experimental setup.

I would like to thank other distinguished professors and colleagues in the Power Electronics and Energy Research (PEER) group. I would like to also take this opportunity to thank all my friends in the PEER group; Amitkumar, Chirag, Rajendra, Gabriel, Shiva, Yang, Ying, Ashutosh and Sumeet and all the members of the PEER Group for being part of the new family I found in Canada.

Last but not least, I would like to thank my loving and caring family. I am truly grateful to my parents, Sohila and Hossein for their endless love and unconditional support. My mother has been brightening up my life with her presence and my father has been always ask me to level up. I would also like to thank my wonderful sisters Niloofar and Negar for emotional support and encouragement. I consider myself the luckiest for having you on my side.

Table of Contents

List of Figures

List of Tables

Chapter 1 Introduction

1.1. Introductions

By the advent of technology, the demand for high energy efficiency and accurate control process are the main task of engineers so as to promote the industry. By introducing the Voltage Source Inverters (VSI) in the 1980s, it is possible to adjust the speed of various AC motors. Typically, the Adjustable Speed Drives (ASD) consist of a motor, and an inverter to drive the load which is mechanically connected to the motor shaft. A typical ASD is presented in Fig. 1- 1.

Mainly two types of AC motor are used in ASD namely Induction Motor (IM) and Permanent Magnet Synchronous Motor (PMSM). Due to the several advantages of the PMSM as compared to the IM namely high efficiency, high power density, rigidness, high-speed operation, good dynamic performance, and less maintenance PMSM are widely used in many application[1]–[4]. These advantages draw attention of researchers to develop many control techniques for PMSM, amongst different control strategies Scalar Control, Field Oriented Control (FOC) and Direct Torque Control (DTC) are mainly used for driving PMSMs [5]. Field oriented control is the most popular control strategy as compared to the other control strategies because of constant switching frequency and fast dynamic response [5].

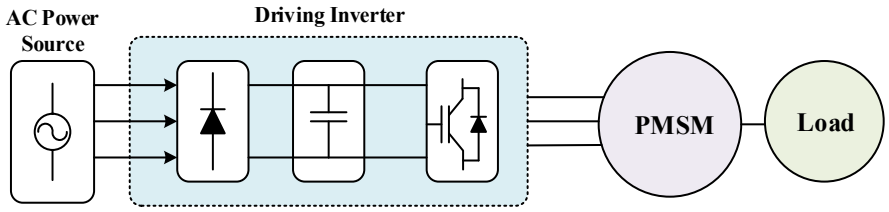

Fig. 1- 1. Typical industrial adjustable speed drive.

The typical power part of the drive consists of three-phase power supply, a diode bridge rectifier and DC link and PWM VSI inverter. In this network AC voltages pass through the diode bridge rectifier so as to rectify to DC voltage. The rectified DC voltage usually has some ripples, which is usually smoothed by the capacitors which are located in the DC link. Then the smoothed DC link voltage inverting back to alternating voltages with the help of PWM inverter. A three-phase PWM inverter generally contains six transistors and six anti-parallel diodes. The diodes are in reverse to the transistor and protect the inverter from overvoltage when they are switched off by letting reverse currents run. The transistor switches are controlled according to

the PWM switching dictated by the required control strategy. The output of the PWM inverter is typically pulses which are applied to the motor terminal. These pulses are switching between the negative DC link voltage to the positive DC link voltage. The transistors which used in VSI inverter are high speed semiconductor devices mostly IGBTs and MOSFETs. These devices are usually made with Silicon or Silicon-Carbide (SiC) or Gallium Nitride (GaN). To operate the inverter in higher switching frequency SiC or GaN power devices are used. SiC are more developed as compared to the GaN transistor as they can operate in higher power and voltage application and GaN transistors are used in application which higher switching frequency is required [6], [7].

These devices mostly offer fast turn-on and turn-off times, so, they offer high switching frequency. Higher switching frequency will result in high rate of change in voltage with respect to the time (*dv/dt*).The high *dv/dt* caused by the inverter output leads to insulation degradation, eddy current losses, and increase the acoustical noise in motor [7], [8]. These failures have devastating effects on the motor which leads to the huge financial losses for the industry. It is shown that 70% of faults in machine stator are due to high *dv/dt* [9]. A universal solution for high *dv/dt* problem at the inverter end is to change the voltage waveform by electrical filters such as LC filters or Sine wave filters. The cut-off frequency of sinusoidal filters is lower than the inverter switching frequency. Thus, this filter smooths the voltage pulses in the inverter output voltage and hence results in a sinusoidal voltage waveform [10], [11].

This sine wave filter or LC filter is located between the inverter output terminal and motor terminal. These conventional LC filters consist of series inductances with capacitances and resistances in parallel for each phase. Fig. 1- 2 illustrates the LC filter for PMSM motor drive. As it can be observed, for each phase one inductor (L), damping resistor (R) and capacitor (C) is required. Fig. 1- 3 presents the measured line voltage before and after inserting the LC filter to the motor drive system from two-level IGBT inverter with a 5 KHz switching frequency. It can be observed that the inverter output voltage is in the form of PWM pulses, and it becomes a smooth sine wave voltage with low residual ripple after the LC filter. In the previous studies, the value of LC filter elements is considered to be identical for all three phases for different applications including motor drive [11]–[13] and grid connected converter [14]–[16]. However, in practical situation it might be difficult to find three identical values for each phase because of the component tolerance. This filter element variation from nominal value causes unbalance LC

filter. Unbalances are considered for inductors, capacitors and damping resistors. For example, in Fig. 1- 2 L_f is the nominal filter inductance and ΔL is the inductance tolerance/variation.

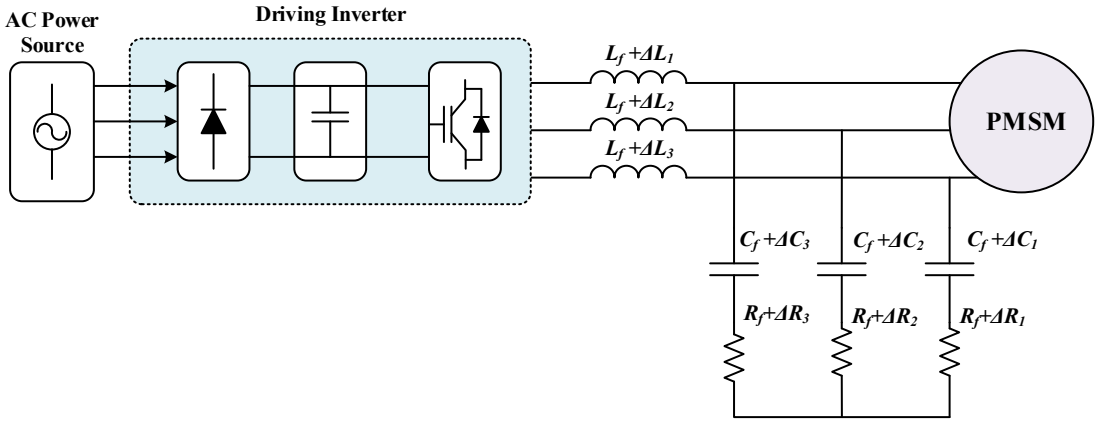

Fig. 1- 2. Adjustable speed drive with unbalance filter.

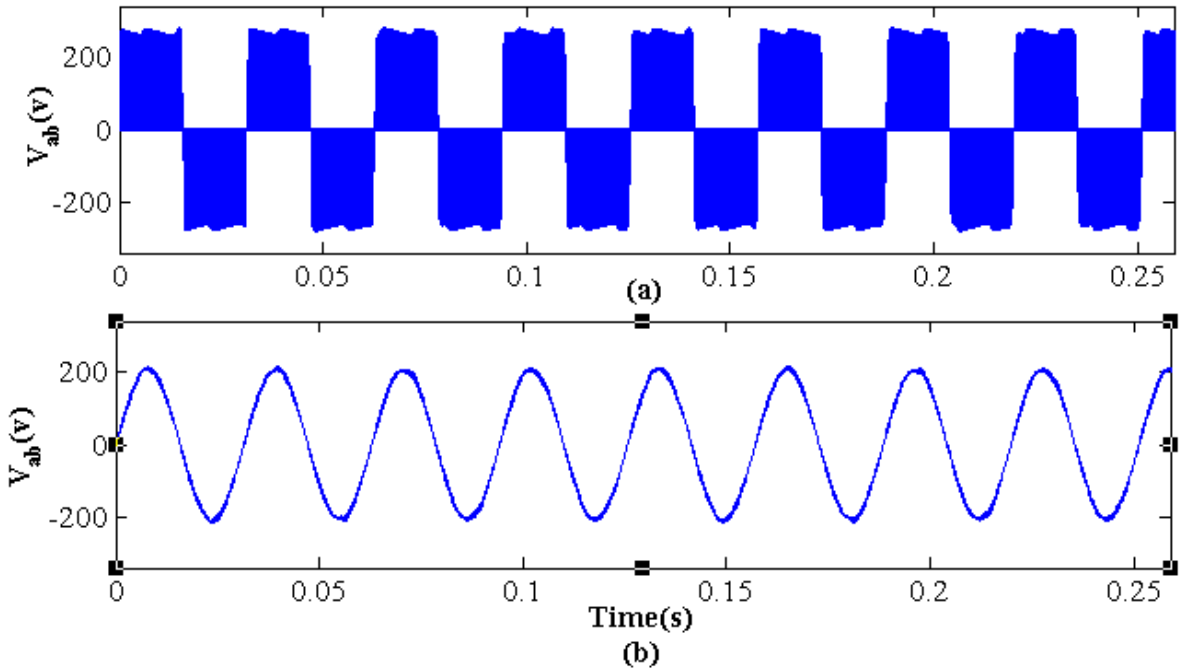

Fig. 1- 3. The inverter line voltages output before and after LC filter.

These non-ideal situations create several problems for the whole machine and drive. Unbalanced winding currents will have negative sequence currents, which in turn produce reverse rotating magnetic field inside the motor, leading to additional heating. The generated heat decreases equipment life and motor efficiency. Moreover, the unbalanced winding currents also causes torque and speed ripple which lead to machine vibration, and possibly mechanical stresses and

failures [17]. In addition, unbalance current leads to the negative sequence current in *dq* frame [18], [19].

1.2. Problem statement

The problem associated with high *dv/dt* due to the use of VSI in PMSM can be eliminated by using an LC filter between the VSI inverter and motor terminal. In theoretical scenario, the values of Inductors and capacitors for all three-phases are considered to be identical. However, in practical scenarios it is difficult to find three identical values for each phase because of component tolerances. Thus, there will be a derivation between each three-phases. This non-ideal condition of filter parameter variation amongst the three phases can cause unbalance in the motor winding currents. Unbalanced winding currents will have negative sequence currents, which in turn produce reverse rotating magnetic field inside the motor, leading to additional heating. The generated heat decreases equipment life and motor efficiency. Moreover, the unbalanced winding currents also causes torque and speed ripple which lead to machine vibration, and possibly mechanical stresses and failures. This thesis investigates the impact of LC filter unbalance on the motor and drive.

1.3. Research objective

The previous section presented some research problems of PMSM with unbalance LC filter. The research objective of this thesis and the problem which will be addressed in this research work are as follows:

1. Comprehensive modeling and analysis of the LC filter unbalance are presented, and its impacts on the machine and drive performances are investigated through MATLAB simulations and experimental tests.
2. A detailed investigation of PMSM drive control, accounting for LC filter unbalance, will be presented in this study. An adaptive PR controller along with the conventional PI controller is proposed to minimize the negative sequence current introduced due to LC filter unbalance and detailed controller design will also be presented and validated with experiments.

1.4. Contributions

The contribution of this research work is the following conference and journal paper

Conference paper:

S. Afrasiabi and C. Lai, "Investigation of LC Filter Unbalance in an Inverter-Fed Permanent Magnet Synchronous Machine Drives," *ICEM2020*– Under review.

Journal Paper:

S. Afrasiabi and C. Lai, "Improved Current Controller Design in a Permanent Magnet Synchronous Motor Drive Considering LC Filter Unbalance," to be submitted to IEEE Transactions on Transportation Electrification.

1.5. Organization of this thesis

The rest of the thesis is divided into the following five chapters.

Chapter 2 starts with the permanent magnet synchronous machine mathematical modeling and its application. Then, parameter measurement of the PMSM under test is presented. Electrical parameters of the machine such as *d*-axis and *q*-axis inductances, stator resistance, back EMF constant, along with machine mechanical parameters including the moment of inertia and viscous friction are measured. Afterwards, the mathematical model of LC filter is presented, and the LC filter components are designed for the laboratory PMSM drive system. At the end, the PMSM model was updated to include a balance LC filter.

Chapter 3 introduces different control strategies for PMSM namely scalar control, vector control and direct torque control. Vector control and direct torque control are evaluated through simulations and experiments in this study to determine their suitability for the proposed research. The experimental setup as well as comparison between these two control methods will be provided in this section. Based on the evaluations of these two advanced control methods, vector control is selected for analysis of PMSM drive performance with balance and unbalance LC filters. This chapter also provided a detailed procedure of controller design for PMSM drive with LC filter.

Chapter 4 presents a comprehensive modeling and analysis of the LC filter parameter unbalance, and its impact on the motor drive performance. These analyses will include the negative sequence current and torque/speed ripples and motor performance deterioration, due to

unbalance in LC filter parameters. This chapter also discusses an allowable range of LC filter unbalance to keep machine performance within the required bounds.

Chapter 5 provides a solution to mitigating the negative impact of unbalance LC filter on PMSM motor drive performance. The adaptive PR controller is implemented in the motor drive to mitigate the second harmonics in the *dq*-axis currents. This PR controller works in parallel with the PI controller to deliver an improved motor drive performance under the unbalanced LC filter condition. The proposed control method will be analyzed in detail through the simulation and experimental tests.

Chapter 6 presents the conclusions and possible future work to extend/improve the research proposed in this thesis.

Chapter 2 Comprehensive Modeling of Permanent Magnet Synchronous Machine Considering LC Filter

This chapter presents the permanent magnet synchronous machine (PMSM) modeling followed by electrical and mechanical parameter measurements of the prototyped surface-mounted PMSM. Also, LC filter design and mathematical modeling of PMSM with LC filter will present in this chapter.

2.1. Permanent magnet synchronous machine

With the introduction of adjustable speed drives (ASD) in the industry, it became possible to adjust the speed of various AC motors. Induction Motor (IM) and Permanent Magnet Synchronous Motor are commonly installed with ASD. As compare to IMs, the PMSMs draw a special attention because of their advantages including higher starting torque, compact size, faster dynamic response for both torque and speed, and higher efficiency as compared to the size [20]. As a consequences of these advantages, PMSMs are used in different industrial applications such as pumps, fans, robotic, aerospace, and electrical vehicles [20].

In general, according to the shape of the back electromotive force (EMF), PMSM is classified into the two main categories. One is sinusoidal back EMF and the other with trapezoidal or square back EMF is normally called Brushless DC motors (BLDC) [21]. The sinusoidal back EMF can be divided in to two category base on the location of the magnets on the rotor. Fig. 2- 1 shows different magnet placements in PMSM.

Fig. 2- 1 (b) is surface-mounted PMSM (SPMSM) which permanent magnet (PM) are mounted on the surface of the rotor core. Due to this, the SPMSM has weak mechanical strength especially at the higher speeds. The generated electromagnetic torque of SPMSM is only generated by the permanent magnet. Thus, designing of this machine is simple. The other type of PMSM is interior PMSM (IPMSM) in which the PMs are buried inside the rotor (Fig. 2- 1 (a)). IPMSM is mechanically more robust then SPMSM at high speed, and it has a reluctance torque component in addition to the torque produced by PMs.

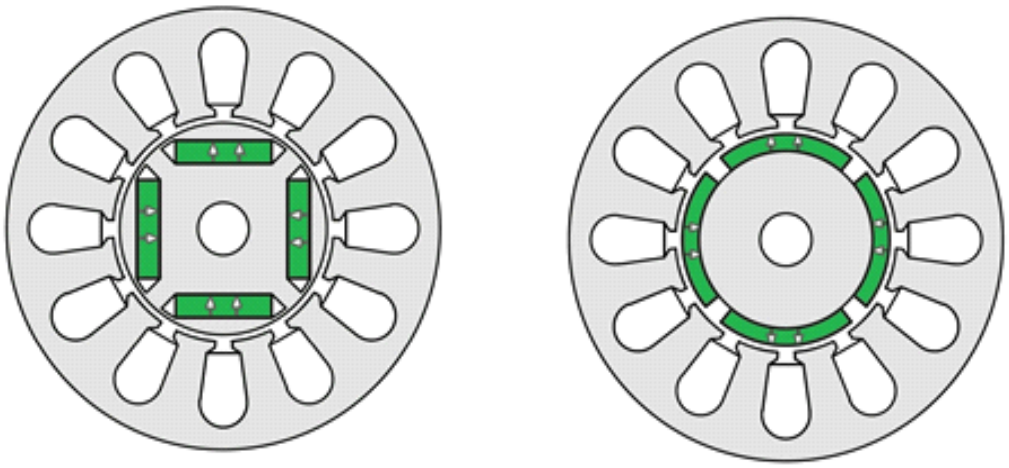

(a) **(b)**

Fig. 2- 1. Different rotor structures for PMSMs (a) Interior PMSM (b) Surface mounted PMSM [22].

2.2. Mathematical model of PMSM

The mathematical model of PMSM is a time-variant, multivariable and nonlinear. The following assumptions are made to simply the modeling of PMSMs [20].

- Core saturation and parameter variation is neglected;
- The stator windings are balanced with sinusoidal back EMF;
- Eddy currents and Hysteresis losses are neglected;

In the *abc* frame, the three-phase winding of the motor is *abc* axes and the actual components of the motor in the coordinate axis are current, voltage, and flux. In this reference frame, the electrical dynamic equation in terms of phase variables can be written as:

$$v_{abc} = R_s i_{abc} + \dot{\psi}_{s,abc} \tag{2-1}$$

where v_{abc}=[v_a v_b v_c]^T is the phase terminal voltage vector, $i_{abc} = [i_a \quad i_b \quad i_c]^T$ is three phase current vector and $\psi_{abc} = [\psi_a \quad \psi_b \quad \psi_c]^T$ is the flux linkage vector of phase *a, b,* and *c*. The flux linkages are generated by the stator currents and the rotor permanent magnets can be expressed as:

$$\psi_{s,abc} = L_s i_{abc} + \psi_{abc} \tag{2-2}$$

where ψ_{abc} is the flux generated by the PMs in the rotor and it changes according to the rotor position. The L_s is inductance matrix can be written as:

$$Z_{ph} = \begin{bmatrix} L_{aa} & M_{ab} & M_{ac} \\ M_{ba} & L_{bb} & M_{bc} \\ M_{ca} & M_{cb} & L_{cc} \end{bmatrix} \tag{2-3}$$

where the M is mutual inductance between each machine phase and L is each phase inductance. In *abc* reference frame, these three variables make machine equation. However, the equation solution is unnecessarily complex. Thus, to simplify the motor model Park transformation is commonly applied. This transformation converts AC variables to the DC components in the *dq* axis. Fig. 2- 2 presents the relationship between *abc* reference frame and *dq* reference frame.

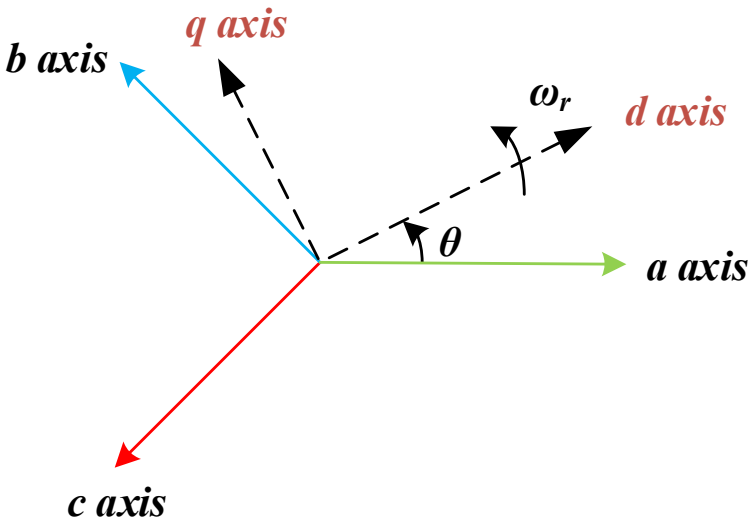

Fig. 2- 2.Three phase stationary frame and equivalent rotating *dq* axis.

The following transformation matrix is used to convert *abc* axis to *dq* axis.

$$u_s = u_d + ju_q = \frac{2}{3}(u_a + u_b e^{\frac{-j2\pi}{3}} + u_c e^{\frac{j2\pi}{3}})e^{-j\theta} \tag{2-4}$$

$$\begin{bmatrix} u_d \\ u_q \\ u_0 \end{bmatrix} = \frac{2}{3}\begin{bmatrix} \cos(\theta) & \cos(\theta - 2\pi/3) & \cos(\theta + 2\pi/3) \\ -\sin(\theta) & -\sin(\theta - 2\pi/3) & -sin(\theta + 2\pi/3) \\ \frac{1}{2} & \frac{1}{2} & \frac{1}{2} \end{bmatrix}\begin{bmatrix} u_a \\ u_b \\ u_c \end{bmatrix} \tag{2-5}$$

Inverse transformation is given by:

$$\begin{bmatrix} u_a \\ u_b \\ u_c \end{bmatrix} = \begin{bmatrix} \cos(\theta) & -\sin(\theta) & 1 \\ \cos(\theta - 2\pi/3) & -\sin(\theta - 2\pi/3) & 1 \\ \cos(\theta + 2\pi/3) & -sin(\theta + 2\pi/3) & 1 \end{bmatrix}\begin{bmatrix} u_d \\ u_q \\ u_0 \end{bmatrix} \tag{2-6}$$

By applying the Park transformation to the (2-1), we have:

$$v_{abc}e^{-j\theta} = R_s i_{abc}e^{-j\theta} + \frac{d}{dt}(\psi_{abc}(t)e^{-j\theta}) \tag{2-7}$$

$$v_d + jv_q = R_s I_d + jR_s I_q + \left(\frac{d}{dt}\psi_{abc}(t)\right)e^{-j\theta} + (\frac{d}{dt}(\psi_{abc}(t))e^{-j\theta} + (\frac{d}{dt}e^{-j\theta})\psi_{abc}(t) \tag{2-8}$$

By doing some simplifications:

$$v_d + jv_q = R_s I_d + jR_s I_q + \frac{d}{dt}(\psi_d + j\psi_q) + j\omega_r(\psi_d + j\psi_q) \tag{2-9}$$

Then, the dynamic model of a PMSM in *dq* rotor reference frame can be expressed as follows:

$$v_d = R_s I_d + \frac{d\psi_d}{dt} - \omega_r\psi_q \tag{2-10}$$

$$v_q = R_s I_q + \frac{d\psi_q}{dt} + \omega_r\psi_d \tag{2-11}$$

$$\psi_d = L_d I_d + \psi_{PM} \tag{2-12}$$

$$\psi_q = L_q I_q \tag{2-13}$$

where, I_d and I_q represent *d* and *q* axes currents, respectively, R_s is the stator resistance, v_d and v_q are *d* and *q* axes voltages, L_d and L_q are the *d* and *q* axes inductances, ω_r is the rotor electrical speed, ψ_q and ψ_d are *d* and *q* axes flux linkages and ψ_{PM} is the permanent magnet flux linkage.

The electromagnetic torque generated by PMSM can be represented as follows:

$$T_e = \frac{3}{2}P(\psi_d I_q - \psi_q I_d) \tag{2-14}$$

$$T_e = \frac{3}{2}P(\psi_{PM} I_q + (L_d - L_q)I_d I_q) \tag{2-15}$$

where T_e is the electromagnetic torque, T_L is the load torque, *P* is the number of pole pairs of the machine, *J* is the rotational inertia, and *B* is the viscous friction coefficient.

The PMSM electromagnetic torque equation consists of magnetic torque and the reluctance torque which are corresponded with the first term and second term of equation (2-15) respectively. The magnet torque is produced by the interaction of the fields produced by the magnets in the rotor and the stator, whereas the reluctance torque is generated by the unequal

reluctances of d and q axes. For the IPMSM with saliency ($L_d \neq L_q$), the reluctance torque is produced with asymmetrical flux paths in d axis and q axis. SPMSM with nonsalient-pole ($L_d = L_q$), has a higher magnet torque due to magnet proximity to the air gap and the reluctance torque is not presented.

Typically, the mathematical model of PMSM is represented by an equivalent circuit base on the mathematic equation. Fig. 2- 3 shows the dq axis equivalent circuit of PMSM.

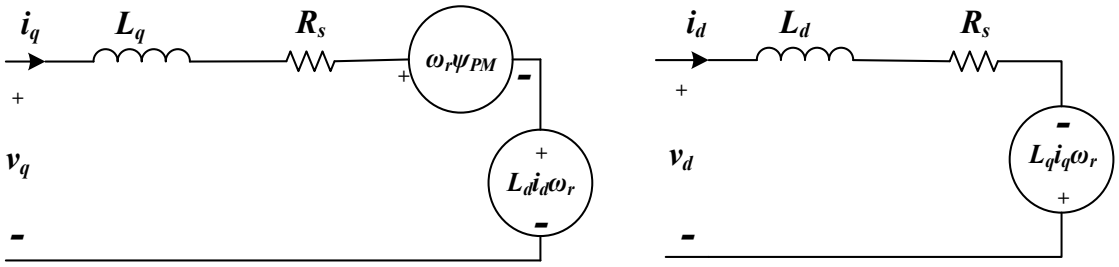

Fig. 2- 3. dq axis equivalent circuit of a PMSM.

2.3. PMSM parameters measurements

An accurate information of motor parameters is necessary for control of electrical machines. The quality of control design depends on the parameters of overall system. Therefore, it is important to measure the electrical parameters of the PMSM which are back-EMF constant, d and q axis inductances and stator resistance. The mechanical parameters are friction coefficient and moment of inertia. In this section the measurement methods for electrical parameter as well as mechanical parameters for PMSM are covered.

2.3.1. Back-EMF constant measurement

To measure the back-EMF constant or flux linkage of the PM is measured base on the following machine setup Fig. 2- 4. The test bench is included a surface-mounted PMSM (SPMSM), a direct current (DC) dynamometer, and a torque transducer. The SPMSM was coupled with a dc dynamometer through a torque transducer. In order to measure the back-EMF constant, the prototyped SPMSM runs as a generator from 200 to 1400 rpm in steps of 200 rpm using a dc dynamometer. Back-EMF was measured and recorded in the Yokogawa SL1000 data acquisition system.

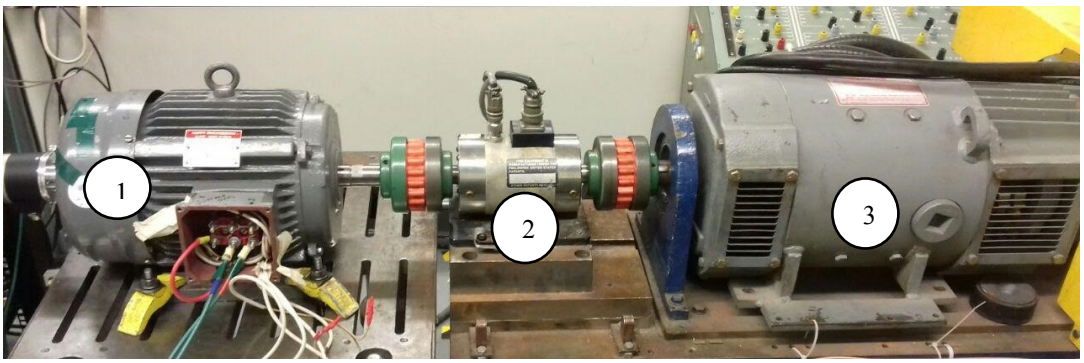

Fig. 2- 4. (1) Permanent magnet synchronies machine, (2) Torque transducer, (3) DC dynamometer.

To calculate the back-EMF constant the peak value of the phase voltage at no-load condition and electrical speed (rad/sec) are required. Electrical speed is calculated from the measured mechanical speed of the machine and the peak value of the phase voltage (V_{ph}) is obtained while the motor rotates as a prime mover at a constant speed. The peak value of the phase voltages at different speeds of the machine is measured and recorded. The back-EMF constant is the ratio between the peak value of the phase voltage and the electrical speed of the machine. The calculated value of the back-EMF constant is listed in the Table. 2- 1 and Fig. 2- 5 shows the measured back-EMF constant (Ke_{ph}).

Table. 2- 1. Back-EMF constant calculation.

Speed(rpm)	**Electrical Speed (rad/sec)**	**V_{LL} (rms)**	**$V_{ph(}$ peak)**	**Ke_{ph} (V.sec/rad)**
200.00	41.89	29.20	23.84	0.57
400.00	83.78	59.00	48.17	0.58
600.00	125.66	88.60	72.34	0.58
800.00	167.55	118.00	96.35	0.58
1000.00	209.44	147.00	120.02	0.57
1200.00	251.33	176.00	143.70	0.57
1400.00	293.22	205.00	167.38	0.57

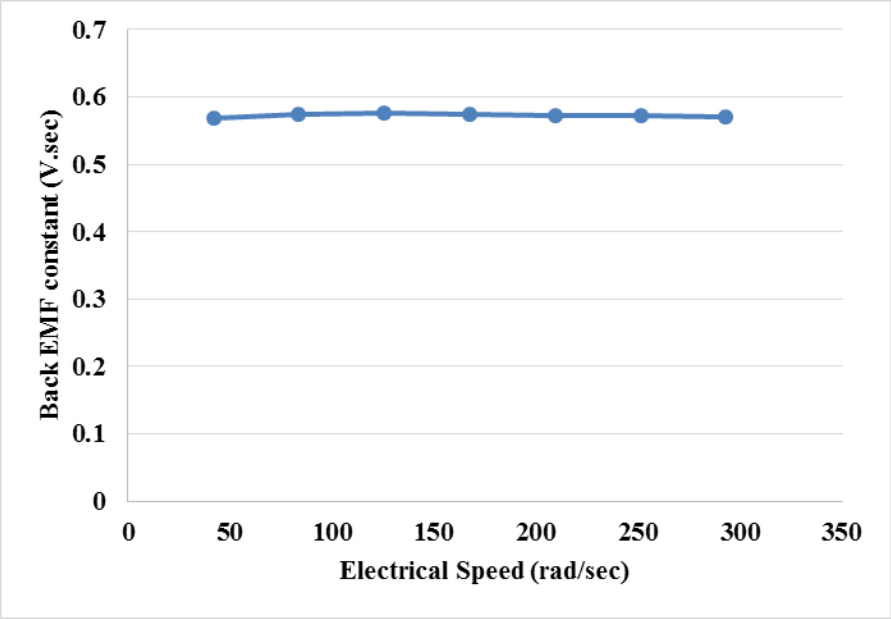

Fig. 2- 5. Back-EMF constant vs. electrical speed for SPMSM.

2.3.2. Resistance measurement

The R_s is considering the stator winding resistances which is depending on the temperature. So, during the measurement the attention has to be paid winding temperature. To measure the winding resistance for PMSM typically two methods are used. The simplest method is using a digital multimeter. This method is operate accurately for the machine with stator resistance more than ($>10\Omega$). For the star connected, star winding, the resistance value is measured in pair and the stator resistance is half of the measured resistance.

The second method for measuring the winding resistance is using the RLC meter or two multimeters. This technique measures current through the winding and voltage across the machine terminal. Moreover, it measures the stator resistance between (10 mΩ-10 kΩ) [23].

2.3.3. Inductances measurement

To determine the inductances of direct and quadrature axes of PMSMs. AC stand still test and DC stand still test are mostly used. In AC stand still test, an AC voltage source at desired magnitude and frequency are supplied to the phase winding of the machine while the rotor is locked at the axis in which the inductance is to be determined. The inductances is measured based on the different current magnitudes and the rms value of voltages, currents and reactive powers are recoded in power meter [23]. The other method is DC stand still test, in this method,

the *q* axis or *d* axis inductances is measured while the machine is lucked at the axis in which the inductance is to be determined.

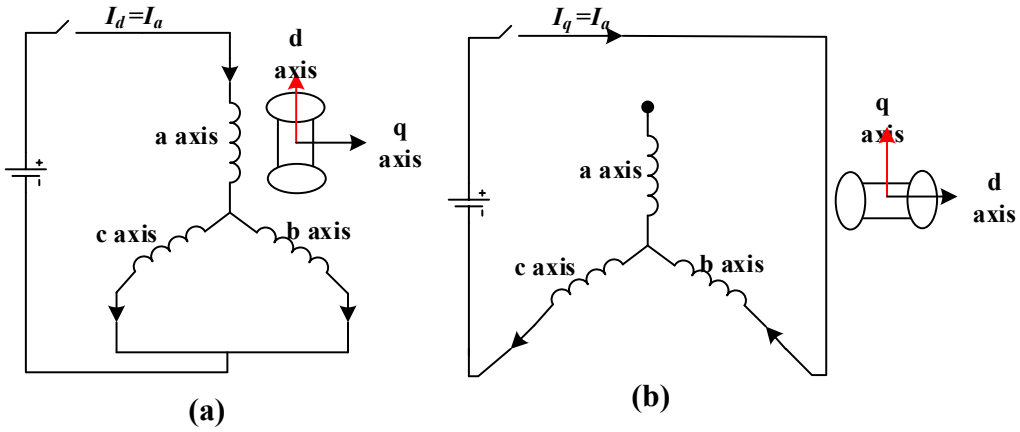

Fig. 2- 6. Circuit diagram of machine terminal connection using DC stand still test method (a) *d* axis inductance measurement connection (b) *q* axis inductance measurement connection.

Fig. 2- 6 illustrates the machine terminal connection for indicating *q* axis inductance and *d* axis inductance. Then, DC step voltage with the desired magnitude is applied to the PMSM thought the phase winding of the machine [24].

The voltage and current curves of the winding are recorded as the supply voltage is switched to zero. The transient response of the machine is measured at different current levels. Fig. 2- 7 presents the measurements result as a DC supply current set to 14 A and then the switched off.

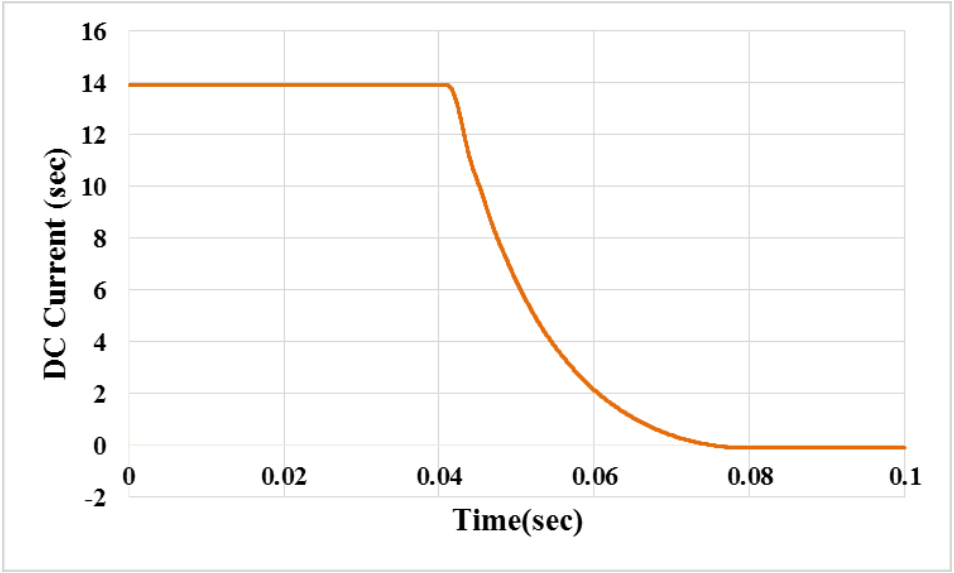

Fig. 2- 7. A current waveform of SPMSM for inductance measurement.

The q axis inductance can be calculated using the following equation [25]:

$$\lambda_q = \int_0^t (v_{dc} - R_s i_{dc}) d\xi \tag{2-16}$$

$$L_q = \frac{\lambda_q}{i_{dc}} \tag{2-17}$$

where $v_{dc}, R_s, i_{dc}, d\xi$ and t are DC voltage, stator resistance, DC current, dummy variable of integration and the time period of integration respectively. The same equation is used to calculate the d axis inductance. Fig. 2- 8 illustrates the measured d axis and q axis inductances for SPMSM.

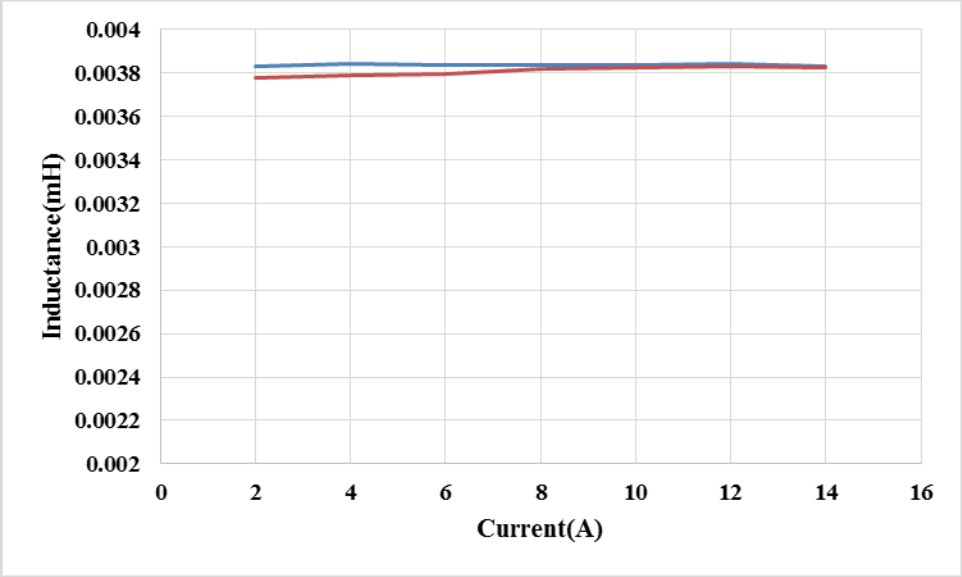

Fig. 2- 8. Measured d axis and q axis inductances of SPMSM.

2.3.4. Moment of inertia and viscous friction measurements

To develop the accurate controller for PMSM, a precise measurement of the motors mechanical parameter is required. The moment of inertia J and viscous friction B can be measured by spin down test. At the start the SPMSM is rotating at a high speed that corresponds to the rated voltage of machine. The voltage source is turned-off instantly with the help of breaker at a given instant and the machine decelerates to a full stop. The SPMSM moment of inertia is calculated by measuring the slop of transient respond (Fig. 2- 9). By neglecting the machine core loss and friction and winding loss the input power and the output power will be measured. From the output power measurement, the induce electromagnetic torque and corresponded viscous friction is calculated.

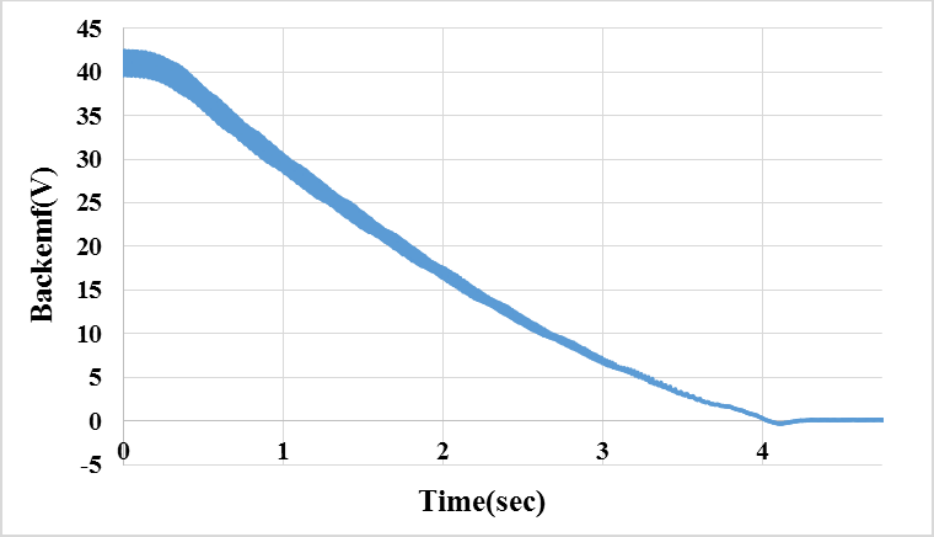

Fig. 2- 9. Measured Back EMF curve of SPMSM in the spin down test.

The parameter values for SPMSM under consideration for simulation and experimental studies are listed in Table. 2- 2.

Table. 2- 2. Parameters of the Permanent Magnet Synchronous Motor

Parameter	**Measurements value**
Rated Power (P_{rated})	3.6 kW
Rated rms line to line voltage (V_{rated})	220 V
Rated rms current (I_{rated})	15 A
Base speed	1350 rpm
Moment of inertia (J)	0.0384 kg/m^2
Viscous friction (B)	0.000425 Nm.s
Number of pols (P)	4
d-axis inductance (L_d)	0.0038 H
q-axis inductance (L_q)	0.0038 H
flux linkage ψ_{PM}	0.5 V.sec
Stator resistance (R_s)	0.1718 Ω

2.4. LC filter modeling

To overcome the problem of high *dv/dt* in the motor terminal due to the VSI. Typically, a low pass LC filters are introduced. LC filters are located between inverter output and motor terminal. Using the LC filter changes the gain and phase of the voltage signals feeding the PMSM [26], [27]. Thus, it is important to model and analyze the behavior of the LC filter. Fig. 2- 10 illustrates the equivalent single phase circuit diagram of LC filter in which L_f, C_f, R_f, V_{inv} and V_m are the filter inductance, filter capacitor, filter damping resistor, inverter output voltage and motor input voltage respectively. The damping resistors are included to limit the current into the capacitor to avoid resonance when the switching frequency is near its resonant frequency.

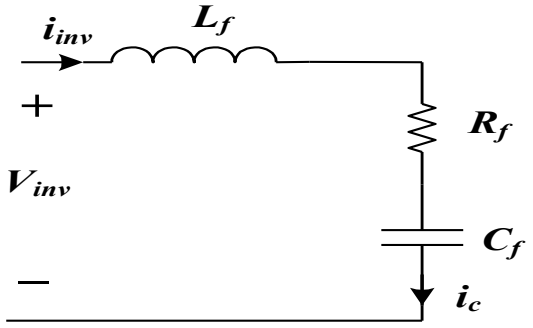

Fig. 2- 10. Equivalent circuit of the LC filter

The following step by step equation can be obtained for total impedance of LC filter:

$$Z_{out} = \frac{1}{c_f s} + R_f \tag{2-18}$$

$$Z_{total} = L_f s + Z_{out} \tag{2-19}$$

where Z_{out} is the output impedance of LC filter and Z_{total} is the total impedance of LC filter. The following open loop transfer function can be written be:

$$G(s)_{LC} = \frac{i_{inv}}{V_{in}} = \frac{C_f s}{L_f C_f s^2 + C_f R_f s + 1} \tag{2-20}$$

Hence, the filter resonance frequency is:

$$f_c = \frac{1}{2\pi\sqrt{L_f C_f}} \tag{2-21}$$

2.5. LC filter design procedure

The LC filter needs to be well designed as there is an amplification in the frequency range near the resonance peak. It is desirable to place the resonance frequency of such a filter greater than the fundamental frequency (f_s) of PMSM and lesser then switching frequency of the inverter (f_{sw}). Thus, it will not amplify the control signal for the PMSM while attenuating the switching frequency. The filter resonance frequency range presents in (2-22) [28].

$$f_s < f_c < f_{sw} \tag{2-22}$$

In this study, the filter resonant frequency is 850 Hz which is placed away from the fundamental frequency and switching frequency (5 kHz). The inductance is selected slightly lesser then the machine inductances. And, the capacitor value is calculated based on the filter resonant frequency and selected inductance using the equation (2-21). This LC filter is designed for a motor drive with switching frequency no less than 5kHz. Table. 2- 3 is listed the value of inductances, capacitors and damping resistances.

Table. 2- 3. The calculated LC filter values

Parameters	**values**
L_f	0.0038 H
C_f	10 μF
R_f	1 Ω
f_c	850 Hz

2.6. Modeling of PMSM along with LC filter

In order to achieve completely sinusoidal motor voltage from the LC filter, it is essential to model the PMSM with LC filter. So, in this section the equivalent circuit of the PMSM with LC filter in *abc* frame is presented. And the transfer function which represents the behavior of input and output of the system is extracted.

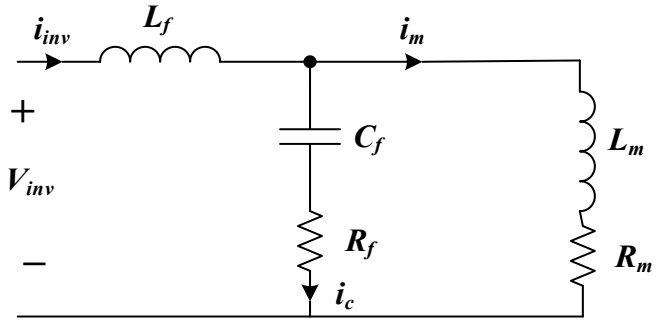

Fig. 2- 11. LC filter along with PMSM equivalent circuit

To examine the behavior of the filter the single phase circuit is needed. The LC filter equivalent circuit along with motor single phase is shown in Fig. 2- 11 where L_f is filter inductance C_f is filter capacitor R_f is filter damping resistance. L_m and R_m are motor inductance and resistance, respectively.

To analysis the filter in frequency domain, the open loop transfer function is obtained. Using the following step by step modeling. By considering the input impedance Z_{in} and the output impedance Z_{out}. First the output impedance is calculated as:

$$Z_{out} = \frac{(L_m s + R_m)(\frac{1}{C_f s} + R_f)}{(L_m s + R_m)} \tag{2-23}$$

Then the input impedance is:

$$Z_{in} = L_f s + Z_{out} \tag{2-24}$$

$$Z_{in} = \frac{L_f L_m C_f s^3 + L_f C_f R_m s^2 + L_f C_f R_f s^2 + L_m C_f R_f s^2 + R_f R_m C_f s + L_f s + L_m s + R_m}{C_f L_m s^2 + R_m C_f s + C_f R_f s + 1} \tag{2-25}$$

Therefore, the transfer function associated with inverter voltage and inverter current ($G(s)_{LC\&PMSM}$) for the PMSM connected with the LC filter can be written as bellow:

$$\frac{i_{inv}}{V_{in}} = \frac{C_f L_m s^2 + R_m C_f s + C_f R_f s + 1}{L_f L_m C_f s^3 + L_f C_f R_m s^2 + L_f C_f R_f s^2 + L_m C_f R_f s^2 + R_f R_m C_f s + L_f s + L_m s + R_m} \tag{2-26}$$

Chapter 3 Development of PMSM Control Strategies with Balanced LC Filter

This chapter presents a comprehensive analysis on different control strategies for PMSM drive system namely scalar control, direct torque control (conventional DTC and PI-DTC) and field oriented control. The principle criteria of each control strategy will be described and simulated in MATLAB/Simulink followed by experimental test. Then the problems associated with each control strategy are evaluated and the motivation for selecting FOC for developing a control strategy for balance LC filter will be presented. The FOC control methodology is developed for controlling a balance LC filter. This is future supported by the simulation and experimental test of the prototyped SPMSM drive.

3.1. Control methods of PMSMs

PMSMs are able to operate at various speeds by the help of variable frequency drive (VFD). Typically, the main control methods for PMSMs are divided into three main categories depending on which quantities they control: scalar control, field oriented control (FOC) and direct torque control (DTC). An overview of these different control strategies is presented in Fig. 3- 1. These sections will introduce each control strategy.

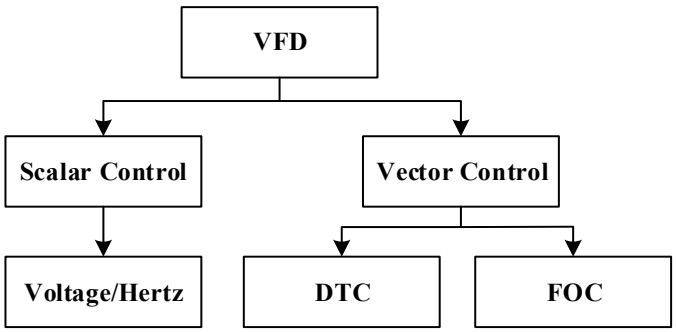

Fig. 3- 1. Overview of PMSM control strategies.

3.1.1. Scalar control

Scalar control or v/f control is the simplest control strategy for controlling a PMSM. In the scalar control, the PMSM speed keeps constant by adjusting the magnitude of stator voltage and frequency. The block diagram of PMSM drive system equipped with V/f control is

illustrated in Fig. 3- 2. In this control strategy, a voltage modulator is used to convert the three-phase voltage references to gate signals for the inverter. Since the scalar control is an open loop control approach without any feedback of motor parameters and position. Also, it focuses only on the steady-state. So, the drive system's transient behavior will not be satisfied. This method is easy to implement, with low demands on computation power of the control hardware. As a result, v/f control is widely used in systems with low dynamic performance such as fans and pump-drivers [29].

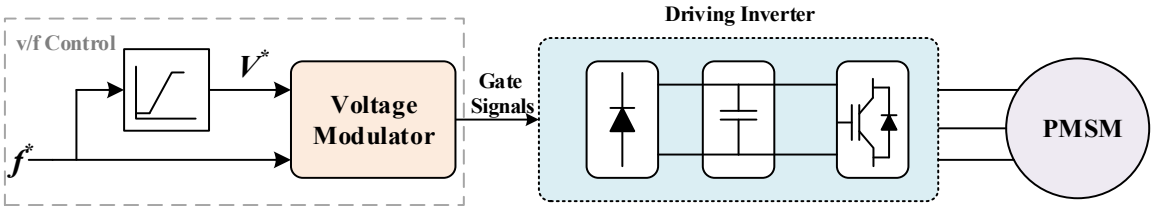

Fig. 3- 2. PMSM scalar control block diagram.

3.1.2. Field oriented control

The idea of field oriented control (FOC) or vector control is controlling an AC machine like the DC machine. In DC motors the produced electromagnetic torque and flux can be independently controlled. However, AC machines do not have such features like DC machines. In 1970s, the FOC technique was first proposed for AC machines that the torque production in AC and DC machines are almost similar. The basic principle of vector control is to transfer the three-phase AC currents to two orthogonal DC components that can be visualized with a vector with the help of Park and Clark transformations. The current components corresponding to the field-magnetizing flux and torque generation in AC machines can be decoupled orthogonally so that the field-magnetizing flux can be controlled without affecting the dynamic response of the torque and vice versa. In this method, the dynamic performance of the electromagnetic torque of AC machine is as accurate as DC machines [30]. Over the years, FOC drives are achieved substantial worldwide market and are used in different applications. Based on the selected directional magnetic field vector control is divided into three categories namely air gap magnetic field orientated, stator magnetic field oriented, and rotor magnetic field oriented. Generally, for the PMSM the rotor magnetic field oriented control is generally adopted because of the constant magnetic flux of the permanent magnet in the rotor.

The general structure of vector control is shown in Fig. 3- 3. In this control strategy the direct axis and quadratic axis currents are independently controlled. The direct axis current is used to weaken the field so it sets as zero and the *q*-axis current is used to control the produced torque. Also, the accurate position control is needed to achieve good dynamic response [31].

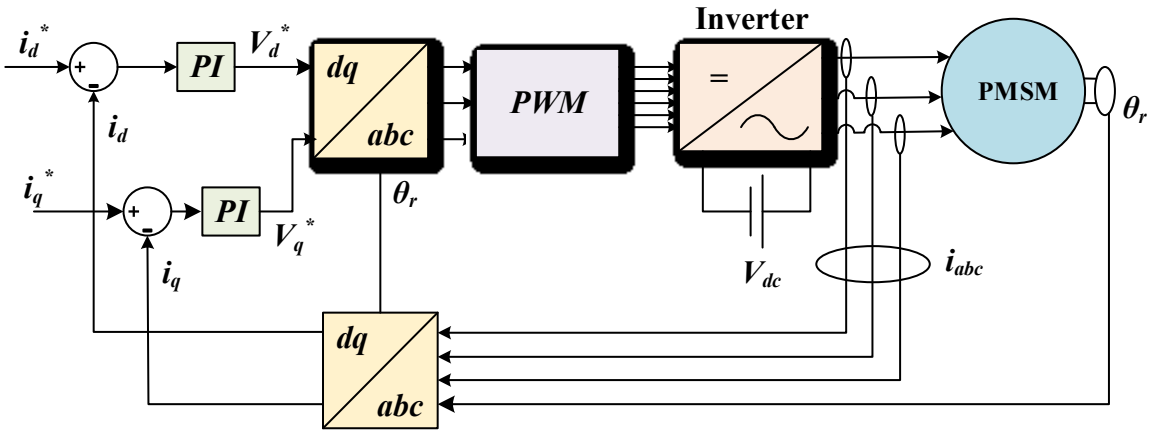

Fig. 3- 3. Block diagram of field-oriented control for PMSM

3.1.3. Direct torque control

After proposed FOC, direct torque control (DTC) was first introduced for induction motors (IM) by a German engineer, Depenbrock, and two Japanese scholars, Takahashi and Noguchi in 1980s [32]. Unlike FOC, DTC control variables are electromagnetic torque and stator flux so that the electromagnetic torque and stator flux can be directly controlled. An important characteristic of this method in comparison with FOC, is fast dynamic performance, robustness to disturbances and simple implementation.

The block diagram of conventional DTC is shown in Fig. 3- 4. In a conventional DTC, the stator flux is estimated by flux estimator, then the sector is determined based on the stator flux value. Next, the electromagnetic torque is calculated. In the next step the actual flux and torque will be compared with the reference value of torque and flux. And a Hysteresis controller or bang-bang control is typically adopted. So, in each control cycle, appropriate voltage vectors are selected according to the outputs of two Hysteresis controllers to generate gate signals for the inverter to control the stator flux and torque of the PMSMs. Using the bang-bang controller in DTC leads to some disadvantages namely torque ripple, flux ripple and variable switching frequency.

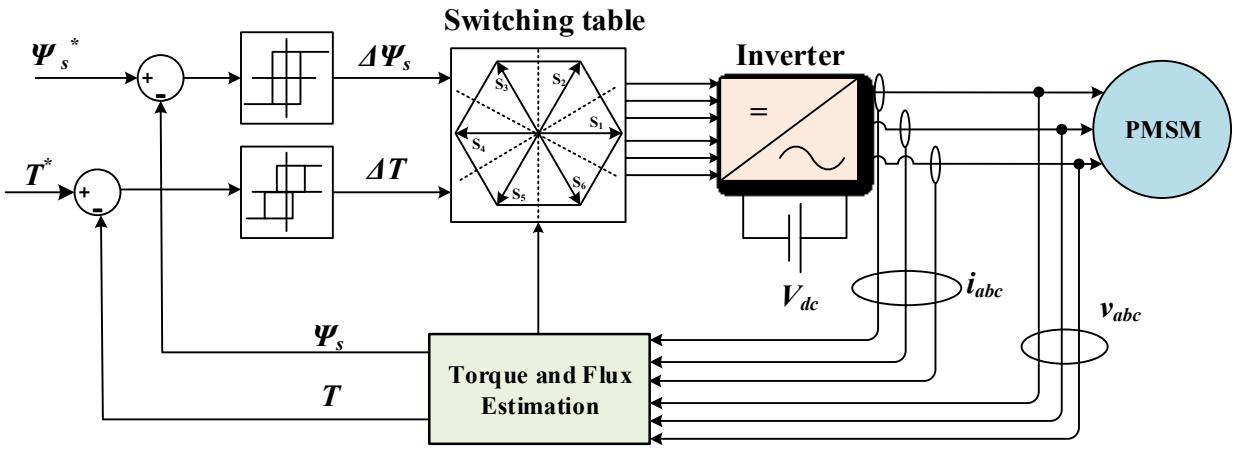

Fig. 3- 4. Block diagram of conventional direct torque control for PMSM.

3.2. Investigations on FOC of PMSMs through simulations and experiments

The Scalar control has been studied in the literature and because of its poor performance; it is not a good candidate for different applications. So, in this section, FOC control strategies will be studied through the MATLAB/ Simulink software and followed by experimental test.

According to Fig. 3- 3, two control loops are used in the FOC control and they are the inner current loop and the outer speed loop. The first two subsections will introduce the controller designs of these two different control loops, and then the FOC of PMSM will be evaluated through simulations and experiments, respectively.

3.2.1. Controller design for current loop

The current loop can be presented by a block diagram shown in Fig. 3- 5 which consists of PI controller, inverter transfer function and motor electrical transfer function. In this section, the transfer function of each part of the current loop is extracted then corresponded PI controller is designed.

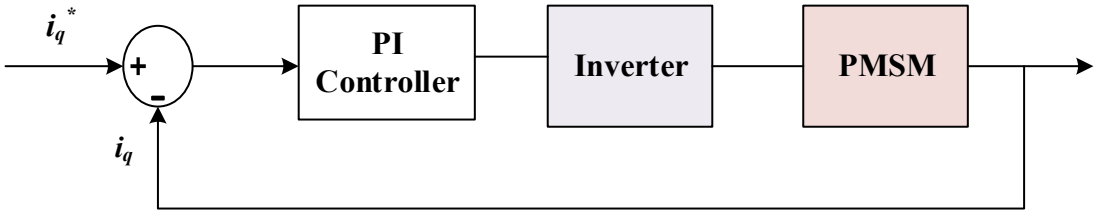

Fig. 3- 5. The simplified block diagram of the PI controller for *q* axis current.

By rewriting the equation (2-10) and (2-11) the following is obtained:

$$\frac{dI_d}{dt} = -\frac{R_s}{L_d} I_d + \frac{L_q}{L_d} \omega_r I_q + \frac{u_d}{L_d} \tag{3-1}$$

$$\frac{dI_q}{dt} = -\frac{R_s}{L_q} I_q - \frac{1}{L_q} \omega_r (L_d I_d + \Psi_{PM}) + \frac{u_q}{L_q} \tag{3-2}$$

By applying the Laplace transformation, into (3-1) and (3-2) the following can be written:

$$u_d = R_s I_d - L_q \omega_r I_q + I_d L_d s \tag{3-3}$$

$$u_q = R_s I_q + \omega_r (L_d I_d + \Psi_{PM}) + I_q L_q s \tag{3-4}$$

$$\frac{I_d}{u_d} = \frac{1}{L_d s + R_s} \tag{3-5}$$

$$\frac{I_q}{u_q} = \frac{1}{L_q s + R_s} \tag{3-6}$$

Thus, the transfer function of the current loop for *d* axis and *q* axis is given in (3-5) and (3-6). The cross coupling terms for *d* axis and *q* axis are $-L_q \omega_r I_q$ and $\omega_r (L_d I_d + \Psi_{PM})$ respectively which will be added to the output of the *q* axis and *d* axis controller.

$$G(s)_{PI} = K_p + \frac{K_i}{s} = K_p \frac{T_i + 1}{T_i s} \tag{3-7}$$

The transfer function of the PI controller is given as (3-7) where K_p and K_i are proportional and integral gains and T_i is the time constant of the controller.

$$G(s)_{inv} = \frac{V_{dc}/2}{1 + \frac{1}{2f_{sw} + T_s} s} \tag{3-8}$$

The inverter transfer function is modeled as a first order transfer function (3-8). In which f_{sw} is inverter switching frequency, T_s is controller delay and V_{dc} is the DC-bus voltage. Thus, the current loop transfer function can be written as the following:

$$G(s)_{current\ loop} = G(s)_{motor} G(s)_{PI} G(s)_{inv} \tag{3-9}$$

The PI controller in equation (3-9) is used to control the *d* axis and *q* axis current. The controller is designed using the zero-pole cancelation method, in which the zero in the PI controller is used to cancel the pole in motor transfer function. The current controller bandwidth can be made to be 1/10 inverter switching frequency. The current loop Bode plot is given in Fig. 3- 6.

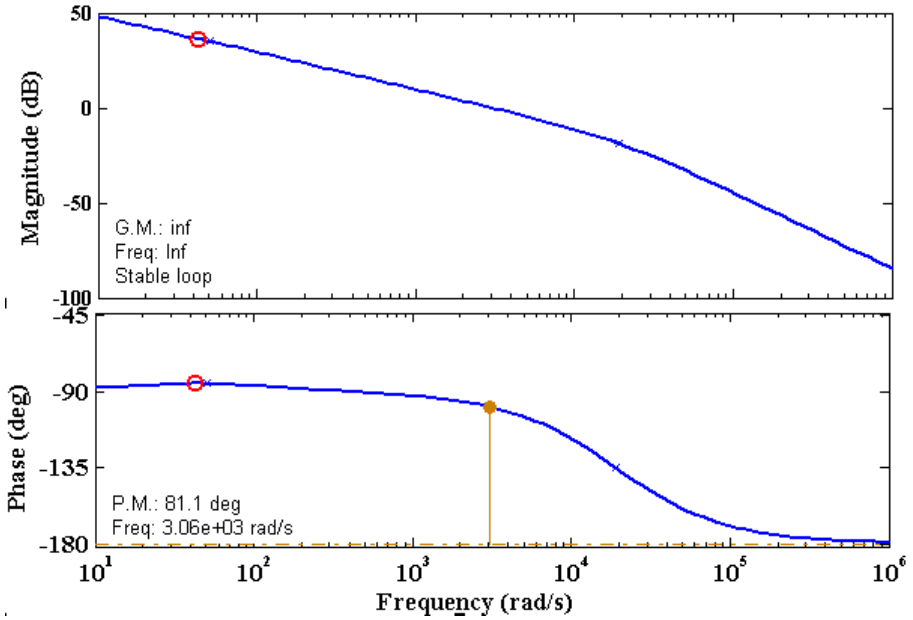

Fig. 3- 6. Bode plot of current loop controller

3.2.2. Controller design for speed loop

The controller design for the speed loop can be represented by the following block diagram which consists of the PI regulator for controlling the speed of the machine, the current loop gain or the inner loop gain and the transfer function of the PMSM. In this section, the transfer function for each part will be extracted and the corresponding PI controller will be designed. The block diagram speed loop controller is shown in Fig. 3- 7.

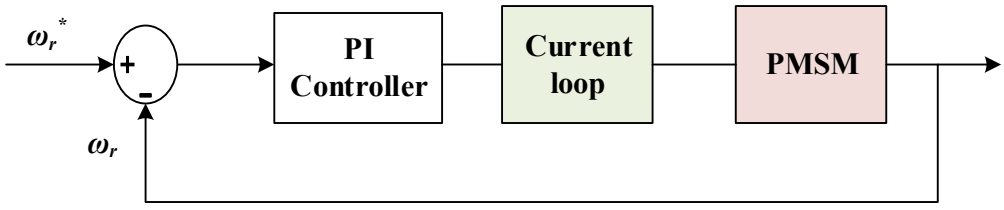

Fig. 3- 7. Block diagram of the PI controller for speed loop.

The mechanical equation for PMSM is presented in (2-14). By considering the no load condition, the load torque is zero (T_L=0) and considering d axis current is zero (I_d=0) and .Then, the following expression can be written:

$$J\frac{d}{dt}\omega_r = \frac{3}{2}P\Psi_{PM}I_q - B\omega_r \tag{3-10}$$

By applying the Laplace transfer function, the following equation is obtained:

$$(Js + B)\omega_r = \frac{3}{2} P\Psi_{PM} I_q \tag{3-11}$$

The equation above can be converted into speed loop transfer function:

$$\frac{\omega_r}{I_q} = \frac{\frac{3}{2} P\Psi_{PM}}{Js + B} \tag{3-12}$$

The simplified current loop transfer function is given below in which T_i is system time constant which can be calculated based on the system bandwidth (ω_i):

$$G(s)_{Currentloop} = \frac{1}{1 + T_i s} \tag{3-13}$$

$$T_i = \frac{1}{\omega_i} \tag{3-14}$$

The open loop transfer function for the speed loop can be driven as follow:

$$G(s)_{Speed} = G(s)_{motor} G(s)_{Currentloop} G(s)_{PI} \tag{3-15}$$

The Fig. 3- 8 presents Bod plot of speed controller loop for FOC of PMSM.

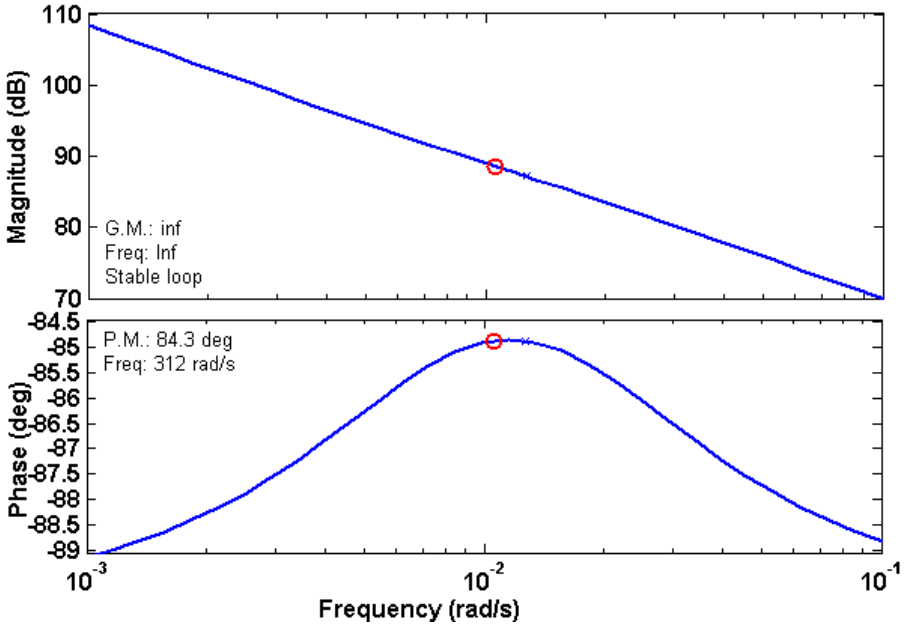

Fig. 3- 8. Bode plot of speed loop controller for FOC of PMSM.

3.2.3. Simulation model of FOC for PMSM

The simulation model of the FOC of PMSM is built in MATLAB/Simulink. Fig. 3- 9 shows the simulation block of FOC of PMSM. The simulation model is includes PMSM, inverter block, PI controller block and transformation block. The PMSM speed is controlled through the PI speed controller. The output of speed controller is the input for the PI controller of *q* axis current. The outputs of the PI current controllers go through the inverse of Park transformation so as the *abc* frame reference voltages are obtained, which are then fed to the PWM block. The space vector pulse width modulation (SVPWM) technique is employed for generating the gate signals for the inverter so as to drive the PMSM.

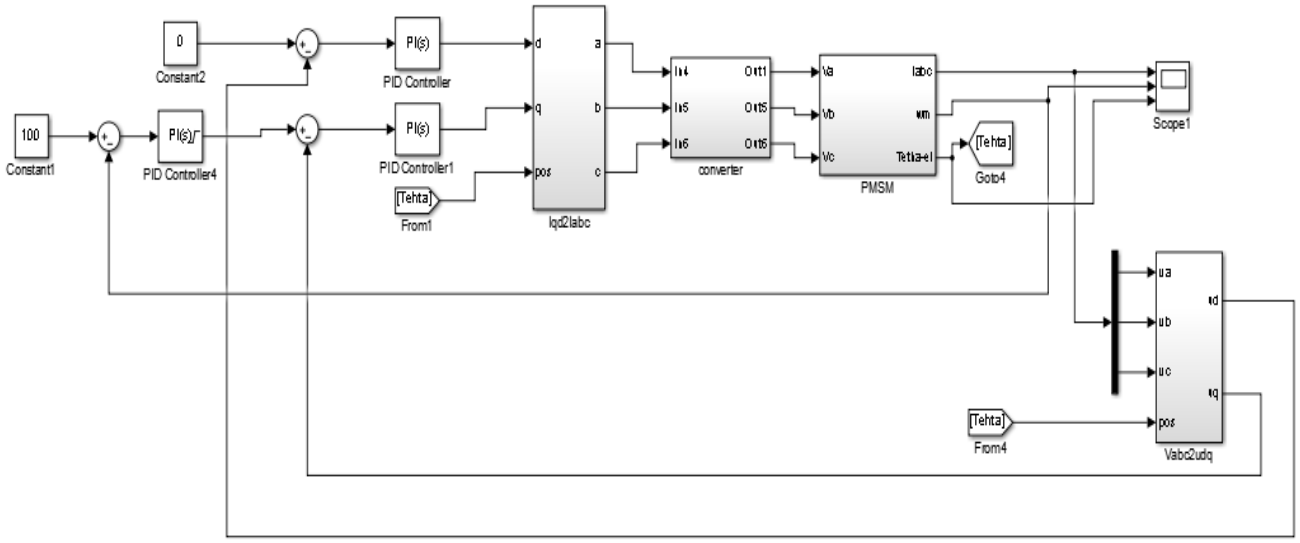

Fig. 3- 9. Simulation model of FOC for PMSM in MATLAB.

3.2.4. Experimental result of FOC for PMSM

In this section, the experimental test is conducted to verify the simulation model. Fig. 3- 10. presents the experimental setup which is used for verifying different control strategies for PMSM.

The SPMSM drive experimental setup is shown in Fig. 3- 10. The experimental setup consists of the driving inverter, which is a standard two-level voltage source inverter composed of IGBT modules, the switching frequency of the driving inverter is 5 kHz .The SPMSM is coupled to a 15-hp DC dynamometer. To measure the shaft torque of SPMSM torque transducer is employed. The control of SPMSM is programmed on dSPACE which is

also shown in Fig. 3- 10. A 12-bit absolute encoder is used to measure the speed and position of the machine. The experimental result is recorded in Yokogawa SL1000 data acquisition system. The sensor board is designed to measure the motor three phase current as well as the inverter DC-bus voltage.

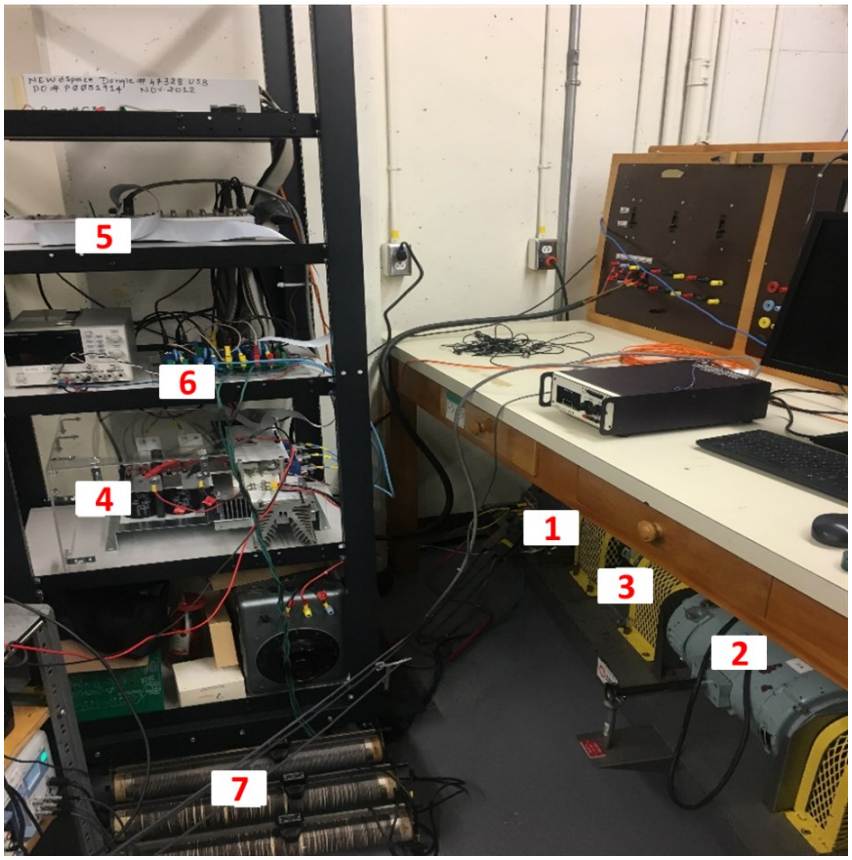

Fig. 3- 10 (1) Surface mounted PMSM, (2) DC dynamometer, (3) Torque transducer, (4) Driving inverter for the PMSM, (5) dSPACE real time simulator, (6) Sensor board, (7) Resistive load.

The test is conducted in different dynamic conditions namely speed reversal change and step change. Fig. 3- 11 presents the result for speed reversal test while the speed is changing from 50 to -50 rad/sec. It can be observed that the magnitude of current is still the same and the controller can work in both directions.

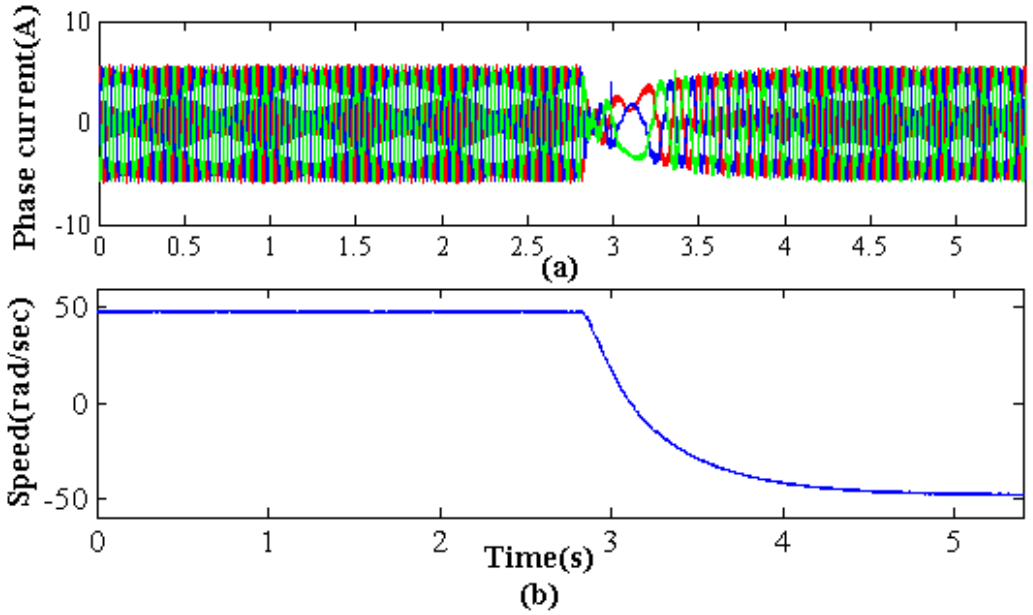

Fig. 3- 11. Experimental results for speed reversal test under FOC of PMSM (a) Three phase current (b) Speed

Fig. 3- 12. presents the machine startup. The reference speed is changing from 0 to 50 rad/sec. This Figure shows machine speed as well as machine three phase currents.

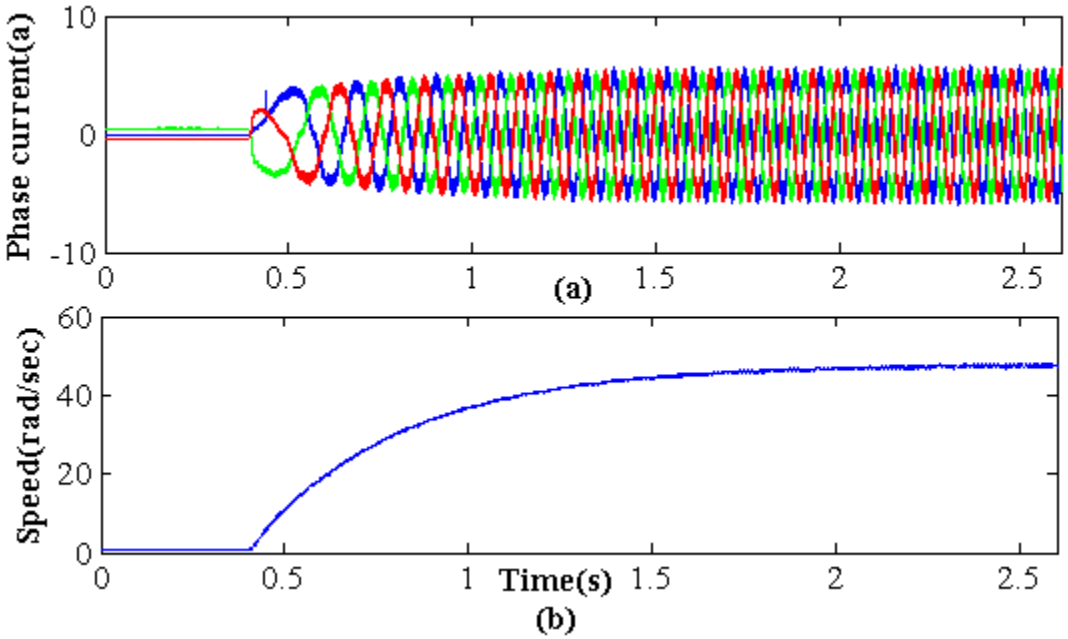

Fig. 3- 12. Experimental results of machine startup for FOC of PMSM (a) Three phase current (b) Speed

3.3. Investigations on conventional DTC of PMSMs through simulations

In this section, a principal of conventional DTC control strategy for PMSM drive will be presented. Then, the simulation test is conducted to validate this control method. Then the problem associated with digitally implementation of this control topology will be discussed in this section.

3.3.1. Principal of conventional DTC

In the introduction the three most important control strategies for PMSM are introduced and compared. In this section, the detailed principal of the DTC is presented. Generally, the three phase PMSM is fed by a two-level voltage source converter (VSC) as in Fig. 3- 13. The voltage source converter makes it possible to connect each of the three phase motor windings to the positive and negative DC-bus voltages. Each leg of the inverter can be represented as an ideal switch, theses switches are called S_a, S_b and S_c. There are eight possible positions of the switches in the inverter. These states correspond to the voltage vectors. Six of them are non-zero or active voltage vectors, and the rest are zero voltage vectors. The stator voltage space vector can be represented by using the switching states and the DC-bus voltage V_{dc} as the following:

$$v_s(S_a, S_b, S_c) = \frac{2}{3} V_{dc}(S_a + S_b e^{j(\frac{2\pi}{3})} + S_c e^{-j(\frac{2\pi}{3})} \quad (3\text{-}16)$$

where the coefficient $\frac{2}{3}$ comes from the Park transformation and v_s is the primary voltage.

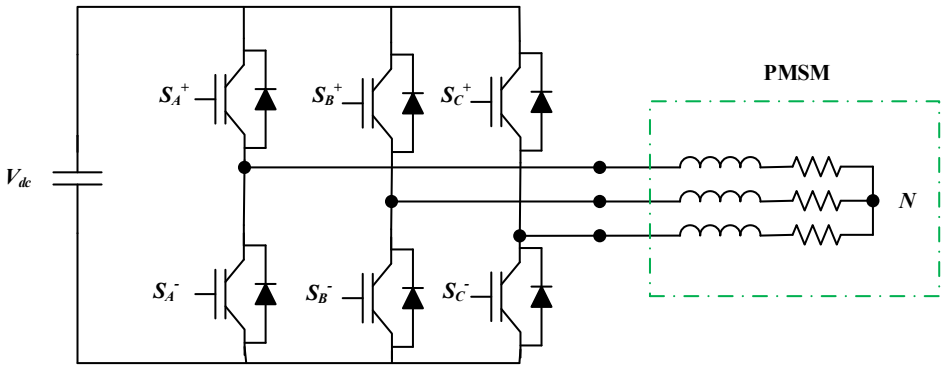

Fig. 3- 13. A voltage source inverter-fed PMSM drive system.

The output voltage vectors are shown in Fig. 3- 14.

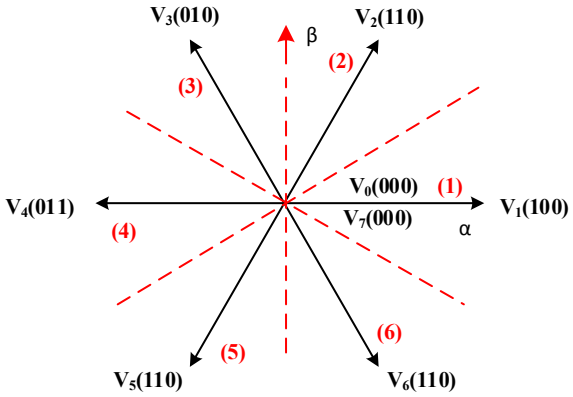

Fig. 3- 14. Voltage vectors and sectors for the two-level VSC.

To control the stator flux, the suitable selection of voltage vectors are required in order to achieve circular stator flux trajectory. Flux linkage vector is in the $\alpha\beta$ stationary reference frame, the voltage sector can be selected based on the location of the stator flux linkage vector. The stator flux estimation is used to select the sector. The equation below shows the exact angular position of the flux vector to determining the motor operating sector.

$$\theta = tan^{-1}\frac{\psi_\alpha}{\psi_\beta} \tag{3-17}$$

In which θ is the angle of stator flux and ψ_α, ψ_β are α axis and β axis flux linkage respectively.

In DTC, accurate flux estimation is required to achieve high drive performance. Mainly three different modeling techniques are used for flux estimation namely voltage modeling, current modeling and combination of these two methods. The flux estimation based on the current method is required the stator current and it will be applied in low frequency. And it depends on the machine inductance which makes the estimation more complicated. Thus, in this study the flux and torque are estimated based on the voltage model. The stator flux vectors in α and β axis are given by:

$$\psi_{s\alpha} = \int (V_{s\alpha} - R_s i_{s\alpha})dt \tag{3-18}$$

$$\psi_{s\beta} = \int (V_{s\beta} - R_s i_{s\beta})dt \tag{3-19}$$

where $\psi_{s\alpha}$ and $\psi_{s\beta}$ are estimated flux for α and β axes respectively. The magnitude of $\psi_{s\alpha}$ and $\psi_{s\beta}$ is considered as the estimated flux (ψ_{es}).

The electromagnetic torque is estimated by the following expression which depends on the flux estimation.

$$T_{es} = \frac{2}{3} P(\psi_{s\alpha} i_{s\beta} - \psi_{s\beta} i_{s\beta}) \tag{3-20}$$

where T_{es} is estimated electromagnetic torque.

To determine the correct control commend on the flux and torque hysteresis comparators are used. The reference stator flux and reference torque are ψ_s^* and T_s^*. The reference values are compared with the estimated or measured values. The Hysteresis controllers evaluate the difference between requested values and estimated values and the estimated flux and torque should be constrained within the Hysteresis band by applying the appropriate voltage vectors. In the conventional DTC of PMSM the digitized output of flux and torque Hysteresis band are as follows:

$$\Psi = \begin{cases} d\psi = -1, & |\psi_s^*| - |\psi_s| < 0 \\ d\psi = 1, & |\psi_s^*| - |\psi_s| > 0 \end{cases} \tag{3-21}$$

$$T_e = \begin{cases} dT_e = 1, & |T_e^*| - |T_e| > 0 \\ dT_e = 0, & |T_e^*| = |T_e| \\ dT_e = -1, & |T_e^*| - |T_e| < 0 \end{cases} \tag{3-22}$$

where ψ_s^* is the stator flux linkage reference, $d\Psi$ is the output of the stator flux linkage regulator, T_e^* is the electromagnetic torque reference and dT_e is the output of the electromagnetic torque regulator. If $d\psi$ =1, it means the stator flux linkage needs to be increased, then according to the sector, appropriate voltage space vector is selected. Else, the stator flux linkage needs to be decreased. If dT_e=1, it means the reference torque is bigger than the actual electromagnetic torque then according to the sector an appropriate voltage vector is applied.

The switching table for the conventional controller based DTC system can be constructed, as Table. 3- 1. Each time, one of the voltage vectors is selected from the switching table based on the sector number and the outputs of the torque and flux Hysteresis comparators.

Table. 3- 1 Switching table in the conventional DTC

$d\psi$	dT_e	S1	S2	S3	S4	S5	S6
1	1	V_2(110)	V_3(010)	V_4(011)	V_5(001)	V_6(101)	V_1(100)
	0	V_7(111)	V_0(000)	V_7(111)	V_0(000)	V_7(111)	V_0(000)

	-1	$V_6(101)$	$V_1(100)$	$V_2(110)$	$V_3(010)$	$V_4(011)$	$V_5(001)$
-1	1	$V_3(010)$	$V_4(011)$	$V_5(001)$	$V_6(101)$	$V_1(100)$	$V_2(110)$
	0	$V_7(111)$	$V_0(000)$	$V_7(111)$	$V_0(000)$	$V_7(111)$	$V_0(000)$
	-1	$V_5(001)$	$V_6(101)$	$V_1(100)$	$V_2(110)$	$V_3(010)$	$V_4(011)$

3.3.2. Simulation model of conventional DTC for PMSM

The conventional DTC of the PMSM is simulated in MATLAB/Simulink. The stator flux linkage references is set as 0.58 V.sec. The bandwidth of the Hysteresis controller for the flux linkage and torque are adjusted as 0.58 V.sec and 0.1 Nm respectively. The model sampling frequency is 20 µs. The SPMSM parameters during this simulation are listed in the Table. 2- 2. The Fig. 3- 15 illustrates the simulation model of conventional DTC for PMSM.

Fig. 3- 16 shows the simulation result of torque, flux linkage, speed and three phase current for conventional DTC. The references for the torque and flux linkage are set to be 10 Nm and 0.58 V.sec respectively and the sampling frequency is 20 µs.

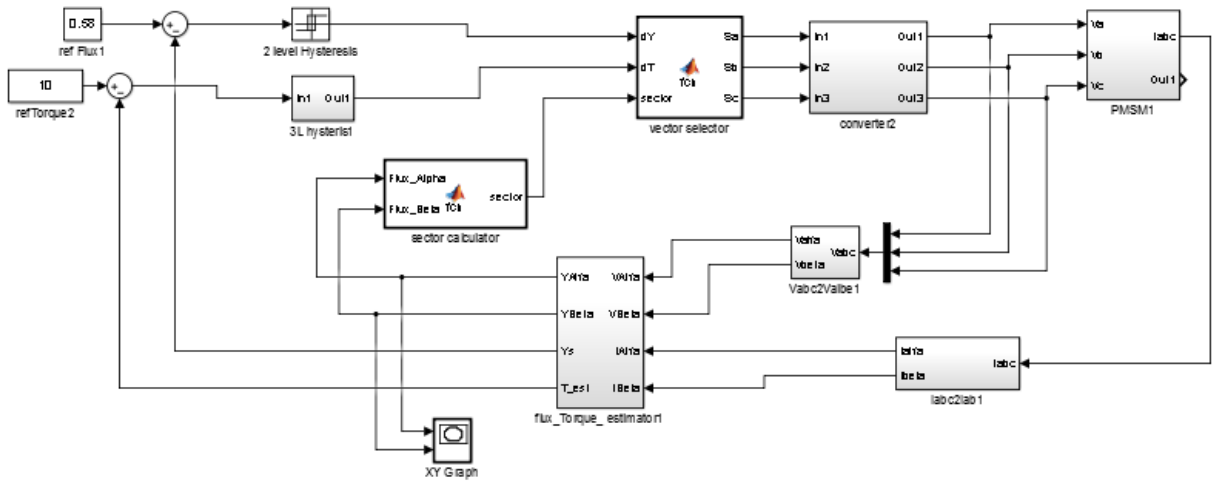

Fig. 3- 15. Simulation model of conventional DTC for PMSM in MATLAB/Simulink

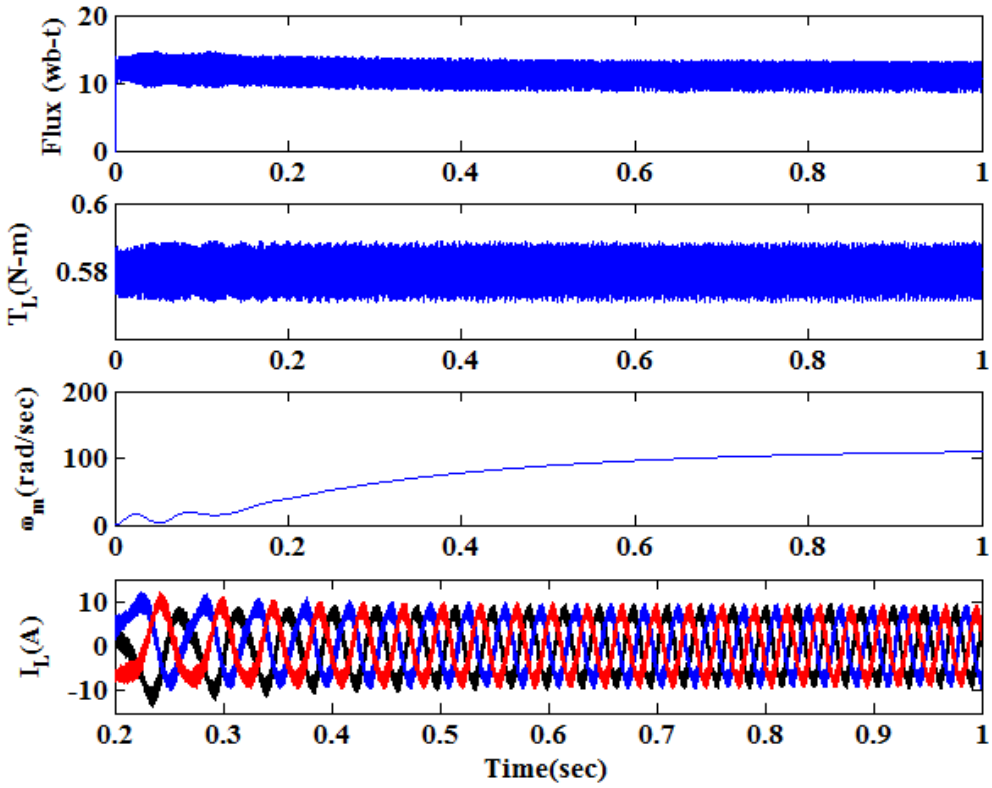

Fig. 3- 16. Simulation results of torque, flux, linkage, currents and speed for the conventional DTC for PMSM.

3.3.3. Digitally implementation of conventional DTC

In conventional DTC, two Hysteresis controllers are used in order to control the stator flux linkage and electromagnetic torque. The performance of the controller is depending on the bandwidth of these controllers. The smaller is the bandwidth leads to the less distortion and torque ripple. Also, it required a higher switching frequency. By implementing the conventional DTC on analog system, it is usually required the switching frequency varied in order to exact control of the estimated torque on the hysteresis band $\pm B_w$ around the reference torque T_e^* as shown in Fig. 3- 17. However, when DTC is implemented in the digital system such as FPGA, DSP or dSPACE [33],the Hysteresis band as well as the sampling time affects the system performance. It can be seen from the Fig. 3- 17(b) that a high sampling frequency is required so control of the estimated torque on the hysteresis band $\pm B_w$ around the reference torque T_e^* as shown in Fig. 3- 17. However, when DTC is implemented in the digital system such as FPGA, DSP or dSPACE [33],the Hysteresis band as well as the sampling time affects the system control

of the estimated torque on the hysteresis band $\pm B_w$ around the reference torque T_e^* as shown in Fig. 3- 17.

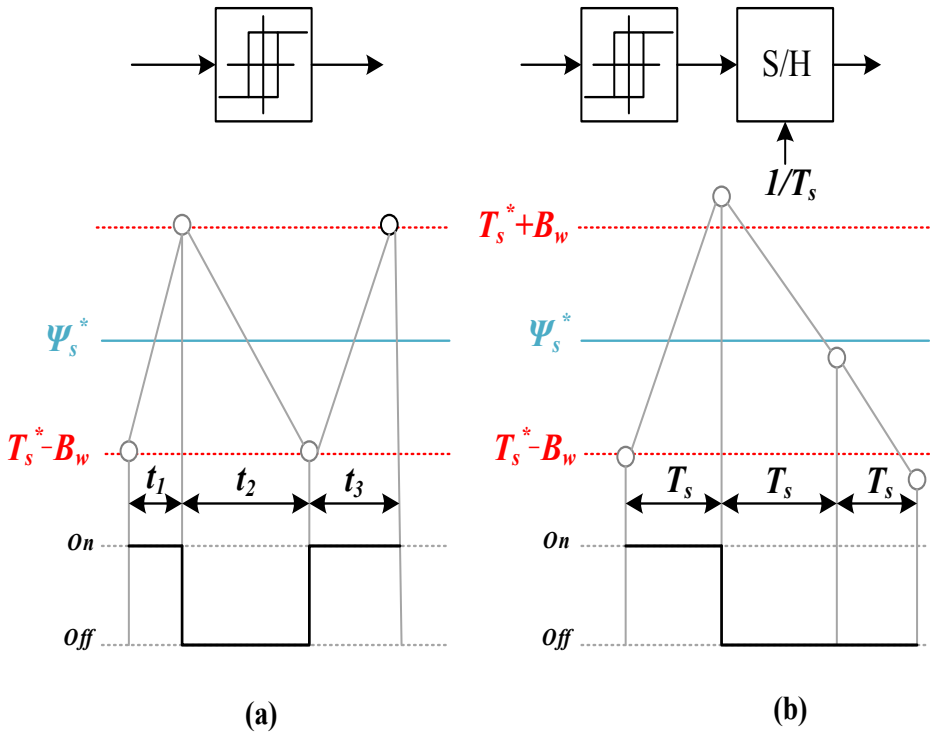

Fig. 3- 17. Comparison of the switching modes of the Hysteresis torque controller in (a) An analog DTC system and (b) A digital DTC system and the resulting torque ripples.

However, when DTC is implemented in the digital system such as FPGA, DSP or dSPACE [33],the Hysteresis band as well as the sampling time affects the system performance. It can be seen from the Fig. 3- 17(b) that a high sampling frequency is required so as the digital system achieve a same performance as an analog system. In addition, because of the lagging nature of the Hysteresis controller, the discrete-time DTC system may not able to perform in timely manner to correct torque and stator flux errors which causes additional torque and stator flux ripples which are larger than the Hysteresis bands (Fig. 3- 17(b)). Thus, higher sampling frequency is required for better performance of the conventional DTC. However, applying a higher sampling frequency is limited by digital controller and the controller with high sampling frequency is required for implementation of conventional DTC in digital controller. Also, an inverter with high switching frequency is needed to achieve a high performance of conventional DTC. Therefore the implementation of conventional DTC in digital controller is challenging. And this study will only present the result of conventional DTC in simulation.

3.4. Investigation on DTC-PI of PMSM through simulations and experiments

In this section the principal of DTC-PI is described. The simulation results followed by experimental results are presented to validate this PMSM control strategy.

3.4.1. DTC-PI principal

Direct flux and torque control with PI controller (DTC-PI) schemes is proposed in order to improve the conventional DTC. The DTC-PI strategies operate at a constant switching frequency. Fig. 3- 18 shows schematic diagram of the PI based DTC for a PMSM.

In the DTC-PI, motor torque and flux are controlled by the torque and flux regulator, which includes a PI controller. Usually, the PI gains are tuned by a trial and error procedure. The output torque and stator flux linkage are estimated based on the analysis in section (3.3.1) to calculate the desired stator flux and electromagnetic torque. Then, a proper voltage vector can be generated by the SVPWM module to achieve fast, accurate torque and flux linkage control.

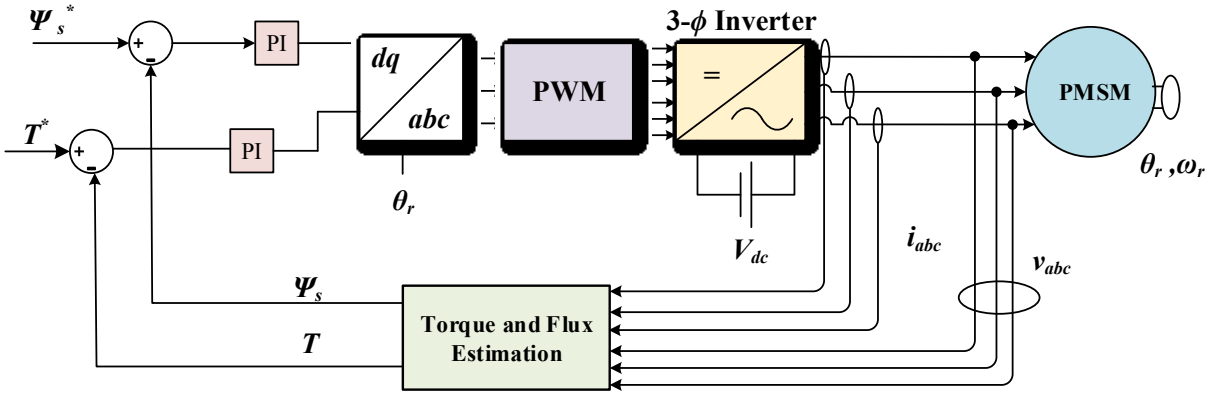

Fig. 3- 18. Block diagram of the DTC-PI for PMSM.

3.4.2. Simulation model of DTC-PI for PMSM

The DTC-PI of the PMSM is modeled in MATLAB/Simulink as illustrated in Fig. 3-19.The simulation model consists of PI regulator block, torque and flux references, torque and flux estimation block, SVPWM block, inverter block and PMSM. Through the PI torque controller block the required voltages are obtained.

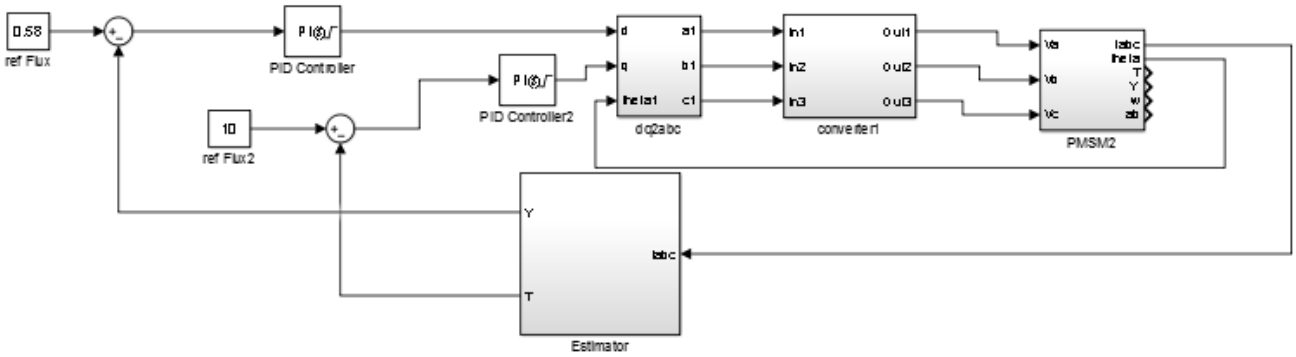

Fig. 3- 19. Simulation model of DTC-PI in MATLAB/Simulink.

Fig. 3- 20 shows the simulation result of torque, flux linkage and three-phase currents for conventional DTC. The sampling frequency is 20 µs. The results are obtained from machine start up test while the torque and flux linkage are changing from 0 to 10 Nm and 0.58 V.sec, respectively.

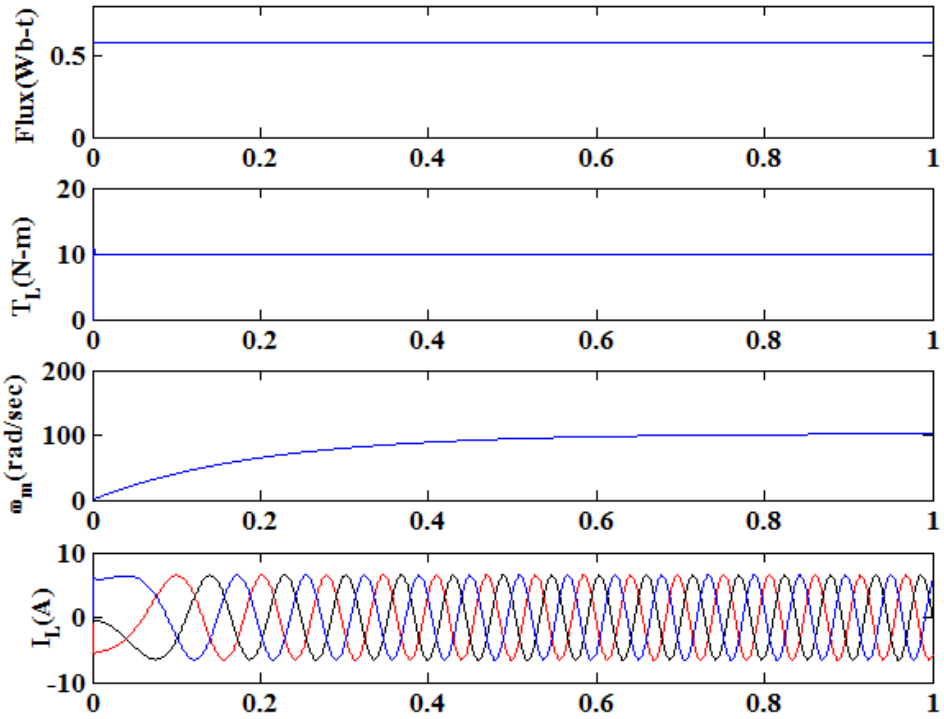

Fig. 3- 20. Simulation results of torque, flux, linkage, speed and three phase current for the DTC-PI in PMSM.

3.4.3. Experimental result of DTC-PI for PMSM

To validate the simulation results for DTC-PI for PMSM, the DTC-PI is tested on a VSI-fed laboratory SPMSM drive system. The switching frequency of the driving inverter is 5 kHz. Fig. 3- 21 presents the results obtained from machine startup in which the torque is changed from 0 to 10 Nm.

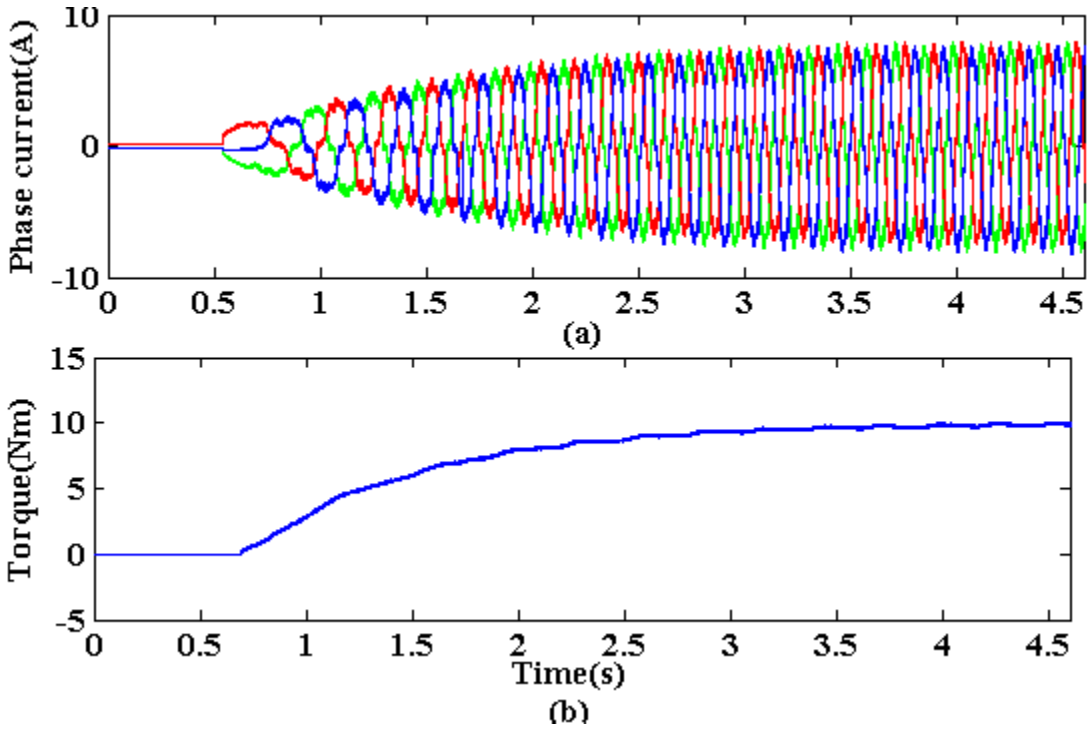

Fig. 3- 21. Experimental results of machine startup with DTC-PI (a) Three-phase current (b) torque

3.5. Comparison between Scaler control, FOC and DTC for PMSMs

Table. 3- 2 summarizes and compares the three control schemes for PMSMs from the aspect of the controllers' features, control variables, dynamic performance and implementation complexity [34].

Table. 3- 2 comparison between Scaler control, FOC and DTC schemes for PMSMs

Comparison property	Scaler control	FOC	DTC
Dynamic response	Slow	Fast	Very fast
Controlled variables	Voltage, frequency	Stator currents	Torque, stator flux

Switching frequency	Constant	Constant	Variable
Torque control	No	Indirect	Direct
Flux control	No	Indirect	Direct
Current control	No	Direct	Indirect
Rotor position requirement	No	Yes	No
Coordinate transformation	No	Synchronous *dq*	Stationary *αβ*
Control tuning	No	PI	Hysteresis bands
Cost	Very cheap	Expensive	Cheap

Based on the table above, both the FOC and DTC can achieve good control performance for PMSMs. However, based on the comparative simulation and experimental studies conducted, DTC requires high bandwidth torque transducer to measure the electromagnetic torque of the machine accurately. Otherwise, estimation/observer-based approaches have to be developed for precise torque estimation/prediction, but it is beyond the scope of this work. The experimental setup which is used in this study has a torque transducer of 4 Hz bandwidth, so it is not suitable for DTC development. Therefore, FOC is selected to be used for the control of PMSM with LC filter and it will be used for the investigations of LC filter unbalance in Chapter 4.

3.6. Control of the PMSM considering LC filter

In this section the control structure for the PMSM with LC filter is presented. And a detailed controller design for the PMSM along with LC filter is described. Finally, to validate the control structure for PMSM with balance LC filter the simulation and experimental tests are conducted.

3.6.1. Control structure

Different approaches are proposed to design a current loop controller for motor drive with LC filter. These methods mainly implemented by using cascaded controller which is required additional sensors [35]. However, in this study, for the low cost implementation of controller of the machine drive with an LC filter, the conventional controller method which is consist of one PI controller is used for the *dq* axis current control. Fig. 3- 22 shows the control structure of the PMSM with LC filter which consists of the two PI controllers for controlling the

d axis and *q* axis current. A desire voltage for the inverter is generated by SVPWM method and the LC filter is located between the inverter output and motor input. This section will introduce the control design for PMSM with balance LC filter.

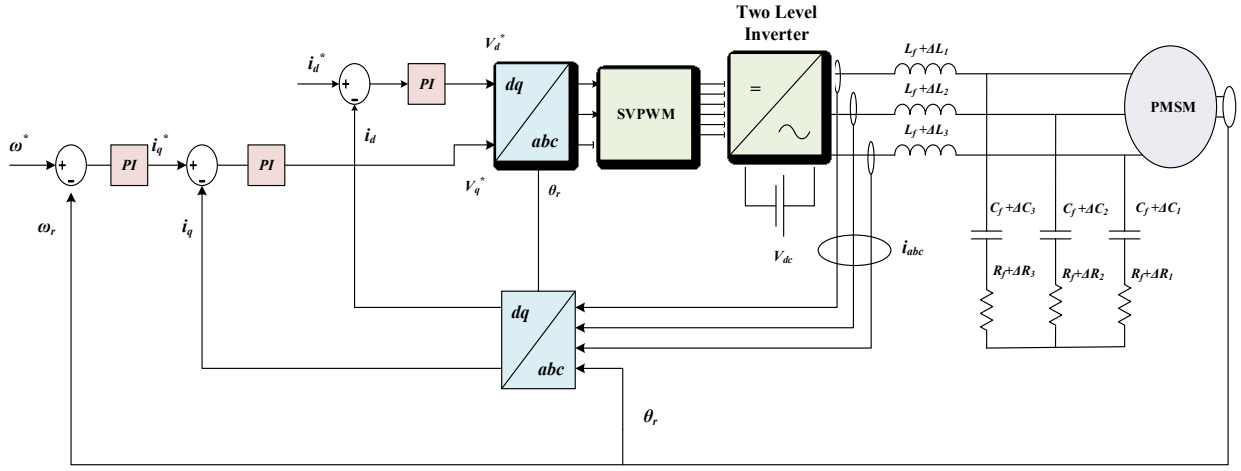

Fig. 3- 22. Schematic of the field oriented based motor drive for PMSM with LC filter.

To design a PI controller for the PMSM with LC filter, it is required to design a controller for the inner loop (current loop). Fig. 3- 23 illustrates the block diagram of current loop for PMSM with LC filter. Thus, it is required to extract a transfer function of the PMSM with LC filter, and an inverter transfer function as well as PI controller transfer function.

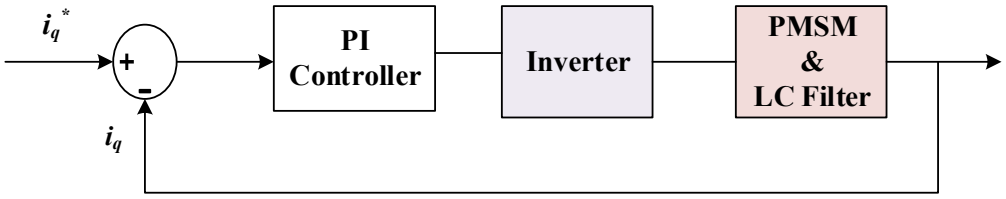

Fig. 3- 23. Block diagram of the current loop scheme for PMSM with LC filter.

In order to design a PI controller for the current loop the transfer function which is associated with PMSM with LC filter can be driven in (2-26). Also, the first order transfer function is approximated for the drive inverter with the gain corresponding to half of the DC-bus voltage ($V_{dc}/2$=150 V) and a time constant corresponding to the sum of PWM sampling time and the controller computation time (sampling time) which is 120 μs (T_f) and a standard PI controller is

used for the compensation. The open loop transfer function of the current loop can be represented as follows:

$$G(s)_{system} = G(s)_{PI}G(s)_{inv}G(s)_{LC\&PMSM} \tag{3-23}$$

$$G(s)_{system} = (K_p + \frac{K_i}{s})(\frac{V_{dc}/2}{1 + \frac{1}{2f_{sw} + T_s}s})\,(G(s)_{LC\&PMSM}) \tag{3-24}$$

The PI controller is designed using the zero-pole cancelation method. The Bode plot of the open loop transfer functions of the current loop is shown in Fig. 3- 24. This figure presents the maximum achievable bandwidth which is limited by the resonant pole.

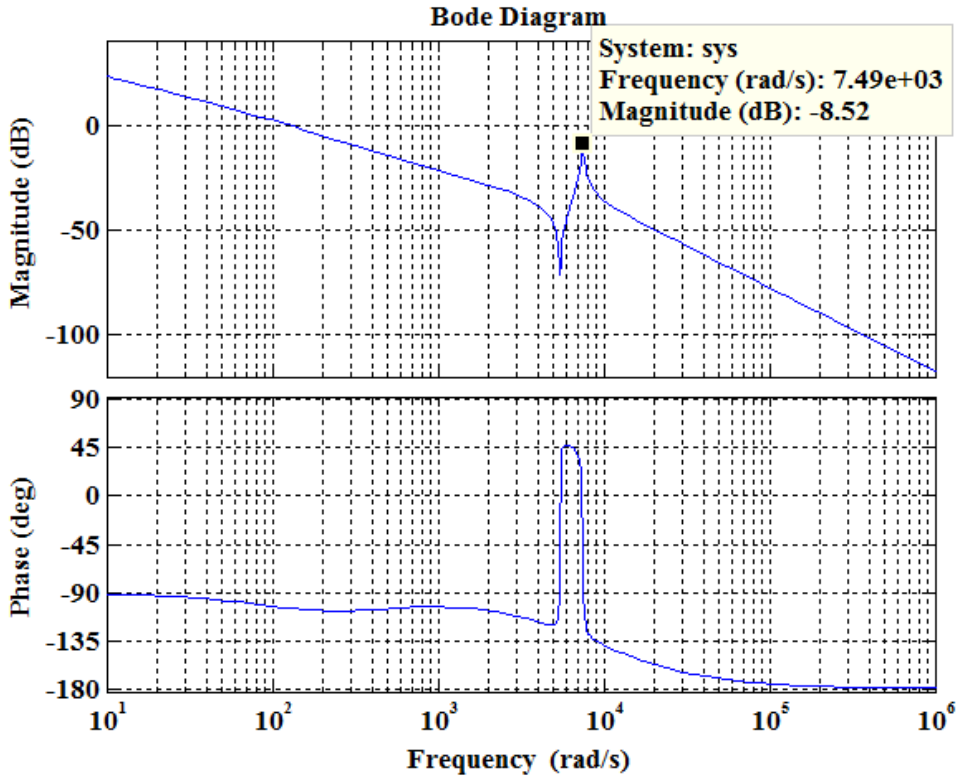

Fig. 3- 24. Open loop Bode plot of current loop for PMSM with LC filter

3.6.2. Simulation results for balance LC filter

A SPMSM with LC filter is simulated in MATLAB/Simulink. The sine-triangle PWM method is employed with a carrier frequency of 5 kHz and the DC-bus voltage is set as 300V Fig. 3- 25 shows the MATLAB simulation model for PMSM with balance LC filter. Fig. 3- *26*presents the simulation result of three-phase current, torque, *q* axis current and *d* axis current

for the balance LC filter with PMSM while the references for *d* axis current and *q* axis current have been kept at 0 A and 11 A respectively.

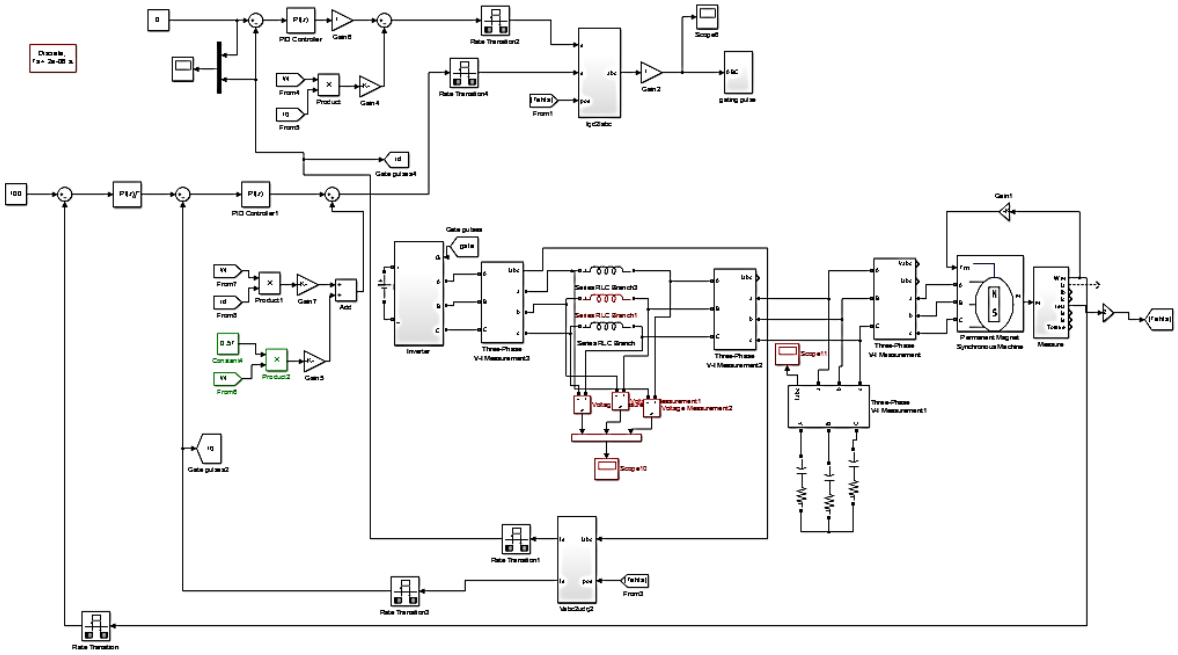

Fig. 3- 25. Simulation model for PMSM drive with balance LC filter.

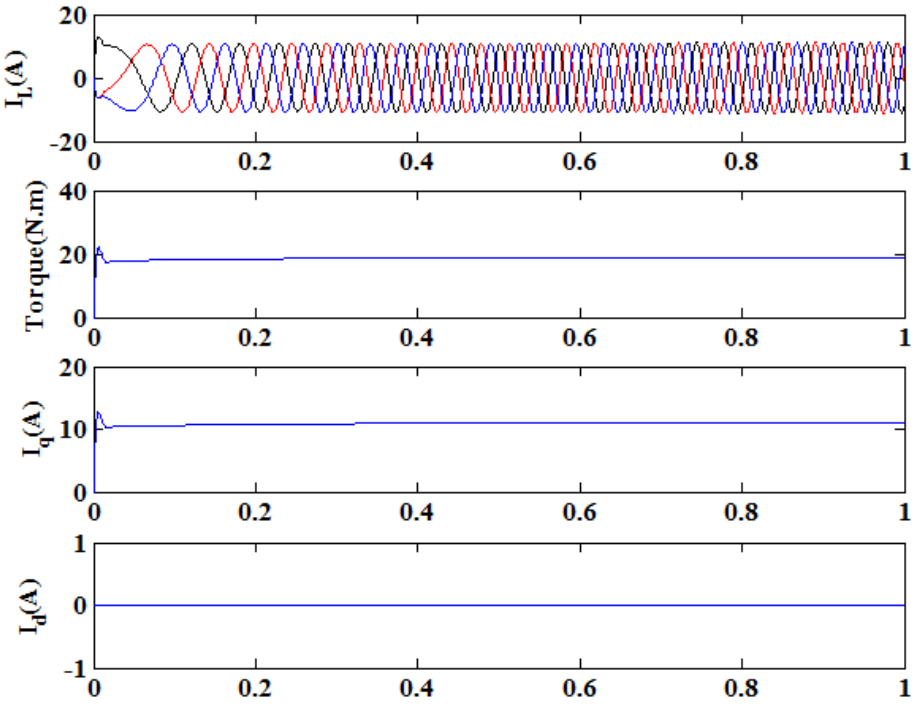

Fig. 3- 26. Simulation result of three phase currents, torque, *q* axis current and *d* axis current respond for balance LC filter with PMSM.

3.6.3. Experimental results of balance LC filter

The simulation model of PMSM with balance LC filter is evaluated on the laboratory SPMSM machine drive system. Fig. 3- 27 presents the result obtained from machine startup while the *q* axis current is changed from 0 to 11 A. Fig. 3- 27 is also presents the experimental results of three-phase current, *d* and *q* axis currents and electromagnetic torque. Fig. 3- 28 presents the result of machine startup test while the speed of the machine is changed from 0 to 50 rad/sec. The three-phase current as well as the torque are shown in this figure as well.

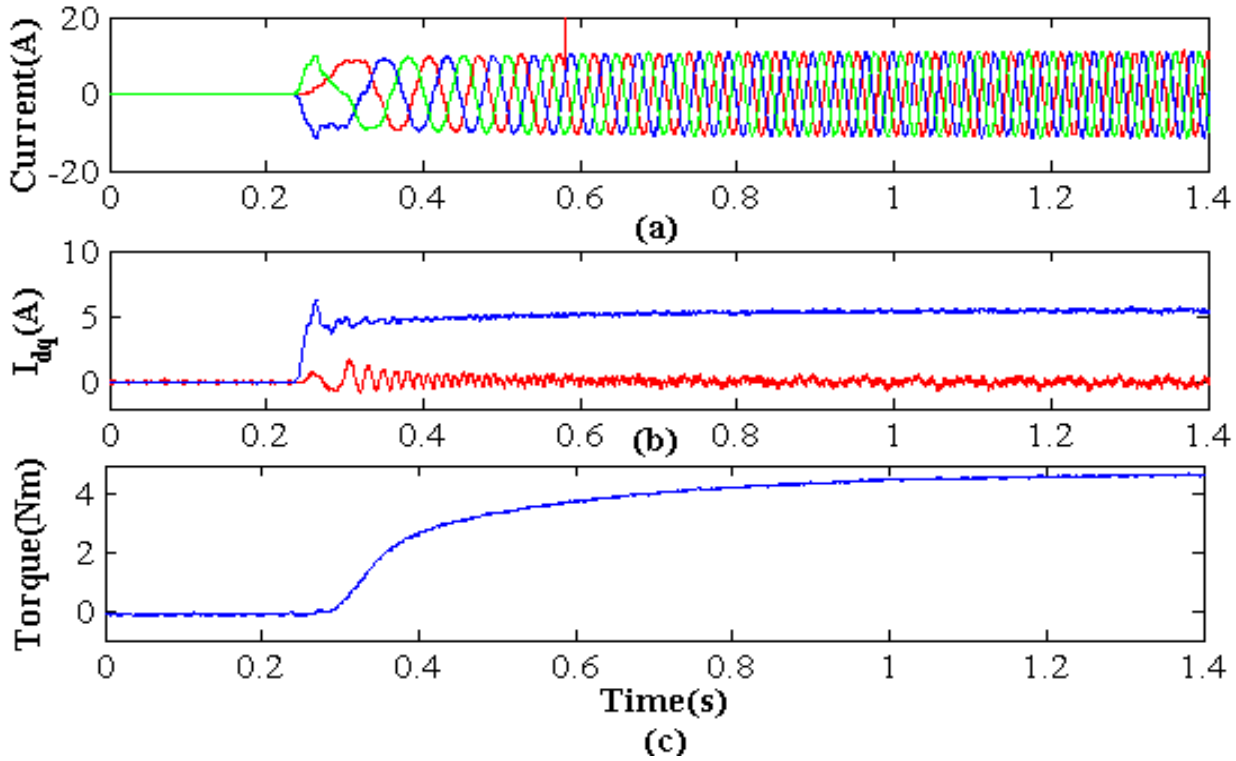

Fig. 3- 27. The experimental results for SPMSM startup with balance LC filter a) Three-phase current b) *dq* axis currents (scale 2A/div) c) Torque (scale 2 Nm/div)

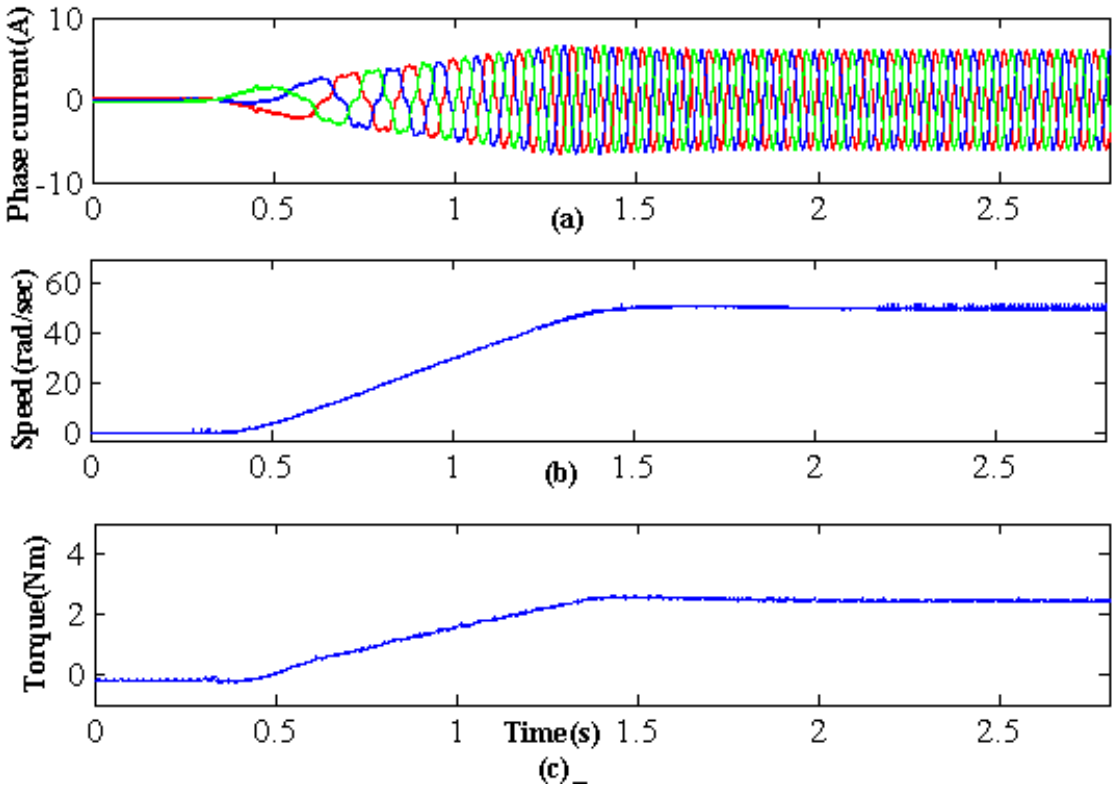

Fig. 3- 28. The experimental results for SPMSM startup with balance LC filter a) Three-phase current b) *dq* axis currents c) Torque (scale 2 Nm/div)

Chapter 4 Modeling and Investigation of the PMSM Drive with Unbalance LC Filter

The motor is supposed to work with balance three-phase currents. However, unbalance currents can arise from different sources such as unbalance load, unbalance voltage supply, unbalance impedance, open phase fault and other faults, etc. The unbalance currents lead to negative sequence current in the motor drive. LC filter unbalance in a PMSM drive also causes negative sequence current inside the motor drive. Therefore, LC filter unbalance can cause the following negative impacts in the motor drive system:

- The presence of negative sequence current produces additional motor losses, which can cause the temperature to rise above the temperature limit and hence reduces motor life.
- Mechanical stresses are increased due to the reverse rotating magnetic field and fluctuating power produced by the negative sequence current. Thus, noise and vibration will be increased. The resulted mechanical vibration can damage the permanent magnet, machine bearings and insulations.
- The unbalance current in the machine reduces the motor efficiency, and hence it increases the input power demand to drive the motor at the same load. This results in an added cost of electricity and maintenance to the users of the motor drive system.

This chapter will present a comprehensive modeling of the PMSM drive system with unbalance LC filter and the investigation results of the LC filter unbalance effects on the motor drive performance.

4.1. Sequence analysis of unbalance LC filter

This section firstly presents the overview of the effect of the negative sequence current on the motor drive, and then presents the comprehensive modelling of positive, negative and zero sequence currents as a result of LC filter unbalance.

4.1.1. Symmetrical components

In a three phase system, phase currents and voltages can be presented in the sets of independent components: positive sequence, negative sequence and zero sequence. Positive sequence components are generated within the system and the direction of the positive sequence is the same as power system voltage and current components. The positive sequence current

exists in the balance operation. The negative sequence current indicates unbalance condition inside the power system. The unbalance exists in voltage and current components. These negative sequence components have the same magnitude as the positive sequence components, but they have opposite rotation direction in the power system. Zero sequence components also exist in unbalance condition. Zero sequence components are equal in magnitude and phase but there is no rotational sequence and it causes a current flow through the neutral of the power system [36]. Fig. 4- 1 illustrates the set of phasors for symmetrical components.

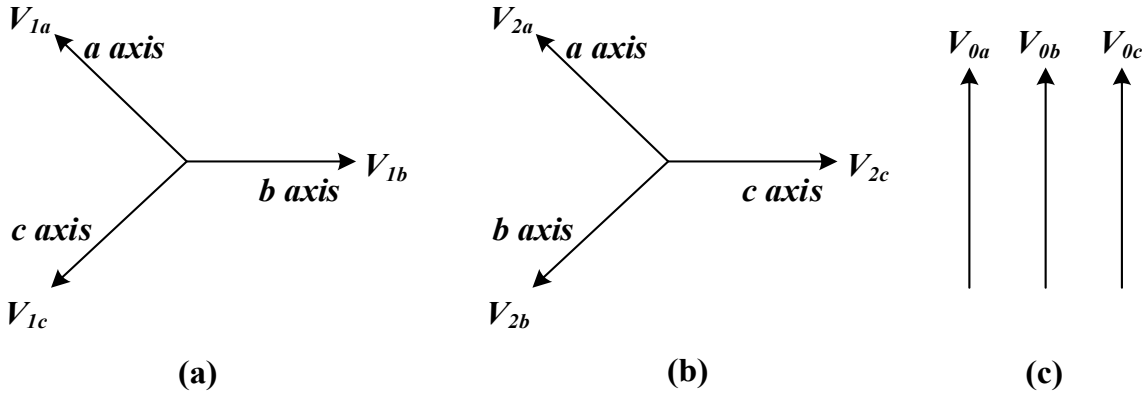

Fig. 4- 1. Symmetrical components (a) Positive sequence components (b) Negative sequence components (c) Zero Sequence components.

In power system all three phase quantities can be presented in symmetrical components. The following equations present the phase voltages in terms of their symmetrical components. Each phase is the sum of positive, negative and zero sequence components:

$$V_a = V_{1a} + V_{2a} + V_{0a} \quad (4\text{-}1)$$

$$V_b = V_{1b} + V_{2b} + V_{0b} \quad (4\text{-}2)$$

$$V_c = V_{1c} + V_{2c} + V_{0c} \quad (4\text{-}3)$$

In which positive sequence components consist of V_{1a}, V_{1b} and V_{1c}, which are three voltage phasors and they are 120 degree apart from each other; V_{2a}, V_{2b} and V_{2c} are negative sequence components, which are also 120 degree apart from each other; the zero sequence components are V_{0a}, V_{0b} and V_{0c}, and there is no phase displacement from each other.

The operator a is used to cause a phasor rotation of 120° in the counterclockwise direction whilst leaving its magnitude unchanged. If twice of a is applied, it will cause a phasor rotation of 240° in the counterclockwise direction:

$$a = e^{j\frac{2\pi}{3}} = -\frac{1}{2} + j\frac{\sqrt{3}}{2} = 1\angle 120° \tag{4-4}$$

$$a^2 = e^{j\frac{4\pi}{3}} = -\frac{1}{2} - j\frac{\sqrt{3}}{2} = 1\angle 240° \tag{4-5}$$

$$a^3 = 1\angle 0° \tag{4-6}$$

From the definition of the sequence components and the definition of operator *a*, the following expression can be written:

$$V_{0a} = V_{0b} = V_{0c} \tag{4-7}$$

$$V_{1b} = a^2 V_{1a}, V_{1c} = aV_{1a} \tag{4-8}$$

$$V_{2b} = aV_{2a}, V_{2c} = a^2 V_{2a} \tag{4-9}$$

The following transformation matrix can be derived, which transfers three voltages into a second set of voltages. The same can be applied to the three phase currents.

$$\begin{bmatrix} V_a \\ V_b \\ V_c \end{bmatrix} = \begin{bmatrix} 1 & 1 & 1 \\ a^2 & a & 1 \\ a & a^2 & 1 \end{bmatrix} \begin{bmatrix} V_1 \\ V_2 \\ V_0 \end{bmatrix} \tag{4-10}$$

The inverse of this transformation is defined as:

$$\begin{bmatrix} V_1 \\ V_2 \\ V_0 \end{bmatrix} = \frac{1}{3} \begin{bmatrix} 1 & a & a^2 \\ 1 & a^2 & a \\ 1 & 1 & 1 \end{bmatrix} \begin{bmatrix} V_a \\ V_b \\ V_c \end{bmatrix} \tag{4-11}$$

To illustrate the model for unbalanced situation in the motor drive by using the symmetrical components, the unbalance voltage due to the unbalance LC filter can be separated into positive sequence voltage, negative sequence voltage and zero sequence voltage. However, zero sequence components usually do not exist in machines because they normally use either delta circuit configuration, so a zero sequence component has no path in the machine. Therefore, unbalanced motor drive system contains only the positive and negative sequence components of the voltage, current, and impedance [37].

4.1.2. Sequence modeling for unbalance LC filter

In the conventional motor drive with LC filter, the inverter voltage is going through the LC filter before it reaches the motor terminals. The following expression between the inverter output voltage and motor current can be written:

$$V_{inv} = Z_{ph} I_{ph} + E_{abc} \tag{4-12}$$

where V_{inv} denotes the inverter output voltage which is equal to $[V_a \quad V_b \quad V_c]^T$, I_{ph} is the three phase current which is equal to $[I_a \quad I_b \quad I_c]^T$, E_{abc} is the PMSM back-EMF which is equal to $[E_a \quad E_b \quad E_c]^T$, and Z_{ph} is the impedance matrix which is consisted of the motor impedances and LC filter impedances. The total impedance can be written using the following matrix:

$$Z_{ph} = \begin{bmatrix} Z_a & Z_m & Z_m \\ Z_m & Z_b & Z_m \\ Z_m & Z_m & Z_c \end{bmatrix} \tag{4-13}$$

where Z_m denotes mutual impedance. It is important to mention, the mutual impedance is considered to be zero as the mutual impedance between each LC filter component is zero and the mutual impedances in the machine is considered to be negligible. Z_a, Z_b, Z_c are the impedances for each phase. In order to model the relationship between the LC filter parameter variations and the amount of unbalance current produced in each phase, the motor current (i_m) should be calculated. Therefore, the single phase equivalent circuit of the motor with LC filter is modeled in Fig. 4- 2 .With such a model, when the LC filter parameter changes, its impact on the negative sequence current, harmonic current and torque in the motor can be determined directly. It is important to mention that the motor parameter variation is not considered in this mathematical model.

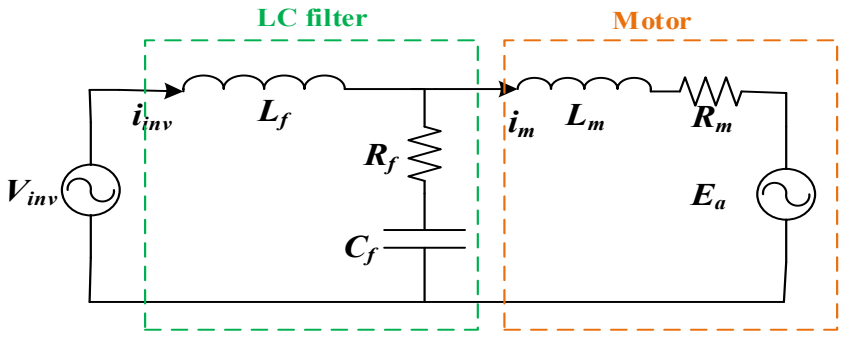

Fig. 4- 2. Single phase equivalent circuit of PMSM with LC filter

To calculate the motor current (i_m) in one phase, the corresponding current (I_{a2}) resulted from the motor back-EMF, and (I_{a1}) resulted from the inverter voltage will be calculated at first. Thereafter, the motor current (i_m) can be calculated as (i_m=I_{a1}-I_{a2}) according to the circuit model. Based on the circuit, current (I_{a2}) is calculated in (4-14) with the inverter voltage equal to zero.

$$\frac{I_{a2}}{E_a} = \frac{L_f C_f S^2 + C_f R_f S + 1}{L_f C_f L_m S^3 + \left(L_f C_f R_f + C_f R_f L_m + R_m L_f C_f\right)S^2 + \left(L_f + L_m + C_f R_f R_m\right)S + R_m} \quad (4\text{-}14)$$

Then, the back-EMF voltage is considered to be zero and the current (I_{a1}) can be expressed as:

$$I_{a1} = \frac{i_{inv}(1/C_f s + R_f)}{1/C_f s + R_f + R_m + L_m s} \quad (4\text{-}15)$$

where the inverter current (i_{inv}) is calculated in (4-16):

$$\frac{i_{inv}}{V_{in}} = \frac{C_f L_m s^2 + R_m C_f s + C_f R_f s + 1}{L_f L_m C_f s^3 + L_f C_f R_m s^2 + L_f C_f R_f s^2 + L_m C_f R_f s^2 + R_f R_m C_f s + L_f s + L_m s + R_m} \quad (4\text{-}16)$$

Therefore, the motor current can be expressed as (4-17):

$$i_m = I_{a1} - I_{a2} \quad (4\text{-}17)$$

With this mathematical model, the motor current can be unbalance due to the unbalance LC filter in different phases. To model the sequence components in a PMSM drive with unbalance LC filter, the symmetrical component transformation is applied so as to calculate the sequence component. Then, by rewriting the symmetrical component transformation (4-11) in the compact form, the following expression can be obtained:

$$v_s = TV_{inv} \quad (4\text{-}18)$$

Where v_s is the vector of sequence voltages, V_{inv} is the vector of three phase inverter voltages and T is transformation matrix:

$$v_s = \begin{bmatrix} V_1 \\ V_2 \\ V_0 \end{bmatrix}, V_{inv} = \begin{bmatrix} V_a \\ V_b \\ V_c \end{bmatrix}, T = \frac{1}{3}\begin{bmatrix} 1 & 1 & 1 \\ a^2 & a & 1 \\ a & a^2 & 1 \end{bmatrix} \quad (4\text{-}19)$$

Then, the inverter voltage vector, phase current vector and back-EMF vector are rewritten in the following form:

$$v_s = TV_{inv},\ I_s = TI_{inv},\ E_s = TE_{abc} \quad (4\text{-}20)$$

where v_s and I_s are the vector of sequence voltage and current vectors respectively. Rewriting (4-20) using the inverse of transformation matrix:

$$V_{inv} = T^{-1}v_s\ ,\ I_{ph} = T^{-1}I_s\ , E_{\ abc} = T^{-1}E_s \quad (4\text{-}21)$$

Based on (4-12) and (4-21), (4-22) can be obtained:

$$T^{-1}v_s = Z_{ph}T^{-1}I_s + T^{-1}E_s \quad (4\text{-}22)$$

The transformation to get the inverter voltage sequence component can be expressed as:

$$v_s = TZ_{ph}T^{-1}I_s + E_s \tag{4-23}$$

By considering $TZ_{ph}T^{-1}$ as L_s, the sequence inductance matrix is defined as:

$$L_s = TZ_{ph}T^{-1} \tag{4-24}$$

The (4-24) emphasizes the fact that the LC filter unbalance can produce the positive, negative and zero sequence components inside the motor. Since zero sequence component does not exist in machines, so it is not considered in this case. Thus, the unbalance LC filter components produce negative sequence current in the motor drive, and hence the resulted impacts from the negative sequence current will investigated in the rest of the chapter.

4.2. LC filter unbalance harmonic modeling

The negative sequence component behaves as an AC oscillation at the frequency of 2ω in the *dq* reference frame. In order to validate the proposed model in previous section, the resulted second harmonic will be modeled in the *dq* reference frame due to LC filter unbalance. Then, the harmonic analysis will be provided to validate the proposed model. In addition, the torque ripple in the motor is one of the major impacts of LC filter unbalance, and hence it will also be investigated in this section.

4.2.1. Current harmonic modeling

The three phase current of machine consist of positive sequence, negative sequence and zero sequence components. So, three-phase machine current can be written in the following format:

$$I_{\boldsymbol{abc}} = I_1 + I_2 + I_0 \tag{4-25}$$

where I_{abc}, I_1, I_2 and I_0 are three-phase currents, positive sequence, negative sequence and zero sequence current components, respectively. In the unbalance situation, the motor current only includes positive sequence current and negative sequence current. The zero sequence is equal to zero in the motor drive system as there is no neural current path. So, we can rewrite (4-25) in the following format in the *abc* frame:

$$I_{\boldsymbol{a}} = Icos(\omega t) + kIcos(\omega t) \tag{4-26}$$

$$I_b = Icos(\omega t - 120) + kIcos(\omega t + \frac{2\pi}{3}) \quad (4\text{-}27)$$

$$I_c = Icos(\omega t + 120) + kIcos(\omega t - \frac{2\pi}{3}) \quad (4\text{-}28)$$

in which the first term presenting the positive sequence current and the second term is the negative sequence current, where *I* and *k* are the magnitudes of the positive and negative current components, respectively. Then, by using the Park transformation for (4-26), (4-27) and (4-28), the following can be obtained:

$$\begin{bmatrix} I_d \\ I_q \\ 0 \end{bmatrix} = \begin{bmatrix} 0 \\ I \\ 0 \end{bmatrix} + \begin{bmatrix} kIsin2\omega t \\ kIcos2\omega t \\ 0 \end{bmatrix} \quad (4\text{-}29)$$

$$\begin{bmatrix} I_d \\ I_q \\ 0 \end{bmatrix} = \begin{bmatrix} kIsin2\omega t \\ I + kIcos2\omega t \\ 0 \end{bmatrix} \quad (4\text{-}30)$$

Above equations show that the negative sequence current causes the second harmonics in the *dq* frame currents.

4.3. Current and torque harmonic analysis for unbalance LC filter

In this section, harmonic analysis for the PMSM with unbalance LC filter will be presented. These analyses include *dq* axis currents and torque/speed harmonics analysis.

4.3.1. *dq* axis current harmonic analysis

In order to validate the proposed mathematical model presented in chapter, it is simulated in MATLAB/Simulink and the second order current harmonics corresponding to the LC filter parameter variation are extracted. Fig. 4- 3 shows the second order harmonic analysis of *q* axis current in the PMSM with LC filter while the inductance tolerances change from 0% to 60%. The fundamental frequency in this case is set as 29.79 Hz, which corresponds to a speed of 93.61 rad/sec in the test motor, and it remains the same for all unbalance conditions. The input voltage level is determined based on I_q=11 A and I_d=0 A, and the motor back-EMF is determined from the motor speed and currents. From the results, it is worth mentioning that as the component tolerance increases the magnitude of the second order current harmonic increases as well. For the highest inductance tolerance of -60%, the second order harmonic current magnitude is 2.38 A, the peak-to-peak current ripple is 2.3A.

With the PI controller in the current loop, the second order current harmonic can be attenuate to some extent, and the analysis results are presented in Fig. 4- 4.The same condition is applied here while the inductance tolerances vary from 0 to 60%. From this result, the highest second order harmonic current magnitude is 0.64 A. This results also shows that as the component tolerance increases the magnitude of second order harmonic current increases as well.

Fig. 4- 5 shows the simulation result from a conventional circuit model with the LC components and the PMSM model from MATLAB/Simulink library. Since this model cannot work properly without the PI controller, only the results with PI controller are presented. The PMSM is controlled to a mechanical speed of 93.61 rad/sec and stator current is 11 A (I_q=11 A and I_d=0 A). Therefore, the fundamental frequency in this case is also 29.79 Hz and it remains the same for all unbalance conditions. This figure illustrates how the second order harmonic in the *q* axis current varies as the inductance tolerance changes. It can be seen that as the inductance tolerance increases, the magnitude of the second harmonic increases. In comparison to the results obtained at a similar condition in Fig. 4- 4, the magnitude of the second order harmonic obtained in this simulation is slightly higher as compared to ones obtained from the proposed model. This could be due to the reason that the inverter model was not considered in the proposed mathematical modelling.

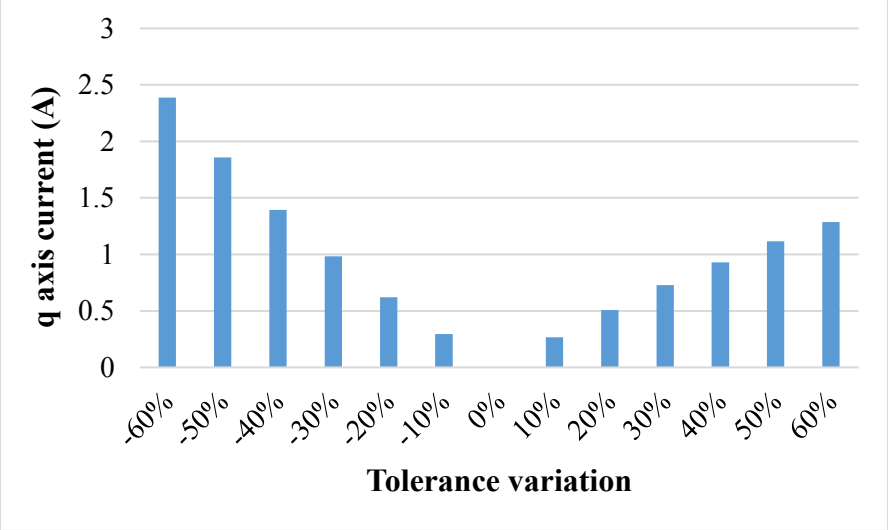

Fig. 4- 3. Second order harmonic analysis using the proposed model for *q* axis current.

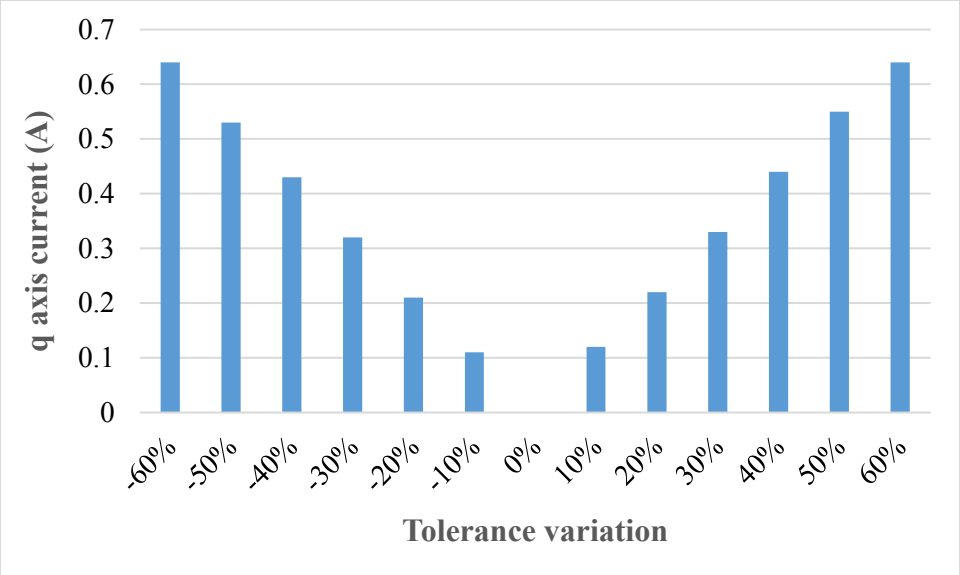

Fig. 4- 4. Second order harmonic analysis using the proposed model with PI controller in the loop for *q* axis current.

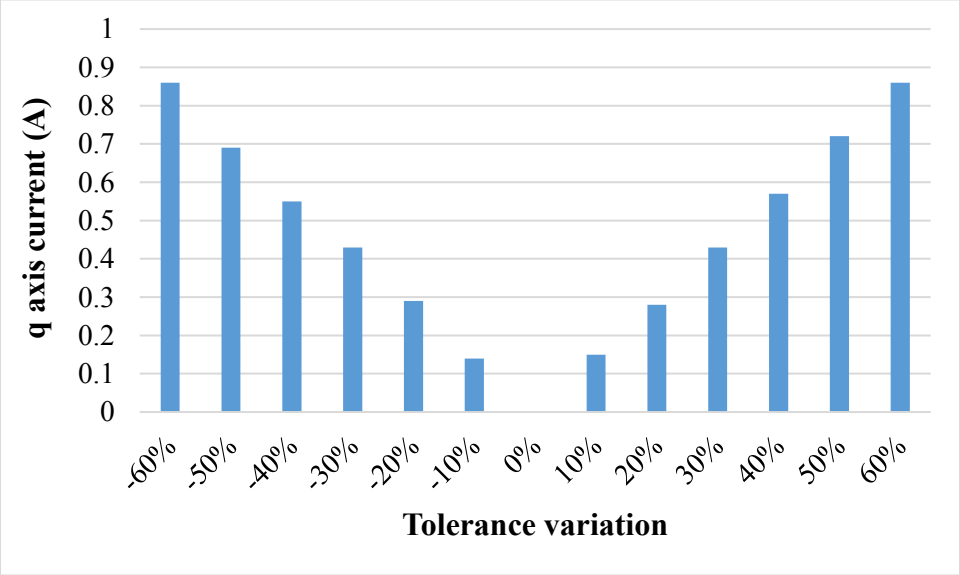

Fig. 4- 5.Second order harmonic analysis using circuit simulation models for *q* axis current.

Fig. 4- 6 Presents a comparison test results between the proposed mathematical model, simulation of PMSM with LC filter and experimental test while the inductance tolerance is reduced by 60% for one of the phases. It can be observed that the magnitude of second order harmonic on the mathematical model with PI controller is almost the same as simulation model and experimental test.

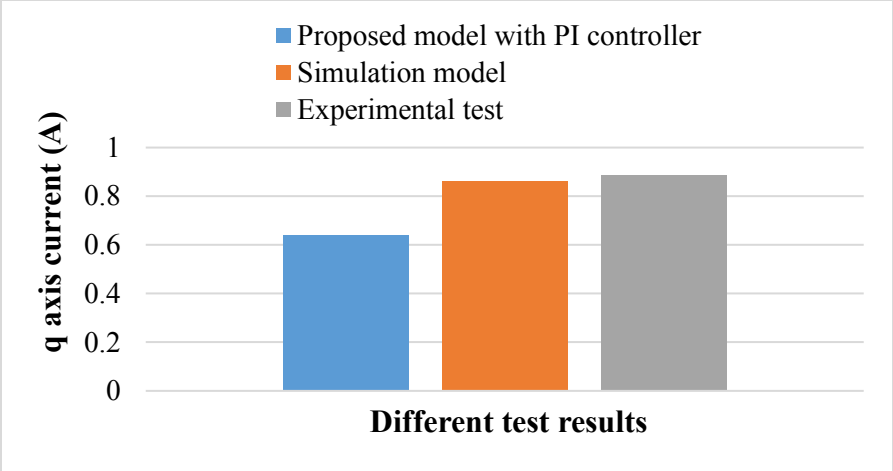

Fig. 4- 6. Second order harmonic analysis for q axis current using different test methods.

4.3.2. Torque harmonic analysis

One of the impacts of unbalance LC filter is the additional torque ripple. In this section, the harmonic analysis for electromagnetic torque under three different conditions namely proposed mathematical model, PMSM drive without PI controller and simulation model of PMSM with LC filter with PI controller.

The following electromagnetic torque expression is driven for PMSM in Chapter2.

$$T_e = \frac{3}{2}P\left(\psi_{PM}I_q + \left(L_d - L_q\right)I_d I_q\right) \tag{4-31}$$

equation (4-31) demonstrates that *dq* axis current directly affects the torque response. Thus, negative sequence current in *dq* axis causes extra torque ripple in the motor drive. Fig. 4- 7 presents the simulation results of torque for LC filter balance and 30% tolerance changes. It can be seen that 30% tolerance change result in additional torque ripple. This additional torque ripple results in second order harmonic.

The torque harmonic analyses using the proposed model presents in Fig. 4- 8 in which the second order harmonics are extracted at different inductance tolerance variation from 0 to 60% while the fundamental frequency is 29.79 Hz. This condition remains the same for all unbalance conditions. These analyses present the fact that as the component tolerance increase the magnitude of second order harmonics is increasing as well.

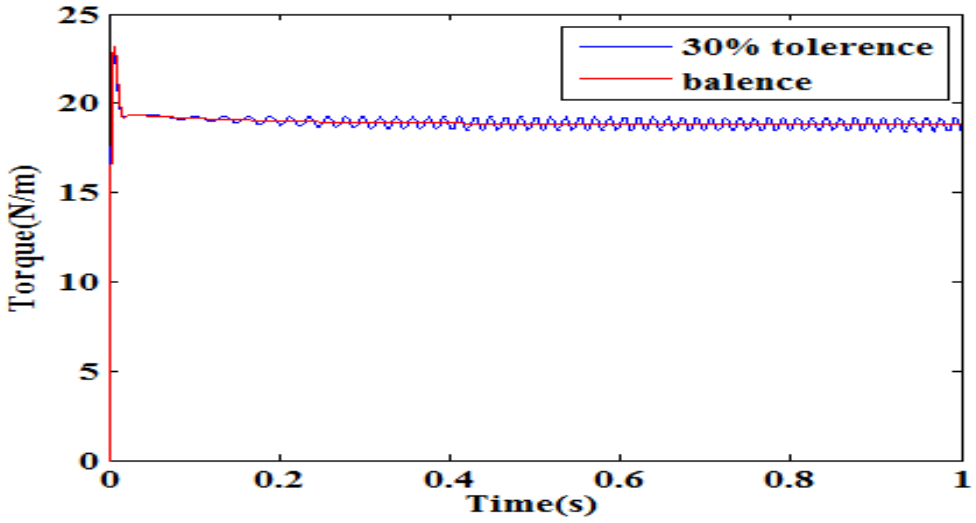

Fig. 4- 7. Torque response under balance and 30% unbalance condition.

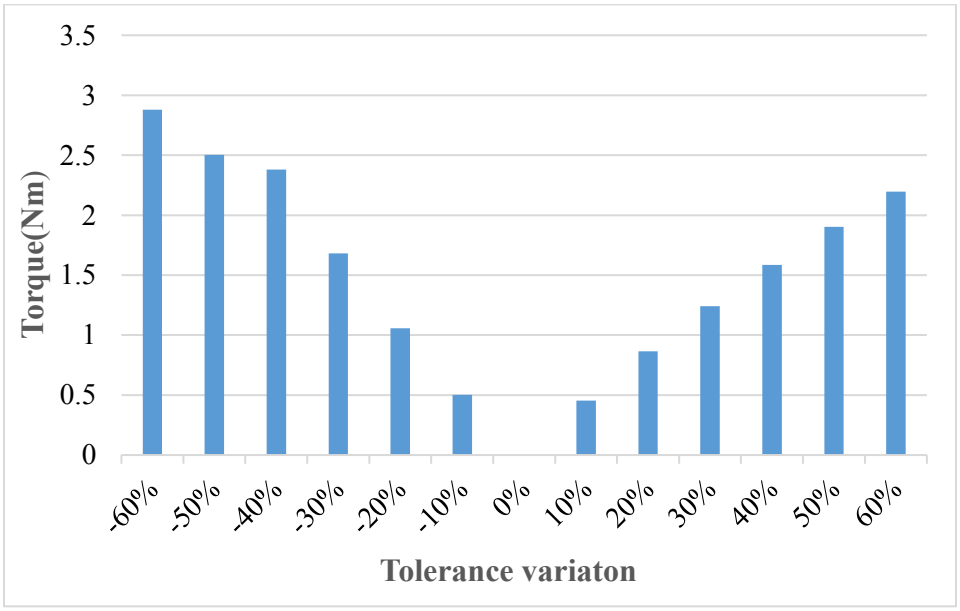

Fig. 4- 8. Second order harmonic analysis using a proposed mathematic model for electromagnetic torque.

Fig. 4- 9 presents the harmonic analysis using a proposed model with PI controller in which the fundamental frequency remains the same and inductance tolerances varied from 0 to 60%. It can be observed as the component tolerance increase the second order harmonics is increasing as well.

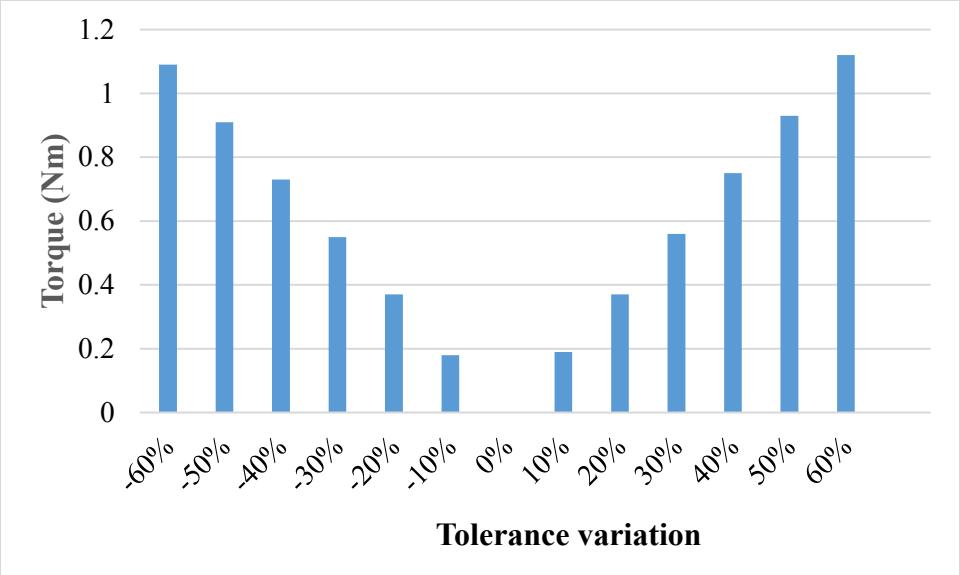

Fig. 4- 9. Second order harmonic analysis using proposed model with PI controller for electromagnetic torque.

The electromagnetic torque harmonic spectrum using the simulation model is given in Fig. 4- 10, where the harmonics are extracted at the different inductance tolerances and the fundamental frequency in this case is 29.79 Hz. It can be seen as the component tolerance increase the magnitude of second order harmonics is increasing as well. Also, the magnitude of the second order harmonics is reduced as compare to the proposed mathematical model and simulation model without PI controller. This is mainly because of the impact of the PI controller on reducing the second order harmonics.

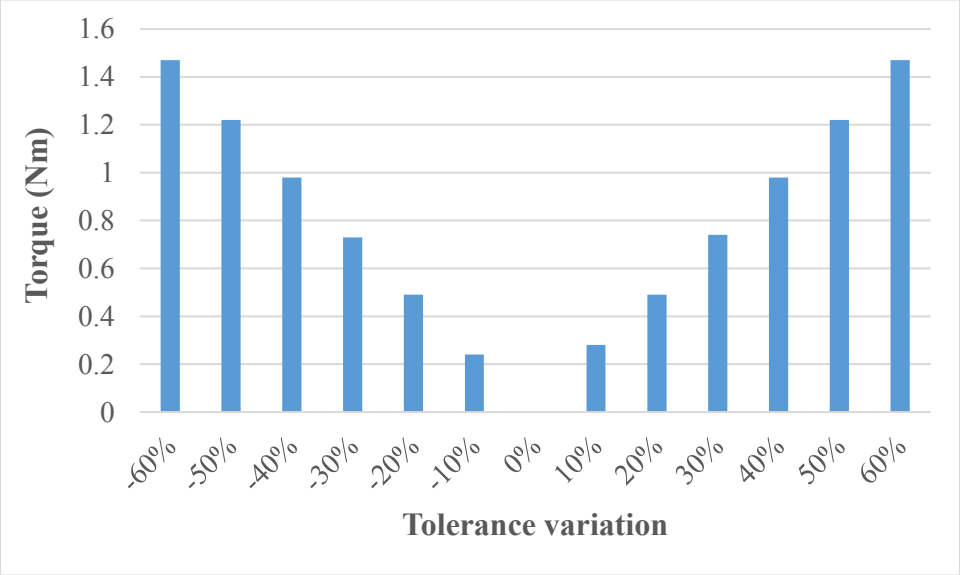

Fig. 4- 10. Second order harmonic analysis using simulation model for electromagnetic torque.

4.4. Resonant frequency analysis

In Chapter 3, the transfer function of the LC filter with PMSM is derived. Also, LC filter is designed in Chapter2. In this section, resonant frequency will be derived from the open loop Bode plot of the PMSM with LC filter. Then, the variation of inductances, capacitors and resistors from the nominal value and the effect of each tolerance variation in resonant frequency will be evaluated.

The open loop magnitude and phase plots of the PMSM with the balance LC filter are given in Fig. 4- 11.

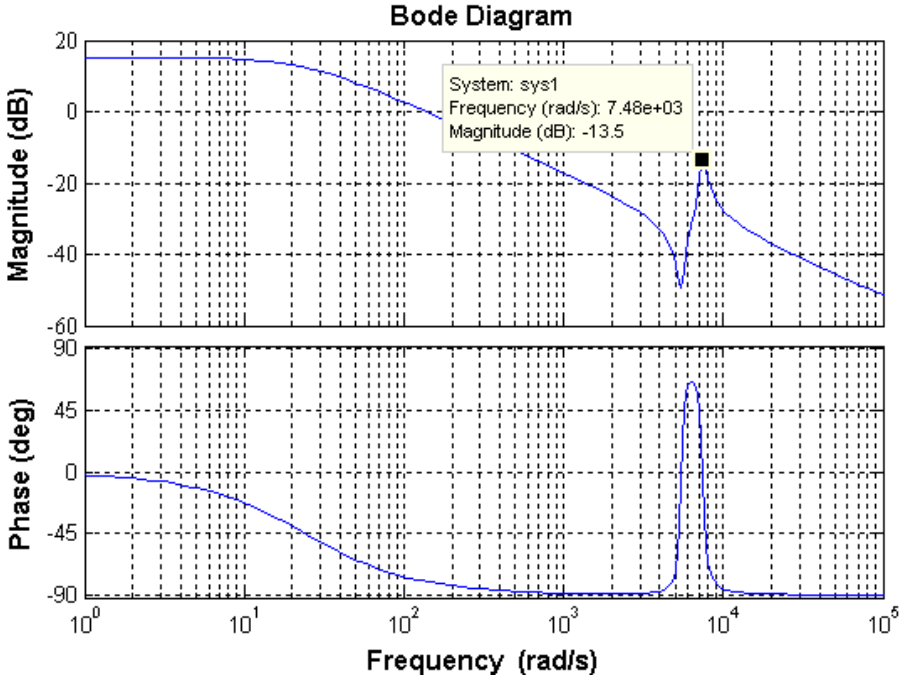

Fig. 4- 11. Open loop magnitude and phase plots for PMSM with balance LC filter.

The Bode plot of PMSM with LC filter is given in Fig. 4- 12 while the inductance tolerance is changing form 60% to -60%. It can be seen that, as the inductor tolerance varied from the nominal value the resonant frequency is varied as well. For the PMSM with LC filter the inductance tolerance is changing from 0 to 60% and corresponding resonant frequency is measured through the Bode the plot. Then, the result of each analysis is listed in the Table.4- 1.

Fig. 4- 13 presents the open loop Bode plot of PMSM with LC filter while the capacitor tolerance is changing from 60% to -60%. It can be seen that, as the capacitor tolerance the resonant frequency is changing as well. The impact of this variation also lists in Table.4- 1.

For the PMSM with LC filter the resistances tolerance variation and corresponding resonant frequency and magnitude are measured through the Bode plot. It is observed that resistances tolerance changes from-60% to 60% do not have any effect on system resonant frequency. Thus, the system resonant frequency is maintained the same which is $7.48*10^3$ rad/sec. However, the resistance variation has direct effect on the magnitude. Fig. 4- 14 illustrates system magnitude variation due to the resistance tolerance changes. As the resistances tolerance reduce the magnitude of resonant peak will increased. Thus, this change will directly affect the PMSM drive stability as explained in Chapter 3 the controller bandwidth is limiting by the resonant peak.

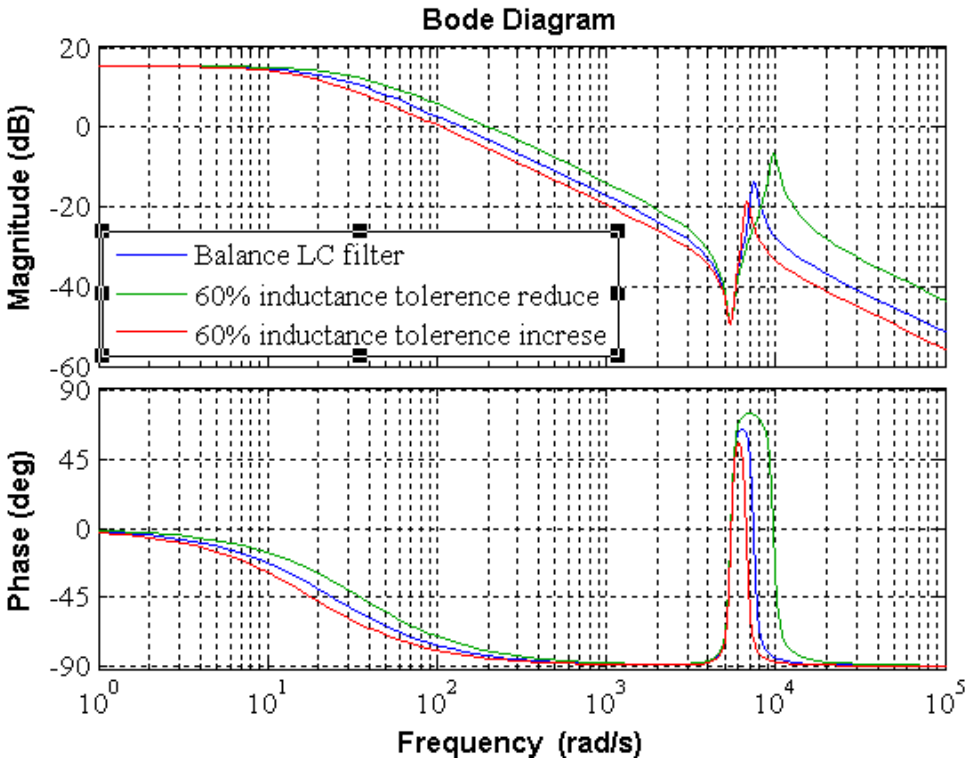

Fig. 4- 12. Open loop magnitude and phase plots for PMSM with LC filter with 60% inductance tolerances changes.

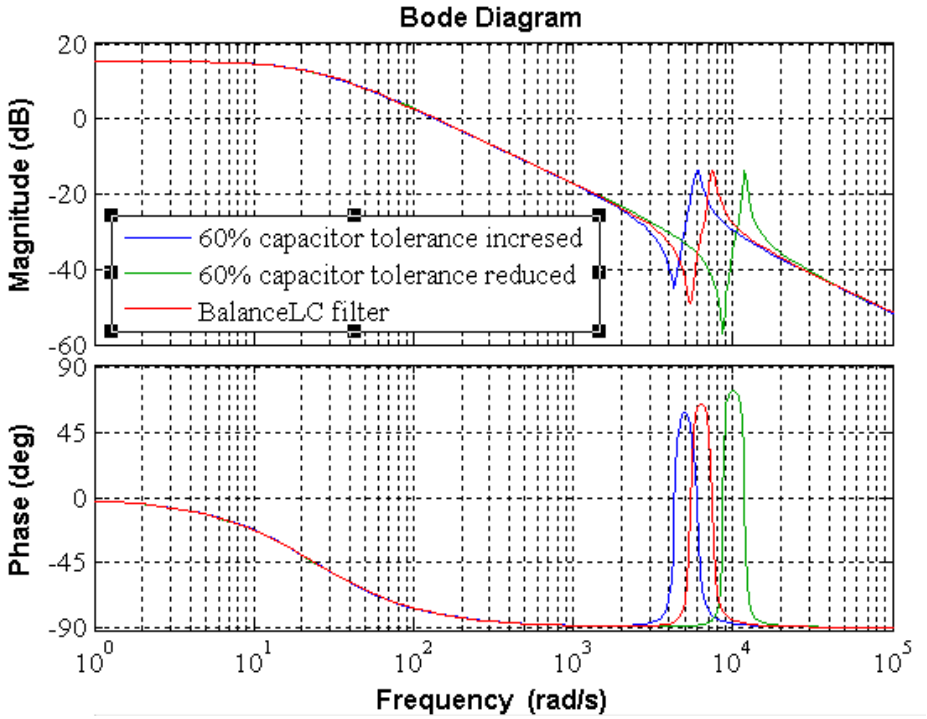

Fig. 4- 13. Open loop magnitude and phase plots for PMSM with LC filter with 60% capacitor tolerance changes.

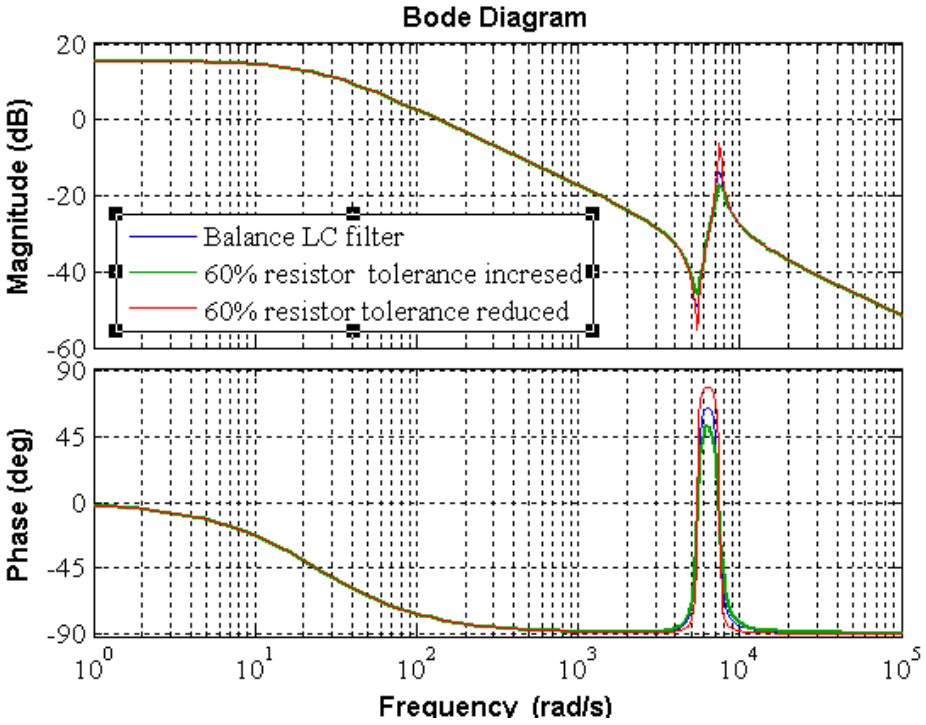

Fig. 4- 14. Open loop magnitude and phase plots for PMSM with LC filter with 60% resistor tolerance changes.

Table.4- 1. The resonant frequency change due to the LC filter components tolerance variation.

Tolerance Change	**Inductor ω_c (rad/sec)**	**Capacitor ω_c (rad/sec)**	**Resistance Magnitude(dB)**
-60%	$9.99*10^3$	$1.16*10^4$	-7.41
-40%	$8.53*10^3$	$9.66*10^3$	-9.48
-20%	$8.08*10^3$	$8.53*10^3$	-11.7
-10%	$7.66*10^3$	$8.05*10^3$	-12.6
0%	$7.48*10^3$	$7.48*10^3$	-13.5
10%	$7.40*10^3$	$7.28*10^3$	-14.3
20%	$7.33*10^3$	$6.82*10^3$	-15.4
40%	$7.1*10^3$	$6.32*10^3$	-17.1
60%	$6.65*10^3$	$6.05*10^3$	-19

Chapter 5 Improved Current Control Development for PMSM Drive under LC filter Unbalance Condition

This chapter looks into mitigating the impact of unbalance LC filter in PMSM drive. The adaptive PR controller working together with PI controller is proposed to eliminating the consequence impacts of LC filter unbalance condition. Additionally, experimental results obtained for the surface-mounted PMSM drive with unbalance LC filter are presented in this chapter.

5.1. Mitigating LC filter unbalance

Based on the investigations presented in Chapter 4, one of the major impacts of LC filter unbalance is the negative sequence current in the PMSM drive. This chapter presents a method to mitigate/compensate the negative sequence current and hence eliminating the consequence impacts. Negative sequence currents lead to second order harmonic currents in the *dq* frame. It can be seen that the LC filter increases the order of the motor drive system and limits the maximum achievable bandwidth in the current control loop. Thus, PI controllers have a low gain at the second order harmonic frequency on the *dq* frame, they are not able to control/ reduce the negative sequence currents, especially at high speeds. Thus, existing controllers are unable to compensate the negative sequence currents in the PMSM drive [38], [39].

To address the unbalance issue in PMSM drives, the produced negative sequence currents must be compensated. A few strategies have been proposed in the literature for other applications. In [40], a Hysteresis controller is developed for non-sinusoidal current control which has a limited performance and a challenging implementation issue due to variable switching frequency. The method proposes in [41] and [42] uses a bandpass filter to extract and compensate negative sequence currents for induction generators. However, this method involves complex computation and has limited performance under low speed conditions. In [43], the master-slave control strategy is implemented for axial-flux PMSM under the unbalance load condition. The repetitive control (RC) is another control strategy for elimination of unbalance current [44], [45] for doubly fed induction generators. However, the tuning process is complex. On the other hand, in applications such as wind power systems and grid-connected power converters [46]–[49], predictive control and decoupled double synchronous frame current control have been developed

to address the unbalance issues. However, it requires different machine parameters information. Recently, the proportional resonant (PR) controller is proposed for unbalance grid conditions in which the grid frequency is fixed [50], [51].

In this research study, an adaptive proportional resonant (PR) controller working together with the PI controller is proposed, to address this issue. The proposed controllers working in tandem will attain a high gain at DC and the second order harmonic current in the *dq* frame. Thus, being able to control both the positive sequence and the negative sequence winding. Fig. 5-1 illustrates the proposed control strategy in PMSM motor drive with unbalance LC filter.

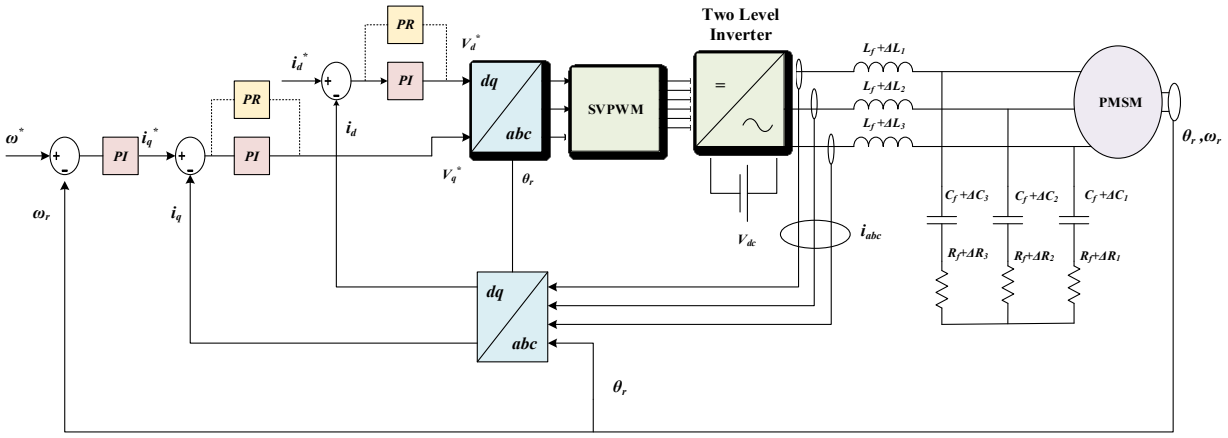

Fig. 5- 1. Block diagram of PR controller along with PI controller in PMSM motor drive with an unbalance LC filter.

5.2. PR controller

In a three-phase systems, PI controllers are typically used due to their simplicity. To implement PI controllers, the quantities on the three-phase *abc* coordinate frame are transferred into the *dq* rotating reference frame. This converts sinusoidal signals in the three-phase *abc* coordinate frame to DC quantities on the *dq* frame. Since PI controllers contain a pole at the origin PI controllers are used to achieve zero steady state error at DC. The PI controller gain starts reducing at other frequencies. Thus, an alternate controller used sometimes in three-phase systems is a PR controller. PR controller is a combination of a proportional term and a resonant term. PR controller is a double integrator which introduce an infinite gain at the selected frequency (resonance frequency) to eliminate the steady-state error at this frequency and to achieve no attenuation outside this frequency and no phase shift and gain at the other frequencies. So, it acts as an integrator with infinite DC gain which makes the steady state-error

to zero at the selected frequency. PR controller is applicable for single-phase or three-phase systems. The ideal resonant controller, can be represented by:

$$G(s)_{PR} = \frac{Aks\omega}{s^2 + ks\omega + \omega^2} \tag{5-1}$$

where k is the damping factor, A is PR controller gain, and ω is the resonance frequency.

5.3. Proposed Controller

A traditional drive inverter controller (PI control) might not be capable of mitigating the negative impact on the motor due to filter unbalance. Negative sequence currents lead to second order harmonic currents in the *dq* frame as discussed in Chapter 4. Since, typically, PI controllers have a low gain at the second order harmonic frequency on the *dq* frame, they are not able to control/ reduce the negative sequence currents in the motor winding. Increasing the current loop bandwidth (gain of PI controller at the second harmonic frequency) could address this issue to a certain extent. However, the maximum achievable bandwidth is limited by the maximum inverter switching frequency as discussed in Chapter 3. Thus, a PI controller would not be sufficient especially at high motor speeds, when the fundamental frequency is high. In this situation, a severe unbalance effect occurs. Hence, existing controllers are unable to compensate for the negative sequence currents in the PMSM drive. Thus, The PI controller along with PR controller is proposed in order to work in tandem to attain a high gain at DC and the second order harmonic current in the *dq* frame. As it discussed in Chapter 4, the *d* axis and *q* axis current contain positive and negative sequence components. Thus, PI controller is controlling the DC part (positive sequence component) of the signal and PR controller is mitigating the second order harmonic in *dq* frame (negative sequence component). Fig. 5- 2 shows the PI and PR effect on each type of the signal. By using this method, the positive sequence and the negative sequence winding currents can be controlled at the required values.

For the drive applications where the fundamental frequency changes, the PR controller need to adaptively changes as well. So, the PR transfer function is needed to change to an adaptive one. For the PMSM drive, the fundamental frequency of the operation drive can be easily obtained as the machine speed is equal to the synchrotrons speed and the PMSM number of pole pairs is known. When the machine accelerates or decelerates, the fundamental frequency will change and the controller transfer function will change automatically. Fig. 5- 3 illustrates the

schematic diagram of the proposed controller in which the PR controller is working together with PI controller in *dq* reference frame.

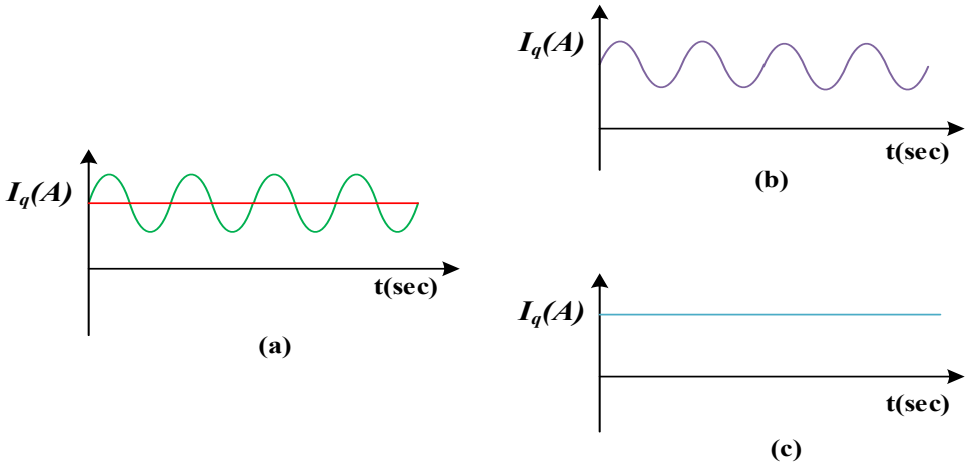

Fig. 5- 2. (a) The current signal components in q axis (b) PR controller is controlling the sinusoidal part of the signal (c) PI controller is controlling the DC part of the signal.

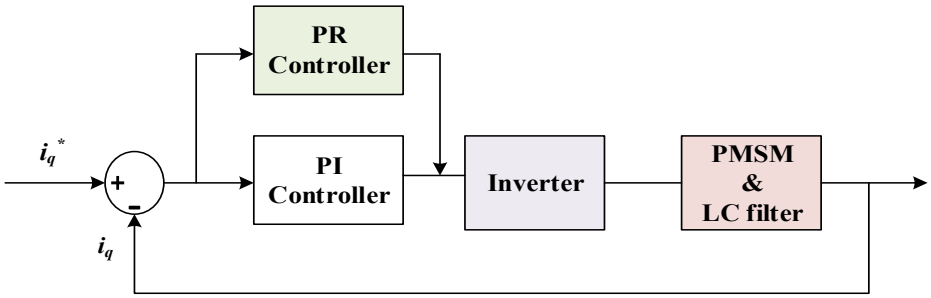

Fig. 5- 3. Block diagram of the close loop LC filter along with PMSM with proposed controller.

The open loop transfer function of the proposed controller for the current loop can be represented by:

$$G(s)_{PR+PI} = \frac{Aks\omega}{s^2 + ks\omega + \omega^2} + \frac{K_{PI}(1 + s\tau_{PI})}{s} \quad (5\text{-}2)$$

$$\text{PRP(s)} = G(s)_{PR+PI}.G(s).\frac{\frac{V_{dc}}{2}}{1+sT_f} \quad (5\text{-}3)$$

where k is the damping factor, A is PR controller gain, and ω is the resonance frequency which changes according to the fundamental frequency. The PR controller gain (A) is selected to achieved total control loop gain of 20 dB .The value of k is selected so as to achieve the resonant controller bandwidth of 10% of fundamental frequency. This ensures selective control action of the resonant controllers for the frequencies of the interest [11]. The implementation of the

proposed controller is shown in Fig. 5- 4.

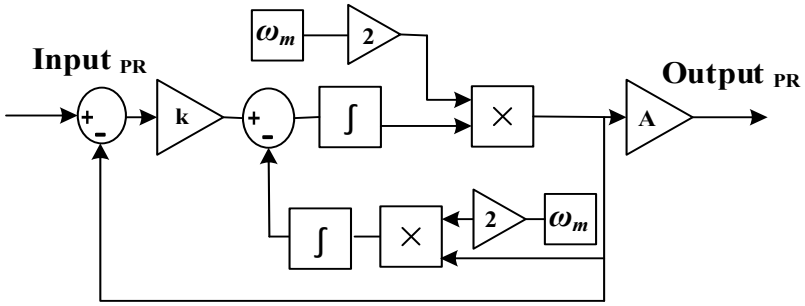

Fig. 5- 4. Implementation diagram of the proposed adaptive PR controller.

Moreover, the PI controller is working in tandem with PR controller to achieve the zero steady state error. The open loop phase and magnitude plots for the PMSM drive with LC filter for the proposed controller are compared with conventional PI controller in Fig. 5- 5. The Fig. 5- 5 shows that the proposed controller adds around 20 dB gain to the selected frequency in this case 20 Hz. Thus, the additional resonant peak is modifying the controller while the phase margin, the gain margin and controller bandwidth is the same. Therefore, the proposed controller leads to more accuracy for the PMSMS drive with unbalance LC filter. For the validation of this method the experimental results will be presented in the next section.

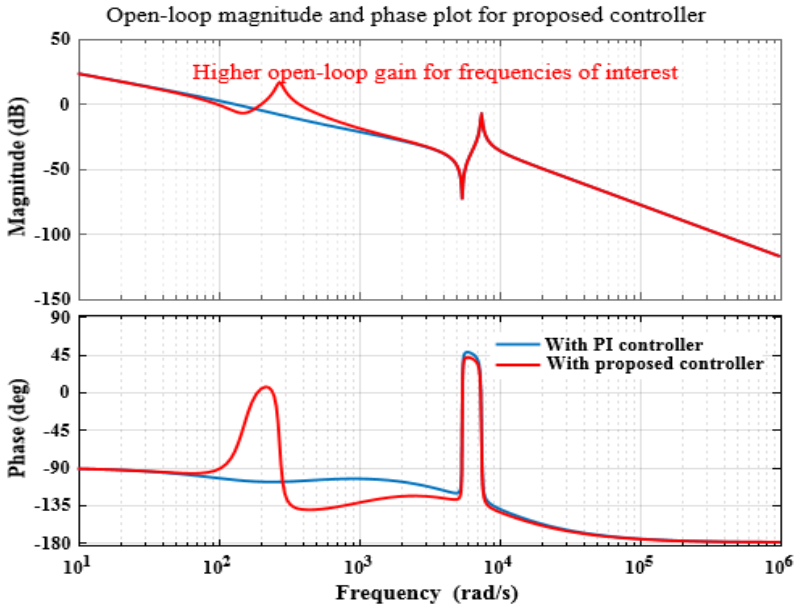

Fig. 5- 5. Open loop magnitude and phase plots for the proposed controller compare with PI controller.

5.4. Simulation model for proposed PR controller

To validate the capability of the proposed PR controller, the vector control of the PMSM along with unbalance LC filter is simulated in MATLAB/Simulink. Fig. 5- 6 presents the simulation model for the proposed adaptive PR controller.

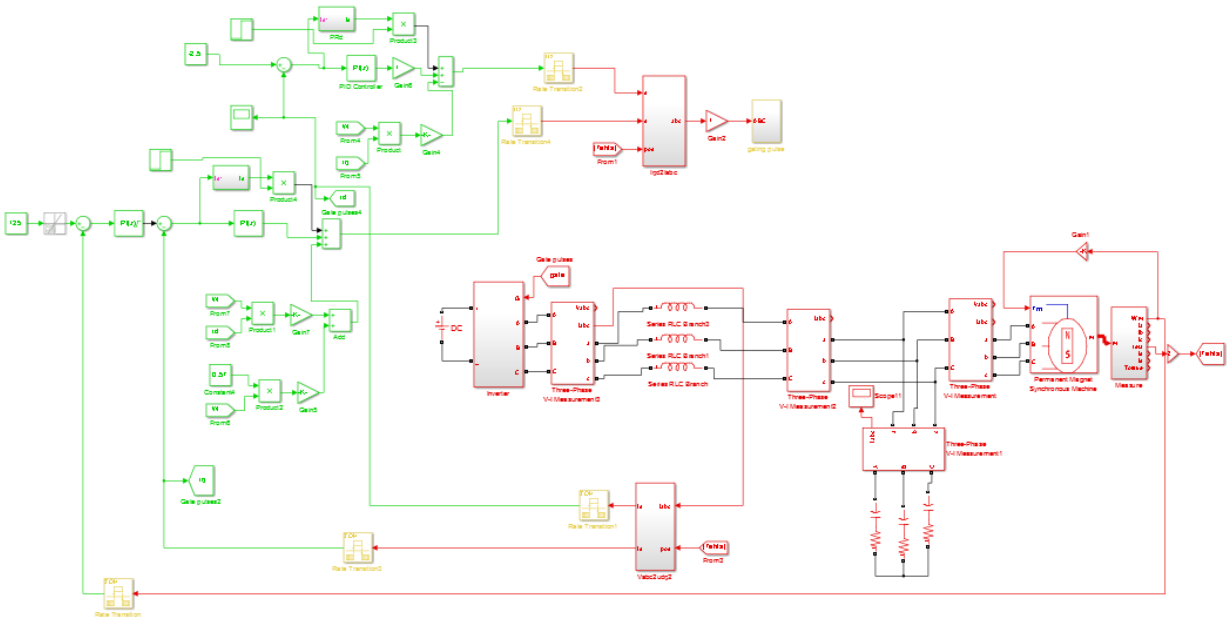

Fig. 5- 6. The simulation model of proposed controller for PMSM with unbalance LC filter.

5.5. Experimental results of the adaptive PR controller

The proposed adaptive PR controller compensation for unbalance LC filter is tested on a VSI-fed laboratory SPMSM drive system as shown in Fig. 5- 7. The experimental setup consists of the driving inverter, which is a standard two-level converter composed of IGBT modules, the switching frequency of the driving inverter is 5 kHz. The driving inverter is connected to the LC filter then connected to the SPMSM which coupled to a DC dynamometer and a torque transducer with the bandwidth of 4 Hz is employed to measure the shaft torque of SPMSM. The control of SPMSM is programmed on dSPACE also shown in Fig. 5- 7. A 12-bit absolute encoder is used to measure the speed of the machine. The experimental result is recorded in Yokogawa SL1000 data acquisition system.

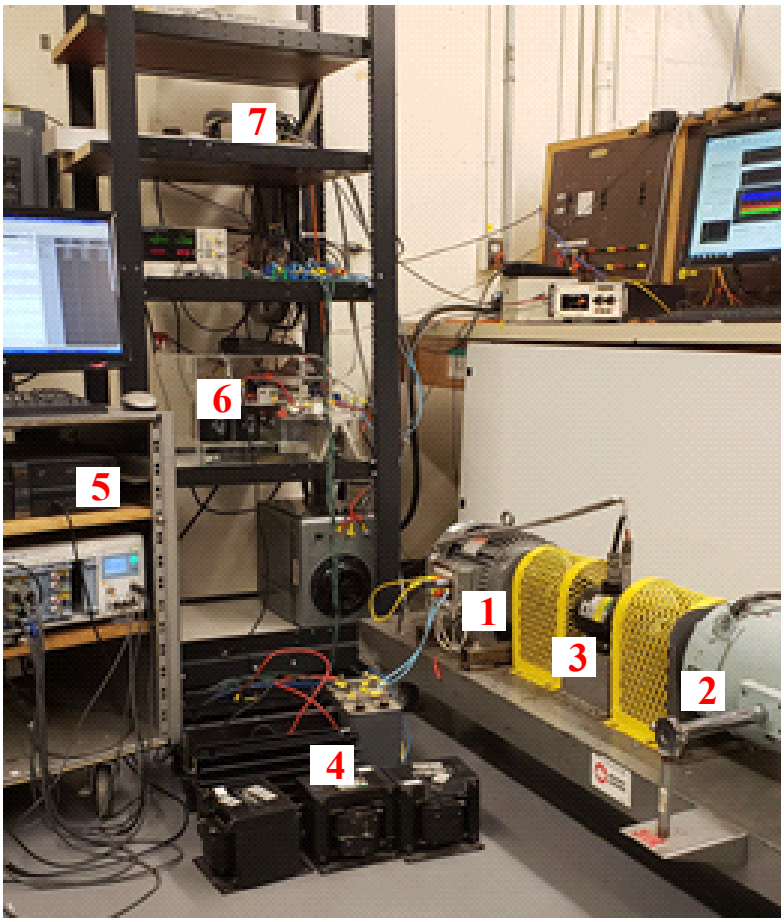

Fig. 5- 7. Experimental setup of PMSM drive with LC filter (1) SPMSM machine (2) Coupled DC dynamometer (3) Torque transducer (4) LC filter (5) Data acquisition (6) Driving inverter (7) dSPACE simulator.

To validate the accuracy of the proposed adaptive controller, the experimental results pertaining to various machine transient conditions are obtained from the prototype machine. These transient conditions are listed below:

A) Startup test

B) Load change test

C) Speed reversal test

D) Different speed conditions test

In addition, in order to clearly observe the unbalance the inductance which is used in one of the phases during the experiment is considered to be 60% tolerance.

Fig. 5- 8 and Fig. 5- 9 present the machine startup without and with the proposed compensation. The reference q axis current is changed from 0 to 9 A. The dq axis current as well as machine three-phase currents are shown in these two figures.

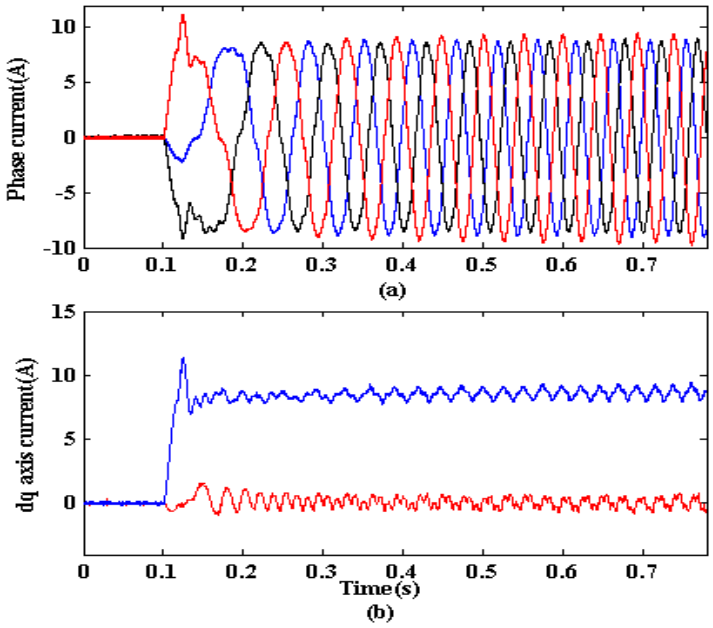

Fig. 5- 8. Experimental results of machine startup without compensation (a) Three-phase current (b) *dq* axis current

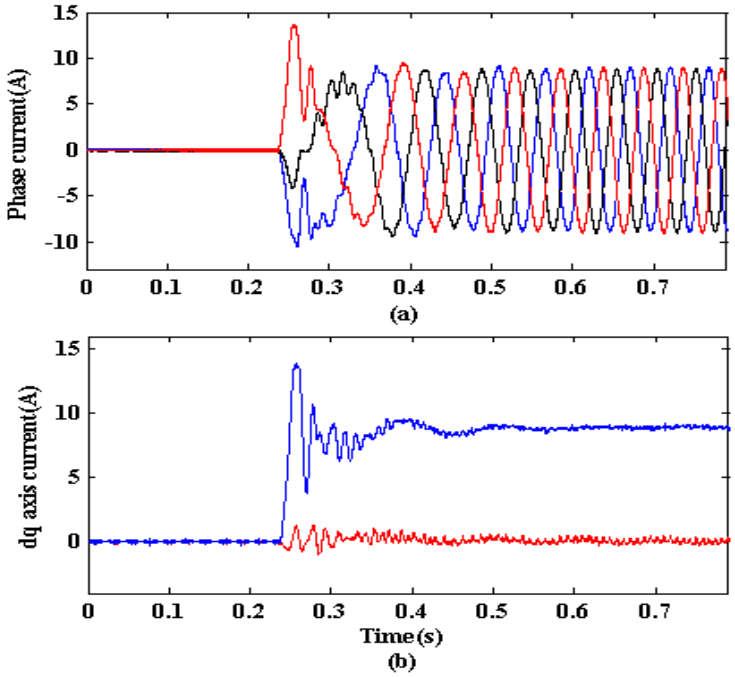

Fig. 5- 9. Experimental results of machine startup with compensation (a) Three-phase current (b) *dq* axis current

Fig. 5- 10 presents results obtained when the load on the SPMSM is suddenly reduced, leading to a higher speed and a subsequent control back to its set value.

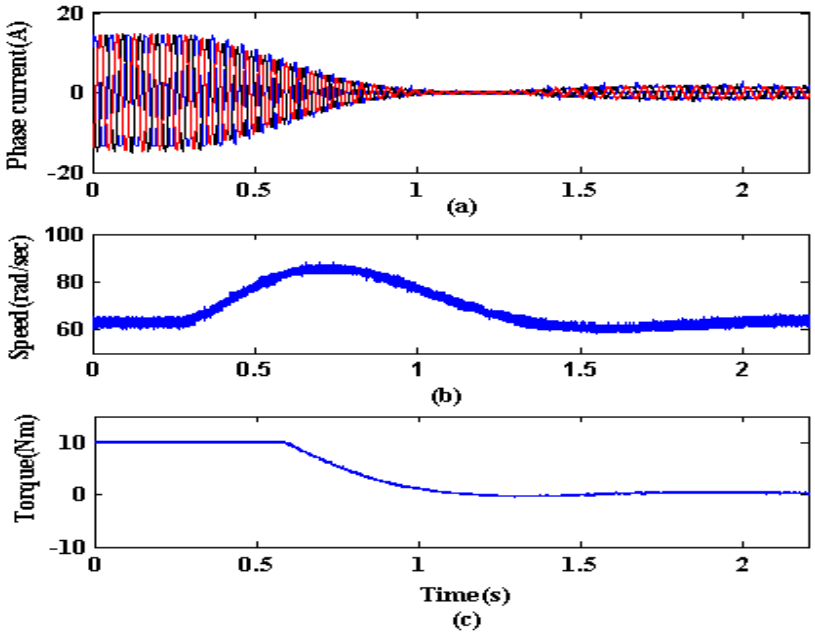

Fig. 5- 10. Experimental results obtained for sudden load change (a) Three-phase current (b) Speed(c) Torque (Scale 2 Nm/div)

Fig. 5- 11 presents the result of speed-reversing test without applying the proposed controller. Fig. 5- 12 presents the results obtained for the speed reversal of the prototype machine while the speed reference is changing from 100 rad/sec to -100 rad/sec. It can be seen from the Fig. 5- 12 that the proposed controller can be applied in both rotational directions and the dynamic performance before/after compensation are similar. Fig. 5- 13 presents the experimental test results with and without proposed adaptive PR controller compensation for the *dq* axis current when the load current is 11 A. The test result is zoomed to show more details about the negative sequence current. It can be seen from the Fig. 5- 13 (a) that after the compensation, the peak to peak current value is around 2 A for the *q* axis current where the proposed method has magnitude of 0.7 A, the peak to peak magnitude is 1.8 A for *d* axis current and after proposed adaptive PR controller compensation is 0.9 A. Fig. 5- 13 (c) presents the actual three-phase motor current waveform before and after applying the proposed controller. The current waveform is unbalanced before the proposed controller compensation; the motor current becomes balance after the proposed controller compensation is used.

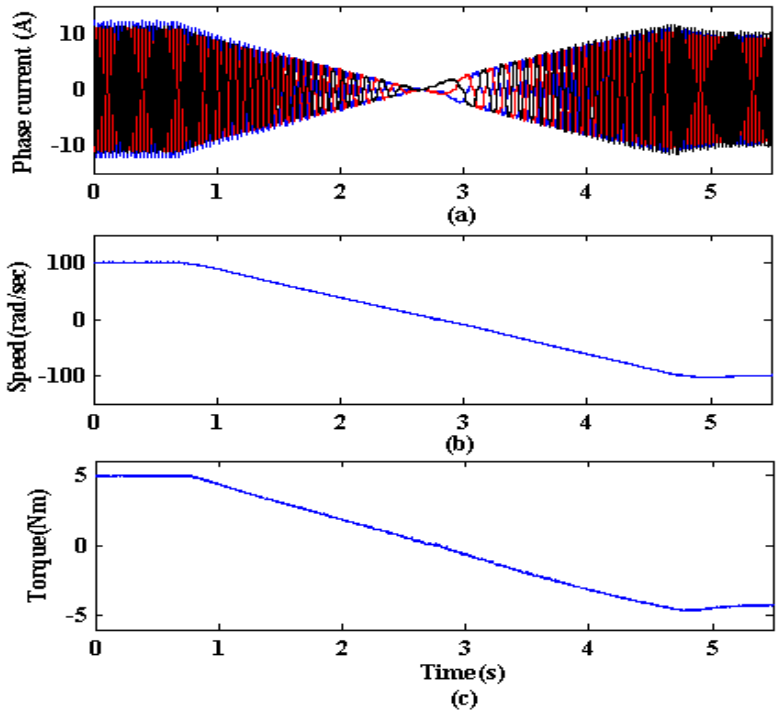

Fig. 5- 11. Experimental results for speed reversal test without compensation (a) Three phase current (b) Speed (c) Torque (Scale2Nm/div)

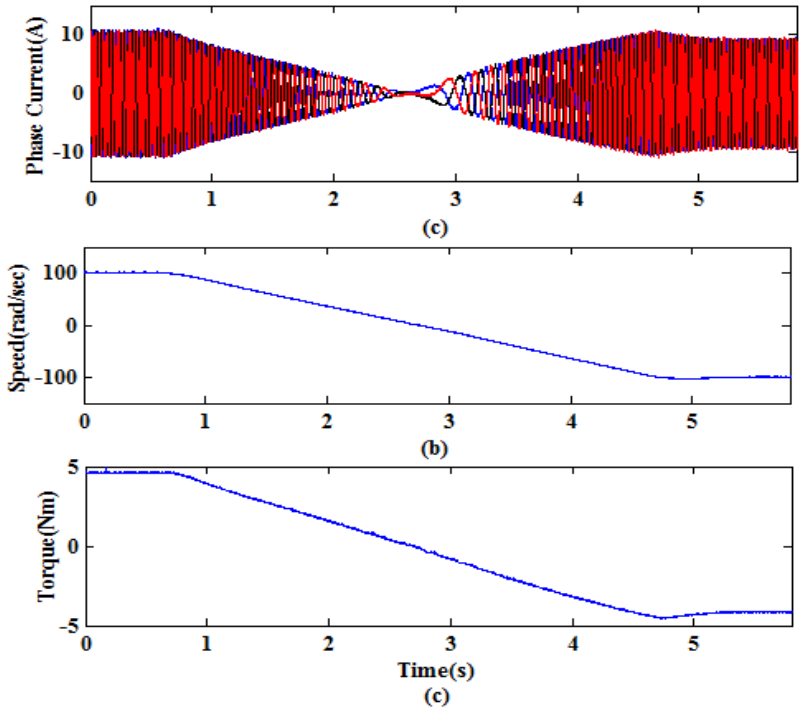

Fig. 5- 12. Experimental results for speed reversal test under proposed controller (a) Three-phase current (b) Speed (c) Torque (Scale 2 Nm/div)

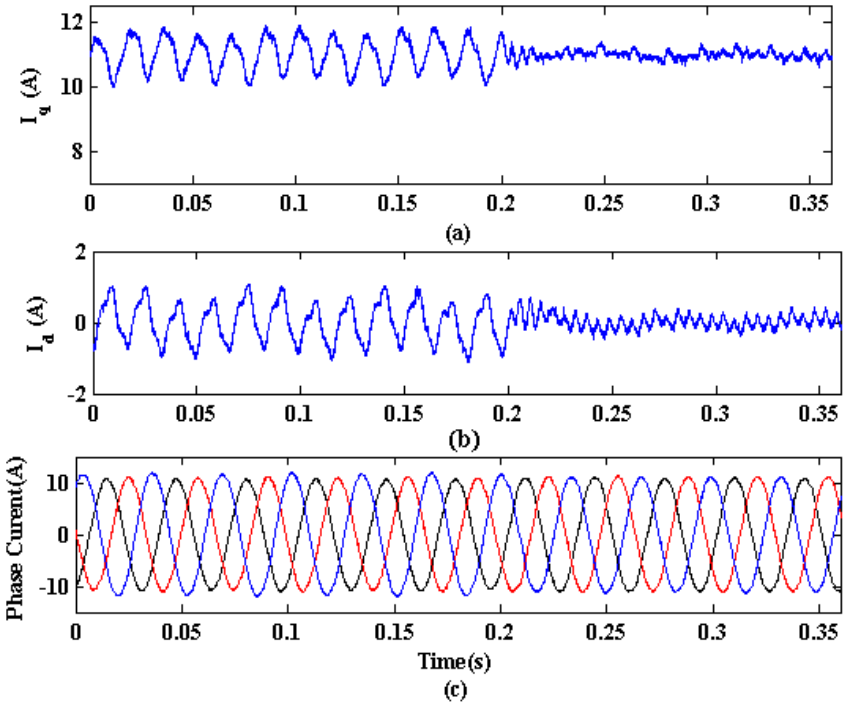

Fig. 5- 13. Experimental result before and after applying the proposed controller (a) Measured *q* axis (b) Measured *d* axis current (c) Measured three-phase current.

Fig. 5- 14 presents the measured harmonics spectrum of the *q* axis current before and after applying the proposed controller while the fundamental frequency is 30 Hz. From the spectrum analysis it can be seen when, the compensation is enabled, the second harmonics of *q* axis current is significantly reduced.

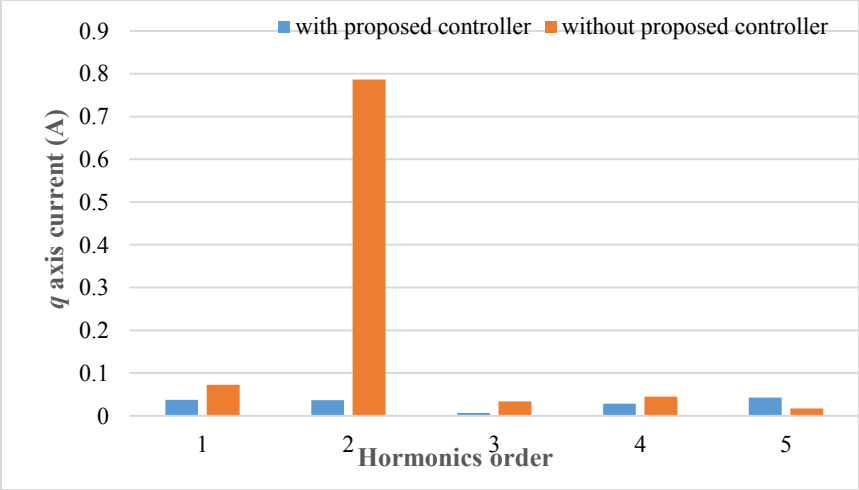

Fig. 5- 14. *dq* axis current harmonic spectrum after and before applying the proposed controller.

Fig. 5- 15 presents the result phase current and the SPMSM different speeds. The speed of machine is changing from 0 to 30 rad/sec then to 60 rad/sec and at the end from 60 rad/sec to 80 rad/sec. It can be observed from Fig. 5- 15 that the proposed controller adaptively adjusted with different speed commands while the three-phase currents remain balance.

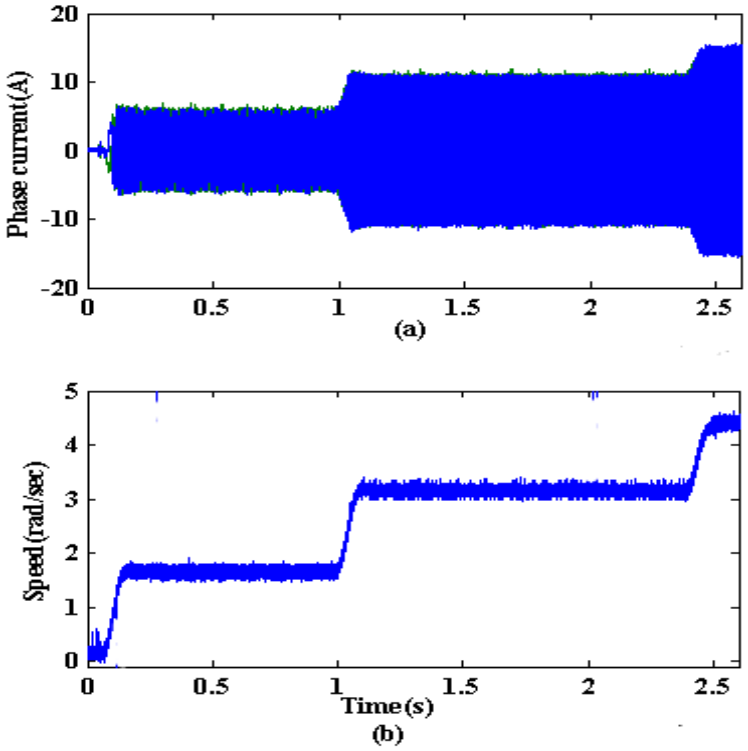

Fig. 5- 15. Experimental results of different speeds with compensation (a) Three-phase current (b) Speed (Scale 20 rad/sec/div).

The experimental results have demonstrated that the proposed adaptive PR controller reduces the negative impact of the LC filter unbalance on the PMSM drive effectively without compromising the machine performance.

Chapter 6 Conclusion and Future Works

The focus of this research work is the investigation of LC filter unbalance in PMSM drive. The main conclusion and future works for this thesis are presented in this chapter.

6.1 Conclusion

This thesis investigated the effect of LC filter unbalance on the PMSM drive performance. A comprehensive mathematical model has been proposed and developed for this investigation by considering both the PMSM and LC filter unbalance. In order to validate the model, its results were compared with the ones obtained from the circuit simulations and experimental tests. It is shown that the proposed model is accurate for motor drive performance analysis with and without LC filter unbalance. Such a model is critical in developing a mitigating approach for LC filter unbalance in the future. It can also be used to detect LC filter unbalance issue in a motor drive system.

The conclusions from each chapter are provided as follows:

Chapter2

In this chapter, the mathematical model of the PMSM and LC filter was studied. Electrical and mechanical parameters of the machine were measured. Moreover, the LC filter modeling and design procedure for considering balance LC filter was presented. Based on this work, the controller of PMSM drive system with and without LC filter can be designed.

Chapter3

In this chapter, different control strategies for PMSM namely scaler control, DTC and FOC are studied and compared. In addition, the FOC and DTC were evaluated in details through simulations and experimental testes. From the evaluations, a simple PI based field oriented control was selected for the proposed investigation of PMSM drive performance considering balance and unbalance LC filters.

Chapter4

In this chapter, the impact of LC filter unbalance on PMSM drive system was investigated. A comprehensive mathematical model was presented to model the PMSM drive system considering unbalance LC filter. Then, the investigation results on current and torque harmonics were presented and compared with a conventional circuit model.

Chapter5

In this chapter, an adaptive PR controller working together with PI controller was proposed in order to mitigate the negative impact of the filter unbalance on the motor drive. The control design procedure to achieve this improvement in drive performance was also presented. The proposed method was validated through simulations and experimental tests.

6.2 Future work

This research work can be further extended to:

- The effect of unbalance LC filter can be extended to include more features of machine losses in motor mathematical model. Therefore, the machine losses can be studied accurately and in more detail.
- This study uses PI controller for regulating the *q* axis and *d* axis currents while the LC filter is included in the motor drive. The LC filter causes control loop bandwidth limitations. Therefore, in future study, this control technique can be modified so as to reach a higher controller bandwidth.
- The effect of LC filter unbalance can be further analyzed under different control strategies for PMSM, such as DTC, so as to validate and compare the machine performance under different control methods.
- In this study, two level IGBT inverter is used to investigate the impacts of LC filter unbalance on PMSM drive. An inverter with higher switching frequency devices, such as GaN transistors, can be used to reduce the size of the LC filter. Then, the comparative studies of motor drives with these two different kinds of inverters can be conducted as part of the future work.

References

[1] T. Jahns, “Getting rare-earth magnets out of EV traction machines: A review of the many approaches being pursued to minimize or eliminate rare-earth magnets from future EV drivetrains,” *IEEE Electrification Mag.*, vol. 5, no. 1, pp. 6–18, 2017.

[2] K. Rajashekara, “Present status and future trends in electric vehicle propulsion technologies,” *IEEE J. Emerg. Sel. Top. Power Electron.*, vol. 1, no. 1, pp. 3–10, 2013.

[3] N. C. Kar *et al.*, “Courting and sparking: Wooing consumers? Interest in the EV market,” *IEEE Electrification Mag.*, vol. 1, no. 1, pp. 21–31, 2013.

[4] T. M. Jahns and W. L. Soong, “Pulsating torque minimization techniques for permanent magnet AC motor drives-a review,” *IEEE Trans. Ind. Electron.*, vol. 43, no. 2, pp. 321–330, 1996.

[5] NED MOHAN, *Electric Machines and Drives*. .

[6] J. Rabkowski, D. Peftitsis, and H.-P. Nee, “Silicon carbide power transistors: A new era in power electronics is initiated,” *IEEE Ind. Electron. Mag.*, vol. 6, no. 2, pp. 17–26, 2012.

[7] W. Yin, L. Durantay, L. Zhang, S. U. Haq, and F. Vannay, “End Winding Protections Improvements Helping To Downsize dV/dt Filter For Medium Voltage Machine Fed By NPP Multi-Levels VSI Drive,” in *2018 IEEE 2nd International Conference on Dielectrics (ICD)*, 2018, pp. 1–4.

[8] M. M. Swamy, J.-K. Kang, and K. Shirabe, “Power loss, system efficiency, and leakage current comparison between Si IGBT VFD and SiC FET VFD with various filtering options,” *IEEE Trans. Ind. Appl.*, vol. 51, no. 5, pp. 3858–3866, 2015.

[9] I. Husain, *Electric and hybrid vehicles: design fundamentals*. CRC press, 2010.

[10] H.-S. Kim and S.-K. Sul, “A novel filter design for output LC filters of PWM inverters,” *J. Power Electron.*, vol. 11, no. 1, pp. 74–81, 2011.

[11] P. Mishra and R. Maheshwari, “Design, Analysis, and Impacts of Sinusoidal LC Filter on Pulsewidth Modulated Inverter Fed-Induction Motor Drive,” *IEEE Trans. Ind. Electron.*, vol. 67, no. 4, pp. 2678–2688, Apr. 2020, doi: 10.1109/TIE.2019.2913824.

[12] H. Kim, B.-H. Kim, and S. Bhattacharya, “The Influence of the LC with Clamping Diodes dv/dt Filter on Current Control of PMSM Drives in Case of Inverter Output Current Sensing and Its Compensation,” in *2019 10th International Conference on Power Electronics and ECCE Asia (ICPE 2019 - ECCE Asia)*, May 2019, pp. 1280–1285.

[13] F. Fan, K. Y. See, X. Liu, K. Li, and A. K. Gupta, “Systematic Common-Mode Filter Design for Inverter-Driven Motor System Based on In-Circuit Impedance Extraction,” *IEEE Trans. Electromagn. Compat.*, pp. 1–12, 2019, doi: 10.1109/TEMC.2019.2944663.

[14] S. Jiang, Y. Liu, W. Liang, J. Peng, and H. Jiang, “Active EMI Filter Design With a Modified LCL-LC Filter for Single-Phase Grid-Connected Inverter in Vehicle-to-Grid Application,” *IEEE Trans. Veh. Technol.*, vol. 68, no. 11, pp. 10639–10650, Nov. 2019, doi: 10.1109/TVT.2019.2944220.

[15] X. Zhang, H. Zhu, F. Li, F. Liu, C. Liu, and B. Li, "An LCL-LC power filter for grid-tied inverter," in *2013 IEEE International Conference of IEEE Region 10 (TENCON 2013)*, Oct. 2013, pp. 1–4, doi: 10.1109/TENCON.2013.6718873.

[16] U. P. Yagnik and M. D. Solanki, "Comparison of L, LC LCL filter for grid connected converter," in *2017 International Conference on Trends in Electronics and Informatics (ICEI)*, May 2017, pp. 455–458, doi: 10.1109/ICOEI.2017.8300968.

[17] A. J. P. Ortega and L. Xu, "Investigation of effects of asymmetries on the performance of permanent magnet synchronous machines," *IEEE Trans. Energy Convers.*, vol. 32, no. 3, pp. 1002–1011, 2017.

[18] "Reduction of Torque and Flux Ripples in Space Vector Modulation-Based Direct Torque Control of Asymmetric Permanent Magnet Synchronous Machine - IEEE Journals & Magazine." https://ieeexplore.ieee.org/abstract/document/7491335 (accessed Apr. 10, 2020).

[19] C. B. Jacobina, M. B. R. Correa, T. M. Oliveira, A. M. N. Lima, and E. R. C. Da Silva, "Vector modeling and control of unbalanced electrical systems," in *Conference Record of the 1999 IEEE Industry Applications Conference. Thirty-Forth IAS Annual Meeting (Cat. No. 99CH36370)*, 1999, vol. 2, pp. 1011–1017.

[20] P. Pillay and R. Krishnan, "Application characteristics of permanent magnet synchronous and brushless DC motors for servo drives," *IEEE Trans. Ind. Appl.*, vol. 27, no. 5, pp. 986–996, Sep. 1991, doi: 10.1109/28.90357.

[21] R. Krishnan, *Permanent Magnet Synchronous and Brushless DC Motor Drives*. CRC Press, 2017.

[22] R. Thike, "A Vector Controlled Drive for Parameter Evaluation of Variable Flux Machines," p. 112.

[23] V. Bobek, "PMSM electrical parameters measurement," p. 16.

[24] M. Mušák and M. Štulrajter, "NOVEL METHODS FOR PARAMETERS INVESTIGATION OF PM SYNCHRONOUS MOTORS," p. 6.

[25] G. Stumberger, B. Polajzer, B. Stumberger, M. Toman, and D. Dolinar, "Evaluation of experimental methods for determining the magnetically nonlinear characteristics of electromagnetic devices," *IEEE Trans. Magn.*, vol. 41, no. 10, pp. 4030–4032, Oct. 2005, doi: 10.1109/TMAG.2005.854992.

[26] V. Dzhankhotov, *Hybrid LC Filter for Power Electronic Drives: Theory and Implementation*. Lappeenranta University of Technology, 2009.

[27] Y. B. Solbakken, "Inductor Design for Filter Applications with high dV/dt," p. 133.

[28] P. S. Chaudhari and S. L. Patil, "Reduction in Harmonics of BLDC Motor Drive Using Controlled LC Filter," *Electr. Power Compon. Syst.*, vol. 46, no. 14–15, pp. 1686–1703, 2018.

[29] Z. Zhang, "Direct Torque Control of Permanent Magnet Synchronous Machines with Applications to Motor Drives and Wind Energy Conversion Systems," *ETD Collect. Univ. Neb. - Linc.*, pp. 1–179, Jan. 2015.

[30] P. Vas, “Sensorless vector and direct torque control,” *CERN Document Server*, 1998. https://cds.cern.ch/record/1604773 (accessed Apr. 10, 2020).

[31] D. W. Novotny and T. A. Lipo, *Vector Control and Dynamics of AC Drives*. Clarendon Press, 1996.

[32] I. Takahashi and T. Noguchi, “A New Quick-Response and High-Efficiency Control Strategy of an Induction Motor,” *IEEE Trans. Ind. Appl.*, vol. IA-22, no. 5, pp. 820–827, Sep. 1986, doi: 10.1109/TIA.1986.4504799.

[33] G. S. Buja and M. P. Kazmierkowski, “Direct torque control of PWM inverter-fed AC motors - a survey,” *IEEE Trans. Ind. Electron.*, vol. 51, no. 4, pp. 744–757, Aug. 2004, doi: 10.1109/TIE.2004.831717.

[34] M. S. Merzoug and F. Naceri, *Comparison of Field-Oriented Control and Direct Torque Control for Permanent Magnet Synchronous Motor (PMSM)*. .

[35] W. Geng, Z. Zhang, and K. Jiang, “A new control strategy of ironless stator axial-flux PM motor fed by inverter with output LC filter,” in *IECON 2015-41st Annual Conference of the IEEE Industrial Electronics Society*, 2015, pp. 002264–002269.

[36] J. Wang and R. Hamilton, “A review of negative sequence current,” in *2010 63rd Annual Conference for Protective Relay Engineers*, 2010, pp. 1–18.

[37] S. Taylor, “Implementation of negative phase sequence protection in the high voltage distribution network,” 2016.

[38] X. Yuan, W. Merk, H. Stemmler, and J. Allmeling, “Stationary-frame generalized integrators for current control of active power filters with zero steady-state error for current harmonics of concern under unbalanced and distorted operating conditions,” *IEEE Trans. Ind. Appl.*, vol. 38, no. 2, pp. 523–532, 2002.

[39] H. S. Che, E. Levi, M. Jones, W.-P. Hew, and N. A. Rahim, “Current control methods for an asymmetrical six-phase induction motor drive,” *IEEE Trans. Power Electron.*, vol. 29, no. 1, pp. 407–417, 2013.

[40] S. B. L. Malesani and P. Mattavelli, “Comparison of current control techniques for active power filters,” *IEEE Trans Ind. Electron.*, vol. 45, 1998.

[41] R. Pena, R. Cardenas, E. Escobar, J. Clare, and P. Wheeler, “Control system for unbalanced operation of stand-alone doubly fed induction generators,” *IEEE Trans. Energy Convers.*, vol. 22, no. 2, pp. 544–545, 2007.

[42] C. J. Ramos, A. P. Martins, and A. S. Carvalho, “Rotor current controller with voltage harmonics compensation for a DFIG operating under unbalanced and distorted stator voltage,” in *IECON 2007-33rd Annual Conference of the IEEE Industrial Electronics Society*, 2007, pp. 1287–1292.

[43] S. Cheng, D. Luo, S. Huang, Z. Chen, and K. Huang, “Control strategy for permanent magnet synchronous motor with contra-rotating rotors under unbalanced loads condition,” *IET Electr. Power Appl.*, vol. 9, no. 1, pp. 71–79, 2014.

[44] Q. Zhao, Y. Ye, G. Xu, and M. Zhu, "Improved repetitive control scheme for grid-connected inverter with frequency adaptation," *IET Power Electron.*, vol. 9, no. 5, pp. 883–890, 2016.

[45] B. Zhang, D. Wang, K. Zhou, and Y. Wang, "Linear phase lead compensation repetitive control of a CVCF PWM inverter," *IEEE Trans. Ind. Electron.*, vol. 55, no. 4, pp. 1595–1602, 2008.

[46] J. He, H. Chen, R. Katebi, N. Weise, and N. A. Demerdash, "Mitigation of uneven surge voltage stress on stator windings of induction motors fed by SiC-MOSFET-based adjustable speed drives," in *2017 IEEE International Electric Machines and Drives Conference (IEMDC)*, 2017, pp. 1–7.

[47] V.-T. Phan and H.-H. Lee, "Improved predictive current control for unbalanced stand-alone doubly-fed induction generator-based wind power systems," *IET Electr. Power Appl.*, vol. 5, no. 3, pp. 275–287, 2011.

[48] P. Cortes, J. Rodríguez, P. Antoniewicz, and M. Kazmierkowski, "Direct power control of an AFE using predictive control," *IEEE Trans. Power Electron.*, vol. 23, no. 5, pp. 2516–2523, 2008.

[49] M. Reyes, P. Rodriguez, S. Vazquez, A. Luna, R. Teodorescu, and J. M. Carrasco, "Enhanced decoupled double synchronous reference frame current controller for unbalanced grid-voltage conditions," *IEEE Trans. Power Electron.*, vol. 27, no. 9, pp. 3934–3943, 2012.

[50] A. O. Althobaiti, "Proportional resonant control of three-phase grid-connected inverter during abnormal grid conditions," PhD Thesis, Newcastle University, 2018.

[51] D. Vanitha and M. Rathinakumar, "Photovoltaic based proportional resonant controlled buck boost converter with coupled inductor," in *2017 IEEE International Conference on Power, Control, Signals and Instrumentation Engineering (ICPCSI)*, Sep. 2017, pp. 1817–1822, doi: 10.1109/ICPCSI.2017.8392029.